IS-T 1742

Matrix Effects in Inductively Coupled Plasma Mass Spectrometry

by

Chen, Xiaoshan

PHD Thesis submitted to Iowa State University

Ames Laboratory, U.S. DOE
Iowa State University
Ames, Iowa 50011

Date Transmitted: July 7, 1995

PREPARED FOR THE U.S. DEPARTMENT OF ENERGY
UNDER CONTRACT NO. W-7405-Eng-82.

DISCLAIMER

DISCLAIMER

Portions of this document may be illegible in electronic image products. Images are produced from the best available original document.

TABLE OF CONTENTS

LIST OF FIGURES vii

LIST OF TABLES x

1. GENERAL INTRODUCTION 1

Matrix Effects 2

Processes in the Plasma 2

Deposition of Salts on the Orifices 4

Matrix Effects in the Ion Extraction 4

Space Charge Effects 5

Alleviation and Correction of Matrix Effects 7

Optimization of Ion Optics 7

Internal Standardization 8

Removal of Matrix Ions 9

Chelating resins 9

Ion exchange 9

Chromatographic methods 9

Other Instrumental Methods 10

Hydride generation 10

Mixed gas plasmas 10

Dissertation Organization 10

References 11

2. POLYATOMIC IONS AS INTERNAL STANDARDS FOR MATRIX CORRECTIONS IN INDUCTIVELY COUPLED PLASMA MASS SPECTROMETRY 19

Abstract 19

Introduction 19

Experimental Section 21

Instrumentation 21

Reagents 21

Procedure 21

Results and Discussion 23

Polyatomic ions from aqueous HNO_3 23

Polyatomic ions from aqueous H_2SO_4 and HCl 24

$M'O^+$ ions from aqueous HNO_3 24

Effect of ionization energy on suppression behavior 25

Effect of desolvation 26

Conclusion 26

Acknowledgments 27

References 27

3. SPATIALLY RESOLVED MEASUREMENTS OF ION DENSITY BEHIND THE SKIMMER OF AN INDUCTIVELY COUPLED PLASMA MASS SPECTROMETER 43

Abstract 43

1. Introduction 44

2. Ion Sampling Process 46

2.1 Gas and Ion Flow Behind the Skimmer 46

2.2 Space-Charge-Limited Flow 49

3. Experimental Section 51

3.1 Instrumentation 51

3.2 Targets for Ion Deposition 52

3.3 Procedure 53

3.4 Reagents 54

4. Results and Discussion 55

4.1 Ion Trajectory Simulation 55

4.2 Ion Deposition Results 57

4.2.1 Ion Intensity and Ion Beam Profile 57

4.2.2 Recovery of Ions 59

4.2.3 Effect of Cs Matrix 60

4.2.4 Effect of Photon Stop 60

4.2.5 Deposition of Yttrium 61

5. Conclusion 62

Acknowledgments 63

References 63

4. AN INDUCTIVELY COUPLED PLASMA MASS SPECTROMETER WITH A MOVABLE QUADRUPOLE MASS DETECTOR 87

Abstract 87

Introduction 87

Experimental Section and Discussion 91

Outer Chamber Design 91

Interface Assembly 91

Sampler and Skimmer 91

Interface Chamber 91

Mach Disk Position 92

Sampler-Skimmer Separation 93

Outer Chamber Assembly 94

Ports 95

Back Flange 95

Inner Chamber Design 96

Inner Chamber 96

X-Y-Z Stage 97

Flanges 97

Motion Mechanism 98

Pumping Considerations 99

Ion Lenses and Mass Analyzer 99

Ion lenses 100

RF Only Rods 100

Main Quadrupole 100

Wiring and Connections 101

Pumping System Design 101

Roughing Pumps 101

Diffusion Pump 102

Turbopump 102

Safety Considerations 103

Quadrupole Control and Data Acquisition System Design 103

Quadrupole Control System 103

Control Process 103

Synchronization 104

Data Acquisition System 105

1) Detector 105

2) CEM Power Supply 106

3) Preamplifier 106

4) Amplifier 107

5) Discriminator 107

6) Counter 107

7) Logic Signal Standards 108

Acknowledgments 109

References 109

5. GENERAL CONCLUSIONS 125

ACKNOWLEDGMENTS 128

LIST OF FIGURES

2. POLYATOMIC IONS AS INTERNAL STANDARDS FOR MATRIX CORRECTIONS IN INDUCTIVELY COUPLED PLASMA MASS SPECTROMETRY

Figure 1. $^{40}Ar_2^+$ as internal standard for $^{75}As^+$. 39

Figure 2. $^{16}O_2^+$ as internal standard for $^{24}Mg^+$. 40

Figure 3. $^{89}Y^{16}O^+$ as internal standard for $^{103}Rh^+$. 41

Figure 4. $^{138}Ba^{16}O^+$ as internal standard for $^{159}Tb^+$. 42

3. SPATIALLY RESOLVED MEASUREMENTS OF ION DENSITY BEHIND THE SKIMMER OF AN INDUCTIVELY COUPLED PLASMA MASS SPECTROMETER

Figure 1. Top view of deposition apparatus. The targets were oriented horizontally. A: sampler. B: skimmer. C: ion optics, including the following elements: a: first cylindrical ion lens, b: second cylindrical ion lens, c: photon stop (not shown here, see Figure 6), d: plate ion lens. D: grid. E: graphite targets. F: water cooled mounting clamp and stand off, potential of -1000 V was provided by an electric feedthrough connected to a high voltage power supply. 71

Figure 2. Top view of the SIMION ion trajectory simulation with all the ion lenses set at ground potential. This is the X-Z plane shown in Figure 1. The grids at the right represent the deposition targets. Each grid is 0.94 mm wide in this and Figs. 3-6. 72

Figure 3. SIMION ion trajectory simulation with all the ion lenses set at ground potential. This is a side view of Figure 2, i.e., the Y-Z plane from Figure 1. The two grids at the right represent the thickness of one of the target electrodes. 73

Figure 4. SIMION ion trajectories for ion lens setting 1. 74

Figure 5. SIMION ion trajectories for ion lens setting 2. 75

Figure 6. SIMION ion trajectories for ion lens setting 3 where a photon stop is present. 76

Figure 7. Deposition profile for Sc at 50 mg L^{-1}. 77

Figure 8. Effect of Cs matrix (1000 mg L^{-1}) on Sc beam profile, lens setting 1. 78

Figure 9. Effect of Cs matrix (1000 mg L^{-1}) on Sc beam profile, lens setting 2. 79

Figure 10. Effect of lens settings on Sc beam profile, with Cs matrix at 1000 mg L^{-1}. 80

Figure 11. Beam profile for Sc at 50 mg L^{-1} with a photon stop. There is less of a dip in the center with the lenses grounded. 81

Figure 12. Beam profile for Sc at 50 mg L^{-1} with Cs matrix at 5000 mg L^{-1} and a photon stop. With matrix element present, grounding the lenses gives moderately higher signals than biasing them. 82

Figure 13. Effect of lens settings on Y beam profile. 83

Figure 14. Effect of lens settings on Y beam profile, with Cs matrix at 1000 ppm. 84

Figure 15. Effect of Cs matrix (1000 mg L^{-1}) on Sc beam profile, lens setting 1. 85

Figure 16. Effect of Cs matrix (1000 mg L^{-1}) on Sc beam profile, lens setting 2. 86

4. AN INDUCTIVELY COUPLED PLASMA MASS SPECTROMETER WITH A MOVABLE QUADRUPOLE MASS DETECTOR

Figure 1. Illustration of an ICP torch and ICP-MS interface. 111

Figure 2. Illustration of a mass spectrometer in ICP-MS. 112

Figure 3. Section view of the ICP-MS device. 113

Figure 4. Lateral motion of the inner chamber. The maximum pivoting angle is 20°. 114

Figure 5. Section view of the ICP-MS device. Axial motion is provided by the axial motion feedthrough. 115

Figure 6.	Top view showing axial motion of the inner chamber.	116
Figure 7.	Top view of the outer chamber.	117
Figure 8.	Section view of the ICP-MS interface.	118
Figure 9.	Front view of the ICP-MS device.	119
Figure 10.	Rear view of the ICP-MS device.	120
Figure 11.	Section view of the inner chamber.	121
Figure 12.	Rear view of the inner chamber.	122
Figure 13.	Top view of the inner chamber. The figure also shows the position of the inner chamber after pivoting 20° from the axis line.	123
Figure 14.	The quadrupole control and data acquisition system.	124

LIST OF TABLES

2. POLYATOMIC IONS AS INTERNAL STANDARDS FOR MATRIX CORRECTIONS IN INDUCTIVELY COUPLED PLASMA MASS SPECTROMETRY

Table 1. ICP-MS operating conditions 31

Table 2. Comparison of signals for analyte metal ions and polyatomic ions as internal standards with cesium as matrix element in HNO_3 32

Table 3. Comparison of signals for analyte metal ions and polyatomic ions as internal standards with cesium as matrix element in H_2SO_4 or HCl 34

Table 4. Comparison of signals for analyte metal ions and metal monoxide ions as internal standards with cesium as matrix element in HNO_3 36

Table 5. Ionization energies of metal atoms and neutral polyatomic molecules studied 38

3. SPATIALLY RESOLVED MEASUREMENTS OF ION DENSITY BEHIND THE SKIMMER OF AN INDUCTIVELY COUPLED PLASMA MASS SPECTROMETER

Table 1. Ion deposition conditions 69

Table 2. Voltages corresponding to different ion lens settings (in volts). Letter (a)-(c) denote the individual lenses, as shown in Fig. 1. 70

1. GENERAL INTRODUCTION

The inductively coupled plasma is an electrodeless discharge in a gas (usually Ar) at atmospheric pressure. Radio frequency energy generated by a RF power source is inductively coupled to the plasma gas through a water cooled load coil (1). In ICP-MS the "Fassel" type quartz torch commonly used in emission (2) is mounted horizontally. The sample aerosol is introduced into the central flow, where the gas kinetic temperature is about 5000 K (3). The aerosol is vaporized, atomized, excited and ionized in the plasma, and the ions are subsequently extracted through two metal apertures (sampler and skimmer) into the mass spectrometer. Figure 1 in Chapter 4 depicts the operation of the inductively coupled plasma, and the extraction of ions into the ICP-MS interface.

In ICP-MS, the matrix effects, or non-spectroscopic interferences, can be defined as the type of interferences caused by dissolved concomitant salt ions in the solution. Matrix effects can be divided into two categories: 1) signal drift due to the deposition of solids on the sampling apertures; and/or 2) signal suppression or enhancement by the presence of the dissolved salts. The first category is now reasonably understood. The dissolved salts, especially refractory oxides, tend to deposit on the cool tip of the sampling cone. The clogging of the orifices reduces the ion flow into the ICP-MS, lowers the pressure in the first stage of ICP-MS, and enhances the level of metal oxide ions. Because the extent of the clogging increases with the time, the signal drifts down. Even at the very early stage of the development of ICP-MS, matrix effects had been observed. Houk *et al.* (4) found out that the ICP-MS was not tolerant to solutions containing significant amounts of dissolved solids.

A solution containing 500 ppm total dissolved solids caused considerable signal drift over the short term, because the sampling orifice was too small (typically 0.5 mm or less) in the early devices. Modern ICP-MS instruments use larger sampling orifices (1.0-1.3 mm) and skimmers (0.7-0.8 mm) and are more tolerant to high levels of concomitant ions. The maximum level of dissolved solids is about 0.2% nominally (1).

The second category of matrix effects is still not well understood, and obviously, further studies are needed. In summary, high concentrations of matrix elements cause signal reduction (5), poor precision (6), and even memory effects (7). This chapter serves as a review of recent research about the matrix effects in ICP-MS. However, because of the amount of research in this area, in some cases only representative examples are given. Subsequent chapters present some research results focusing on this topic.

Matrix Effects

Using the same sample preparation procedures, the same plasma source, and the same type of nebulizer as ICP-AES, ICP-MS has its unique matrix effects. There have been some comprehensive studies (7) and good reviews (1, 8) to document matrix effects.

Processes in the Plasma

Atomic emission spectrometry using the ICP as the atomization and excitation source is relatively free from ionization interferences caused by easily ionizable elements in solution (4). However, the interference effects in ICP-MS was found to be more severe than in ICP-AES. Olivares and Houk (5) studied the suppression of analyte signal of Co by five salts: NaCl, $MgCl_2$, NH_4Br, and NH_4Cl. The extent of the suppression agreed with the order of ionization energies (IE). The concomitant salt with the most easily ionized element gave

the most severe suppression. They concluded that the suppression of analyte signal is due to the total ion density increase with the presence of some easily ionized concomitant ions in the solution. At high dissolved salt concentrations (above 1%), the measurement was complicated by orifice clogging and transport loss of the salt and analyte in the desolvation system.

Beauchemin (7) found that some easily ionized elements, such as Na, Mg, K, Ca and Cs can enhance analyte signal, while others, such as Al, B, and U, cause suppression for analytes V, Cr, Mn, Ni, Co, Cu, Zn, Cd and Pb in ICP-MS. Li was observed to be a neutral matrix. Gregoire (9) suggested that ambipolar diffusion in the ICP is responsible for matrix effects in ICP-MS. The model states that the excess electrons from the easily ionized matrix elements diffuse out from the central channel, causing light analyte ions to follow, hence there is a decrease in the analyte signal. He believed that the matrix suppression in ICP-MS is strongly mass dependent. Hobbs and Olesik (10) observed significant suppression effects when matrix ions were added to the solution using both laser fluorescence and ICP-MS. They believe that matrix effects appear to originate in the plasma. They agree with Gregoire (9) in that ambipolar diffusion is a possible explanation of the matrix effects in the plasma. But they believe that the matrix effects should not be dependent on the atomic weight of the analyte or the concomitant species. The radially resolved measurements in their studies confirm the lack of atomic weight dependence.

Thompson and Houk (11) concluded that in general the matrix elements cause suppression under all the experimental conditions tested, including forward power, gas flow rates, ion lens voltages, and two different nebulizers. Olesik *et al.* (12, 13) recently studied

matrix effects in ICP-AES and ICP-MS using monodisperse dried microparticulate injector and laser fluorescence techniques. They observed that the Li^+ temporal signal in the presence of 150 ppm Pb became broader and concluded that the matrix effects originate from the ICP rather than from the mass spectrometer. Tripkovic and Holclajtner-Antunovic (14, 15) believed that the matrix effects in the ICP strongly depend on the IE of the matrix elements. The easily ionized elements can increase the electron concentration significantly.

Deposition of Salts on the Orifices

Houk *et al.* (4) observed significant ICP-MS signal decrease when solutions containing Na at 500 ppm were nebulized in the earliest ICP-MS work. Olivares and Houk (5) recorded the Co signal reduction with the presence of high concentration of Na, which is due mainly to the clogging of their sampling cone. It is now clear that progressive clogging of the sampling orifice causes the analyte signal to deteriorate. Using flow injection to alleviate the clogging has been suggested (16, 17), and enlarged sampling and skimming orifices have been used (18-20). The drawback of the larger orifices is that a more powerful pumping system is necessary. Usually, when the total solids content is 0.1% or less in the solution, clogging of the sampling cone is not a severe problem (21).

Matrix Effects in the Ion Extraction

Early studies of matrix effects provided some conflicting information. For example, Tan and Horlick (22) studied matrix effects of Na, Cs, Zn, K, Rh, In, Cd, Sn and Sb on a range of analyte elements with different masses and first IEs. They found that the matrix effects depend strongly on aerosol gas flow rate. At low aerosol flow rates, the matrix suppresses sensitivity while at high flow rates, it enhances sensitivity, while plasma power

and sampling depth have no serious effect. They believed that pressure diffusion and Mach-number focusing caused the mass separation, where lighter ions diffuse away and heavier ions are focused towards the axis.

Despite the differences encountered in the observations, there are some general trends that can be summarized (8, 22, 23). 1) Lighter analyte ions are subject to more severe matrix effects. 2) Heavier matrix elements cause more severe suppression. 3) Easily ionized matrix elements cause more suppression than moderately ionized matrix elements. 4) The absolute amount of matrix element present in the solution rather than the mole ratio of matrix to analyte is important in the suppression. Kawaguchi *et al.* (24, 25) proposed that the lighter analyte ions are more susceptible to collision loss than the heavier ones in the presence of heavy matrix elements.

Space Charge Effects

Space charge effects exist in an ion beam with excess positive charge, where the charges on the ions repel each other to form space-charge-limited flow. Olivares and Houk (26) first noted that space charge could be important in the optics of their ICP-MS device, but they did not connect the space charge to the matrix effects. Gillson *et al.* (27) were the first to propose that the space charge effects within the skimmer change the flux and composition of the ion beam, which in turn is responsible for the matrix effects in the ICP-MS. Douglas and French (28) proposed that between the sampler and the skimmer, and at the entrance of the skimmer, the extracted gas beam is still neutral, so the flow of the gas can thus be treated as a plasma beam. Tanner (29) included space charge effects in a theoretical model to predict the ion trajectories behind the skimmer in ICP-MS. The results

showed that heavier elements with higher kinetic energies have higher transmission through the ion optics under the space-charge-limited flow, while lighter elements with lower kinetic energies are more susceptible to space charge repulsion and deviate from the center of the ion beam. Hence, light ions are transmitted less efficiently than heavy ions.

Hieftje *et al.* (30-32) believe that the gas dynamic theory developed by Douglas and French (28) for a neutral beam is inadequate for ion beams in ICP-MS, based on the following considerations. 1) Langmuir probe measurements indicated that the collision frequency of the electron with the sampling cone is high enough to cause significant charge separation in the extracted plasma gas. 2) The theoretical optimal sampler-skimmer separation (33) produced the lowest ion sensitivities, where analyte ions are scattered by columbic repulsion. 3) Skimming the ions near the Mach disk resulted in much better sensitivity and reduced matrix effects.

Tanner *et al.* (34, 35) recently described an ICP-MS device with a three-aperture vacuum interface. The results can be summarized as follows. 1) The device has a much lower total ion current than regular ICP-MS instruments yet still maintains similar sensitivity for analyte ions. 2) The beam entering the skimmer is still neutral. 3) The device has a more uniform ion signal response curve than most instruments. 4) More importantly, matrix effects are much less severe than with regular instruments. The success is believed to be due to the reduced ion current, hence a lower space charge effect. The formation of a shock wave in front of the third aperture facilitates matrix-free ion sampling.

Alleviation and Correction of Matrix Effects

A successful and easy way of overcoming the matrix effects due to high concentrations of concomitant elements present in the solution is to dilute the samples such that the total matrix concentrations are less than 500-1000 $\mu g\ ml^{-1}$ (9, 36), provided that the analyte elements are still above the detection limits. Calibration using matrix matched standards is also a practical method of correction if the composition of the sample is known and high purity standards are available. The standard additions method (37-39) has been used as a traditional way of overcoming the matrix effects with some success in ICP-MS as well as in almost all techniques of spectroscopy.

Optimization of Ion Optics

It has been reported that matrix effects can be alleviated to some extent by optimizing the instrumental parameters, including forward power, gas flow rates (especially nebulizer gas flow rate), ion optical potentials, sampling position, and type of nebulizer. Wang and Caruso *et al.* (40, 41), and others (42) successfully used instrumental optimization to alleviate the matrix effects. Evans and Caruso (43) further used simplex optimization to select the ion lens conditions with zero matrix suppression with some success. They found that the extraction lens potential was the most critical factor. A small sampling orifice (0.4 mm) resulted in very little matrix effect, although the sensitivity was also significantly reduced. Hu and Houk (44) optimized the ion lens potential to alleviate the matrix effects and maximize the ion signal. Chen and Houk (45) used Simion (a computer program) to study the ion trajectory in the second stage of an ICP-MS device (described in Chapter 3). They found that the matrix effects can be alleviated if the ion beam is brought into the ion

lens stack with a relatively broad profile, due to reduced ion density. The ion deposition experiments in Chap. 3 agree with their conclusion. Ross and Hieftje (46) were convinced that the ion-optical configuration can have a substantial influence on mass dependent matrix effects. They found that removing the second stage lenses in the ICP-MS eliminated the matrix effects. They further removed the photon stop and it didn't seem to affect the analytical performance of the system. Vaughan and Horlick (47) used MacSimion (a commercial computer program) to study the ion trajectories under the influence of ion optics without considering the space charge effects. The optimal conditions were dependent on the ion kinetic energies. They believe that the model can be used to predict relative signal intensities for a range of ion masses as a function of lens potentials and these are shown to agree with experimentally measured data. In a different theoretical model including space charge effects, Tanner (29) pointed out that increasing the ion energies by accelerating the ions after the skimmer can alleviate matrix effects. But he also pointed out that decelerating the ions before the quadrupole would once again induce space charge effects.

Internal Standardization

Internal standardization in ICP emission spectrometry to improve precision can be traced back to Barnett and Fassel (48, 49). It has been used in ICP-MS as a practical method of overcoming the matrix effects with some success, because in principle, the matrix element will affect the analyte ion(s) and the internal standard element(s) the same way if the internal standard is carefully chosen. Munro *et al.* (50) were the first to apply the technique in ICP-MS. Thompson and Houk (11) suggested that the elements used as internal standards must closely match both the atomic weight and the ionization energy of the analyte elements.

Chapter 3 covers this topic and will give more reviews.

Removal of Matrix Ions

Perhaps the most satisfactory method to eliminate the matrix effects is to remove the matrix elements altogether. In recent years the use of a chelating or ion exchange column to isolate and preconcentrate trace elements from matrices such as sea water has drawn considerable interest (51-58). Discussed here are the methods that can ultimately be used as on-line methods to remove matrix elements.

Chelating resins Beauchemin and McLaren *et al.* (37, 59, 60), and later Orians (61) used silica-immobilized 8-hydroxyquinoline to preconcentrate trace metals from sea water to remove the matrix interferences and improve the detection limits by up to 7-fold for several elements. Lyon *et al.* (62) used gel filtration to de-salt protein samples and removed Cl, so ^{77}Se could be determined. Analysis of Au from sea water was done by preconcentration and sometimes flow injection technique (63-65). Miyazaki (66) used Chelex-100 to preconcentrate Pb to determine Pb isotope ratios and concentrations.

Ion exchange Kawabata (67) used a cation exchange resin to separate and determine the rare earth elements. Ketterer (68) separated Re from the matrix elements Na, Mg, Al, K and Ca in ground water samples. An iminodiacetate-based chelating ion exchange column (Dionex Metpac CC-1) has been successfully used to isolate alkaline earths, first row transition metals and Pb from NaCl in sea water samples (55, 69).

Chromatographic methods Chromatographic method has been demonstrated able to separate trace analyte elements from the rest of the matrix elements, and to provide speciation information. Houk *et al.* (70-73) showed that As, Pb, Hg, Sn and Se can be

separated using reversed phase, ion exchange, ion-pairing and size exclusion chromatography methods. Caruso *et al.* (74-81) showed that the HPLC and supercritical fluid chromatography could be coupled with ICP-MS to separate organo-metal compounds, and to remove matrix elements. Braverman (82) separated rare earth elements using reversed phase HPLC. Vela and Caruso (83) reviewed the HPLC-ICP-MS for trace metal speciation. Hill (84) reviewed the coupling of HPLC with ICP-AES and ICP-MS.

Other Instrumental Methods

Only those methods that can be used on-line with ICP-MS to alleviate or remove the matrix effects are reviewed here.

Hydride generation Hydride generation is a unique way of determining As, Se, Sn, Sb, Ge, Te, Pb, Bi, and elemental Hg in the presence of matrix in ICP-MS (85-96). The analyte elements in the gaseous hydride form are swept by Ar into the ICP-MS, thus they are isolated from the matrix. The advantages include high transport efficiency, good separation of analyte from the matrix and high recovery.

Mixed gas plasmas Beauchemin *et al.* (97-99) found that adding N_2 to the outer plasma gas flow can reduce the matrix suppression considerably.

Dissertation Organization

This dissertation consists of five parts: the general introduction, three papers submitted or to be submitted to scientific journals, and the general conclusion. Each paper has its own abstract, introduction, conclusion, acknowledgments, references. The tables and figures in the papers have their own numbering system. The references are formatted according to specifications of the corresponding journal.

The general introduction (the beginning of this section) gives a relatively detailed review over the recent research over the dissertation topic.

The first paper has been submitted for publication to *Journal of Analytical Atomic Spectrometry*. The second paper has been submitted for publication to *Spectrochimica Acta*. The third paper is to be submitted to *Journal of American Society of Mass Spectrometry*.

References

1. Jarvis, K. E.; Gray, A. L. and Houk, R. S., Handbook of Inductively Coupled Plasma Mass Spectrometry; Blackie: New York, 1992.
2. Scott, R. H.; Fassel, V. A.; Kniseley, R. N. and Nixon, D. E., Anal. Chem., 1974, 46, 76-80.
3. Barnes, R. M., CRC Crit. Rev. Anal. Chem., 1978, 7, 203-296.
4. Houk, R. S.; Fassel, V. A.; Flesch, G. D.; Svec, H. J.; Gray, A. L. and Taylor, C. E., Anal. Chem., 1980, 52, 2283.
5. Olivares, J. A. and Houk, R. S., Anal. Chem., 1986, 58, 20-25.
6. Wilson, D. A.; Vickers, G. H. and Hieftje, G. M., J. Anal. At. Spectrom., 1987, 2, 365-368.
7. Beauchemin, D.; McLaren, J. W. and Berman, S. S., Spectrochim. Acta, Part B, 1987, 42, 467-490.
8. Evans, E. H. and Giglio, J. J., J. Anal. At. Spectrom., 1993, 8, 1-18.
9. Gregoire, D. C., Spectrochim. Acta, Part B, 1987, 42, 895-907.
10. Hobbs, S. E. and Olesik, J. W., Appl. Spectrosc., 1991, 45, 1395-1407.
11. Thompson, J. J. and Houk, R. S., Appl. Spectrosc., 1987, 41, 801-806.

12. Olesik, J. W. and Hobbs, S. E., Anal. Chem., 1994, 66, 3371-3378.

13. Olesik, J. W., Abstracts of Papers of the Pittsburgh Conference, Abstract # 193, 1995.

14. Tripkovic, M. R. and Holclajtner-Antunovic, I. D., J. Anal. At. Spectrom., 1993, 8, 349-357.

15. Holclajtner-Antunovic, I. D. and Tripkovic, M. R., J. Anal. At. Spectrom., 1993, 8, 359-365.

16. Dean, J. R.; Ebdon, L.; Crews, H. M. and Massay, R. C., J. Anal. At. Spectrom., 1988, 3, 349-354.

17. Hutton, R. C. and Eaton, A. N., J. Anal. At. Spectrom., 1988, 3, 547-550.

18. Crain, J. S.; Houk, R. S. and Smith, F. G., Spectrochim. Acta, Part B, 1989, 44, 1355.

19. Vaughan, M. A. and Horlick, G., Spectrochim. Acta, Part B, 1990, 45, 1289-1299.

20. Hu, K.; Clemons, P. S. and Houk, R. S., J. Am. Soc. Mass Spectrom., 1993, 4, 16-27.

21. Taylor, H. E. and Garbarino, J. R., in Inductively Coupled Plasmas in Analytical Atomic Spectrometry; Montaser, A. and Golightly, D. W.VCH Publishers: New York, 1992, pp 651-677.

22. Tan, S. H. and Horlick, G., J. Anal. At. Spectrom., 1987, 2, 745-763.

23. Horlick, G. and Shao, Y., in Inductively Coupled Plasmas in Analytical Atomic Spectrometry; Montaser, A. and Golightly, D. W.; 2nd ed., VCH Publishers: New York, 1992, pp 551-611.

24. Kawaguchi, H.; Tanaka, T.; Nakamura, T.; Morishita, M. and Misuike, A., Anal. Sci., 1987, 3, 305.

25. Kim, Y. S.; Kawaguchi, H.; Tanaka, T. and Mizuiki, A., Spectrochim. Acta, Part B, 1990, 45, 333-339.

26. Olivares, J. A. and Houk, R. S., Anal. Chem., 1985, 57, 2674-2679.

27. Gillson, G. R.; Douglas, D. J.; Fulford, J. E.; Halligan, K. W. and Tanner, S. D., Anal. Chem., 1988, 60, 1472-1474.

28. Douglas, D. J. and French, J. B., J. Anal. At. Spectrom., 1988, 3, 743-747.

29. Tanner, S. D., Spectrochim. Acta, Part B, 1992, 47, 809-823.

30. Chambers, D. M.; Poehlman, J.; Yang, P. and Hieftje, G. M., Spectrochim. Acta, Part B, 1991, 46, 741-760.

31. Chambers, D. M.; Ross, B. S. and Hieftje, G. M., Spectrochim. Acta, Part B, 1991, 46, 785-804.

32. Chambers, D. M. and Hieftje, G. M., Spectrochim. Acta, Part B, 1991, 46, 761-784.

33. Campargue, R., Proceedings of the 6th International Symposium on Rarefied Gas Dynamics, Academic Press, New York, 1969, pp 1003.

34. Tanner, S. D.; Cousins, L. M. and Douglas, D. J., Appl. Spectrosc., 1994, 48, 1367-1372.

35. Tanner, S. D.; Douglas, D. J. and French, J. B., Appl. Spectrosc., 1994, 48, 1373-1378.

36. Ridout, P. S.; Jones, H. R. and Williams, J. G., Analyst, 1988, 113, 1383-1386.

37. McLaren, J. W.; Mykytiuk, A. P.; Willie, S. N. and Berman, S. S., Anal. Chem., 1985, 57, 2907-2911.

38. McLaren, J. W.; Beauchemin, D. and Berman, S. S., J. Anal. At. Spectrom., 1987, 2, 277-281.

39. McLaren, J. W.; Beauchemin, D. and Berman, S. S., Anal. Chem., 1987, 59, 610-613.

40. Wang, J.; Shen, W. L.; Sheppard, B. S.; Evans, E. H.; Caruso, J. A. and Fricke, F. L., J. Anal. At. Spectrom., 1990, 5, 445-449.

41. Wang, J. S.; Evans, E. H. and Caruso, J. A., J. Anal. At. Spectrom., 1991, 6, 605-608.

42. Marshall, J. and Franks, J., J. Anal. At. Spectrom., 1991, 6, 591-600.

43. Evans, E. H. and Caruso, J. A., Spectrochim. Acta, Part B, 1992, 47, 1001-1012.

44. Hu, K. and Houk, R. S., J. Am. Soc. Mass Spectrom., 1993, 4, 28-37.

45. Chen, X. and Houk, R. S., Spectrochim. Acta, Part B, 1995, submitted.

46. Ross, B. S. and Hieftje, G. M., Spectrochim. Acta, Part B, 1991, 46, 1263-1273.

47. Vaughan, M. A. and Horlick, G., Spectrochim. Acta, Part B, 1990, 45, 1301-1311.

48. Barnett, W. B.; Fassel, V. A. and Kniseley, R. N., Spectrochim. Acta, Part B, 1968, 23, 643-664.

49. Barnett, W. B.; Fassel, V. A. and Kniseley, R. N., Spectrochim. Acta, Part B, 1970, 25, 139-161.

50. Munro, S.; Ebdon, L. and McWeeny, D. J., J. Anal. At. Spectrom., 1986, 1, 211-219.

51. Shabani, M. B. and Masuda, A., Anal. Chim. Acta, 1992, 261, 315-321.

52. Shabani, M. B.; Akagi, T. and Masuda, A., Anal. Chem., 1992, 64, 737-743.

53. Shabani, M. B.; Sahoo, S. K. and Masuda, A., Analyst, 1992, 117, 1477-1480.

54. Akatsuka, K.; Mclaren, J. W. and Berman, S. S., Bunseki Kagaku, 1993, 42, 423-428.

55. Ebdon, L.; Fisher, A.; Handley, H. and Jones, P., J. Anal. At. Spectrom., 1993, 8, 979-981.

56. Ebdon, L.; Fisher, A. S. and Worsfold, P. J., J. Anal. At. Spectrom., 1994, 9, 611-614.

57. Hall, G. E. M. and Pelchat, J. C., J. Anal. At. Spectrom., 1993, 8, 1059-1065.

58. Yang, H. J.; Huang, K. S.; Jiang, S. J.; Wu, C. C. and Chou, C. H., Anal. Chim. Acta, 1993, 282, 437-443.

59. Beauchemin, D.; McLaren, J. W.; Mykytiuk, A. P. and Berman, S. S., J. Anal. At. Spectrom., 1988, 3, 305.

60. Beauchemin, D. and Berman, S. S., Anal. Chem., 1989, 61, 1857-1862.

61. Orians, K. J. and Boyle, E. A., Anal. Chim. Acta, 1993, 282, 63-74.

62. Lyon, T. D. B.; Fell, G. S.; Hutton, R. C. and Eaton, A. N., J. Anal. At. Spectrom., 1988, 3, 601-603.

63. Bakowska, E.; Falkner, K. K.; Barnes, R. M. and Edmond, J. M., Appl. Spectrosc., 1989, 43, 1283-1286.

64. Falkner, K. K. and Edmond, J. M., Anal. Chem., 1990, 62, 1477-1481.

65. Gomezgomez, M. M. and McLeod, C. W., J. Anal. At. Spectrom., 1995, 10, 89-91.

66. Miyazaki, A. and Reimer, R. A., J. Anal. At. Spectrom., 1993, 8, 449-452.

67. Kawabata, K.; Kishi, Y.; Kawaguchi, O.; Watanabe, Y. and Inoue, Y., Anal. Chem., 1991, 63, 2137-2140.

68. Ketterer, M. E., Anal. Chem., 1990, 62, 2522-2526.

69. Bloxham, M. J.; Hill, S. J. and Worsfold, P. J., J. Anal. At. Spectrom., 1994, 9, 935-938.

70. Thompson, J. J. and Houk, R. S., Anal. Chem., 1986, 58, 2541-2548.

71. Shum, S. C. K.; Pang, H. M. and Houk, R. S., Anal. Chem., 1992, 64, 2444-2450.

72. Shum, S. C. K.; Nedderson, R. and Houk, R. S., Analyst, 1992, 117, 577-582.

73. Shum, S. C. K. and Houk, R. S., Anal. Chem., 1993, 65, 2972-2976.

74. Shen, W. L.; Vela, N. P.; Sheppard, B. S. and Caruso, J. A., Anal. Chem., 1991, 63, 1491-1496.

75. Vela, N. P. and Caruso, J. A., J. Anal. At. Spectrom., 1992, 7, 971-977.

76. Alrashdan, A.; Vela, N. P.; Caruso, J. A. and Heitkemper, D. T., J. Anal. At. Spectrom., 1992, 7, 551-555.

77. Carey, J. M.; Vela, N. P. and Caruso, J. A., J. Anal. At. Spectrom., 1992, 7, 1173-1181.

78. Vela, N. P.; Olson, L. K. and Caruso, J. A., Anal. Chem., 1993, 65, A585-&.

79. Vela, N. P. and Caruso, J. A., J. Chromatogr., 1993, 641, 337-345.

80. Kumar, U. T.; Vela, N. P.; Dorsey, J. G. and Caruso, J. A., J. Chromatogr. A, 1993, 655, 340-345.

81. Carey, J. M.; Vela, N. P. and Caruso, J. A., J. Chromatogr. A, 1994, 662, 329-340.

82. Braverman, D. S., J. Anal. At. Spectrom., 1992, 7, 43-46.

83. Vela, N. P. and Caruso, J. A., J. Anal. At. Spectrom., 1993, 8, 787-794.

84. Hill, S. J.; Bloxham, M. J. and Worsfold, P. J., J. Anal. At. Spectrom., 1993, 8, 499-515.

85. Powell, M. J.; Boomer, D. W. and Mcvicars, R. J., Anal. Chem., 1986, 58, 2864-2867.

86. Wang, X. R.; Viczian, M.; Lasztity, A. and Barnes, R. M., J. Anal. At. Spectrom., 1988, 3, 821-827.

87. Ting, B. T. G.; Mooers, C. S. and Janghorbani, M., Analyst, 1989, 114, 667-674.

88. Janghorbani, M. and Ting, B. T. G., Anal. Chem., 1989, 61, 701-708.

89. Haraldsson, C.; Westerlund, S. and Ohman, P., Anal. Chim. Acta, 1989, 221, 77-84.

90. Akagi, T.; Hirata, T. and Masuda, A., Analytical Sciences, 1990, 6, 397-400.

91. Heitkemper, D. T. and Caruso, J. A., Appl. Spectrosc., 1990, 44, 228-234.

92. Sarzanini, C.; Abollino, O.; Mentasti, E.; Porta, V. and Liberatori, A., Appl. Spectrosc., 1991, 45, 312-315.

93. Branch, S.; Corns, W. T.; Ebdon, L.; Hill, S. and Oneill, P., J. Anal. At. Spectrom., 1991, 6, 155-158.

94. Buckley, W. T.; Budac, J. J.; Godfrey, D. V. and Koenig, K. M., Anal. Chem., 1992, 64, 724-729.

95. Marawi, I.; Wang, J. S. and Caruso, J. A., Anal. Chim. Acta, 1994, 291, 127-136.

96. Vanelteren, J. T.; Das, H. A.; Deligny, C. L.; Agterdenbos, J. and Bax, D., J. Radioanal. Nuc. Chem., 1994, 179, 211-219.

97. Beauchemin, D. and Craig, J. M., Spectrochim. Acta, Part B, 1991, 46, 603-614.

98. Craig, J. M. and Beauchemin, D., J. Anal. At. Spectrom., 1992, 7, 937-942.

99. Xiao, G. and Beauchemin, D., J. Anal. At. Spectrom., 1994, 9, 509-518.

2. POLYATOMIC IONS AS INTERNAL STANDARDS FOR MATRIX CORRECTIONS IN INDUCTIVELY COUPLED PLASMA MASS SPECTROMETRY

A paper submitted to the Journal of Analytical Atomic Spectrometry

Xiaoshan Chen and R. S. Houk

ABSTRACT

Several strong polyatomic ion signals common in inductively coupled plasma mass spectrometry (ICP-MS) can be used as internal standards to correct for matrix interferences. Signals for most of the polyatomic ions, including metal oxides, are suppressed by a Cs matrix to the same extent as analyte ion signals at nearby m/z values. Examples include $^{14}N_2^+$ and $^{24}Mg^+$, $^{35}Cl^{16}O^+$ and $^{55}Mn^+$, $^{40}Ar^{16}O^+$ and $^{59}Co^+$, $^{32}S^{16}O^+$ and $^{45}Sc^+$, $^{40}Ar_2^+$ and $^{75}As^+$, and $^{89}Y^{16}O^+$ and $^{103}Rh^+$. The count rates for these polyatomic ions are often measured anyway to determine interference corrections for spectral overlap, so these signals should reduce the number of added elements necessary to correct for matrix interferences.

INTRODUCTION

Spectral interferences and matrix effects have been observed ever since the first publications describing ICP-MS[1-7] and have been summarized in several good reviews.[8-14] Overlap between strong polyatomic ion signals and analyte ions complicates the determination of several important elements. Examples of these interferences include $^{16}O_2^+$

on $^{32}S^+$, $^{40}Ar^{16}O^+$ on $^{56}Fe^+$, $^{40}Ar_2^+$ on $^{80}Se^+$, $^{14}N_2^+$ on $^{28}Si^+$, $^{40}ArN^+$ on $^{54}Fe^+$, $^{35}Cl^{16}O^+$ on $^{51}V^+$, $^{35}Cl^{16}OH^+$ on $^{52}Cr^+$, and $^{40}Ar^{35}Cl^+$ on $^{75}As^+$, $^{32}S^{16}O^+$ on $^{48}Ti^+$ and $^{32}S^{16}O_2/^{32}S_2^+$ on $^{64}Zn^+$. The deleterious effects of polyatomic ion interferences are minimized by employing a) alternative methods of sample preparation (e.g. avoiding HCl, $HClO_4$ and H_2SO_4 in the final sample solution[15-17]), b) separations during or before sample introduction (e.g., desolvation[18-20] or liquid chromatographic separations[13]), c) high resolution MS,[14, 21, 22] or d) correction procedures involving elemental equations.[23, 24]

In ICP-MS, the analyte signal also generally depends on both the concentration and the atomic weight of the matrix constituents. Usually, the analyte signal is suppressed by the matrix, and the suppression gets more severe as the concentration and the atomic weight of the matrix increases.[7, 25-29] Internal standardization is generally used to correct for this matrix effect. A variety of internal standard elements that span the m/z range are often employed,[30-35] e.g., ^{9}Be, ^{59}Co, ^{115}In and ^{205}Tl.[36] This procedure requires multielement spikes and usually precludes determination of the spike elements in the original sample.

As an alternative, if ions that are already present in the spectrum can be used as internal standards, fewer spike elements are necessary. McLaren and Beauchemin and co-workers found that $^{12}C^+$ and $^{40}Ar_2^+$ served as reasonable internal standards for analysis of marine sediments.[25,35] This paper extends this concept to a variety of other polyatomic ions such as N_2^+, ArO^+, ClO^+, SO^+ and MO^+. The signals for these ions are often measured anyway to determine interference corrections. Why not use them as internal standards, as long as their signals are suppressed by the matrix to the same extent as that for analyte ions ?

EXPERIMENTAL SECTION

Instrumentation

The ICP-MS device used for this work was the ELAN 250 from Perkin-Elmer SCIEX (Thornhill, Ontario, Canada) with Fassel-type torch,[37] upgraded ion optics, electronics and ELAN 5000 software. The nebulizer gas flow rate was regulated by a mass flow controller (Model 8200, Matheson Scientific, East Rutherford, NJ). The sample was introduced using an ultrasonic nebulizer (Model U-5000, CETAC Technologies, Omaha, NE). The operating conditions and the measuring parameters are listed in Table 1.

Reagents

The high purity acids (HNO_3, H_2SO_4, HCl) and $CsNO_3$ standard solution used were from GFS Chemicals (Columbus, OH). Other reagents used were from PLASMACHEM Associates, Inc. (Armingdale, NJ). The samples were diluted with high purity water (18 MΩ-cm resistivity) from a 5-stage Milli-Q Plus Water System (Millipore Corporation, Bedford, MA).

Procedure

The instrument was optimized by nebulizing a solution containing 100 ppb Li, Sc, Y, Cs and Bi and adjusting the torch position, ion lens voltage, and nebulizer flow rate to maximize all the ion signals. The acid blank and matrix blank solutions of cesium were all analyzed and no analyte ion was found. Then solutions containing one analyte ion with various concentrations of the matrix element cesium were analyzed. The parameter files were set up so that the strong signals of some polyatomic ions were recorded with a count rate close to or less than 10^6 cps to avoid errors due to nonlinearity of the detector. In each of

the three acid systems, single element standard solutions (1.5 μM unless indicated otherwise) with various Cs matrix concentrations were nebulized, and signals from one polyatomic ion and the analyte ion were monitored. The analyte ions studied were selected so that their major isotopes yielded peaks at m/z values reasonably close to those for common polyatomic ions.

Some metal oxide ions were also studied as possible internal standards at high m/z values. In this case, a solution of two metals (M and M′) was added to provide the analyte (M^+) and the internal standard ($M'O^+$). For example, Tb^+ (m/z=159) was the analyte in one case, Ba was added to provide BaO^+, and the effect of cesium concentration on the signals for Tb^+ and BaO^+ was measured. The concentrations of additives were chosen to provide proper count rates for the ions of interest.

Cesium was used as the matrix element because it was easily ionized and had a relatively high atomic weight. The figures give the relative ion signals as functions of cesium concentration. The signal ratios of analyte ion to the internal standard are also given. Illustrative data representing both the best and the worst cases of agreement between the suppression of polyatomic ions and that of analyte ions were chosen for the figures. The ion signals of the internal standard and the analyte are compared in normalized scales for all the cases studied in Tables 2-4. The maximum signal of each ion is set to 100 for convenience.

RESULTS AND DISCUSSION

Polyatomic ions from aqueous HNO_3

The polyatomic ions in the HNO_3 solvent system include $^{14}N_2^+$, $^{40}Ar^{14}N^+$, $^{40}Ar^+$, $^{16}O_2^+$, $^{40}Ar^{16}O^+$ and $^{40}Ar_2^+$, which exist when any aqueous solution is nebulized. Nitric acid is therefore considered the first acid of choice in ICP-MS because the background is relatively simple and close to that of water alone. In this study, a series of 1.5 μM standard solutions of Mg, Co, or As with various cesium matrix concentrations were studied, and one polyatomic ion and one analyte ion signal were monitored for each solution. Note that the 50 ppm Cs solution nebulized with the ultrasonic nebulizer is more like a 500-1000 ppm Cs solution with a conventional pneumatic nebulizer, so that a more severe matrix effect is expected.

The matrix effect for a typical polyatomic ion, $^{40}Ar_2^+$, is shown in Figure 1. Henceforth, we will simply use the symbol for an ion to mean the signal for that ion, to save space and avoid constant repetition of the term "signal for." Figure 1 shows that $^{75}As^+$ and $^{40}Ar_2^+$ are suppressed substantially by the Cs matrix, as expected. Both ions are suppressed to virtually the same extent, as shown previously for Ar_2^+ by Beauchemin *et al.*[25, 35] Table 2 shows similar results for most of the other pairs of ions studied. The suppression induced by cesium is extensive but is very similar for $^{24}Mg^+$ and $^{14}N_2^+$, and for $^{59}Co^+$ and $^{40}Ar^{16}O^+$. These three pairs of ions should serve as good internal standards for each other. As expected, lighter ions like $^{24}Mg^+$ are suppressed more extensively than heavier ions like $^{40}Ar_2^+$.[38, 39]

Table 2 and Figure 2 also show that $^{24}Mg^+$ is suppressed much more extensively than

$^{16}O_2^+$, so $^{16}O_2^+$ is not an effective internal standard ion for $^{24}Mg^+$. Of the various sets of ions studied, this pair showed the poorest agreement in suppression behavior. Possible reasons for the anomalous behavior of $^{24}Mg^+$ and $^{16}O_2^+$ are described in the discussion section.

Polyatomic ions from aqueous H_2SO_4 and HCl

These acids contribute a variety of polyatomic ions, including $^{32}S^{14}N^+$, $^{40}Ar^{32}S^+$, $^{32}S^{16}O^+$, $^{32}S_2^+$, $^{32}S^{16}O_2^+$, $^{35}Cl^{14}N^+$, $^{35}Cl_2^+$, $^{35}Cl^{16}O^+$, $^{35}Cl^{16}OH^+$ and $^{40}Ar^{35}Cl^+$, in addition to the other ions common from aqueous solutions. The acid concentrations were chosen to restrict the polyatomic ions to convenient levels. The solution analyzed were a) Sc and Cu in 0.1% H_2SO_4 and 1% HNO_3, and b) Mn in 0.5%HCl and 0.5% HNO_3.

The results are listed in Table 3. Sc^+ and Cu^+ showed very similar suppression effects as SO^+ and SO_2^+/S_2^+, respectively, and gave plots very similar to Figure 1, relative to the precision (~2% RSD) of each signal measurement. The signal for ClO^+ was suppressed somewhat more extensively than that for Mn^+.

$M'O^+$ ions from aqueous HNO_3

The polyatomic ions tested previously occur below m/z=80. However, the magnitude of the matrix effect usually depends on the atomic weight of the analyte.[38, 39] Several internal standards that span the m/z range are commonly used for multielement analysis.[36, 38, 39] For these reasons, the effects of cesium matrix on $^{45}Sc^{16}O^+$, $^{89}Y^{16}O^+$, $^{138}Ba^{16}O^+$, $^{169}Tm^{16}O^+$, and $^{184}W^{16}O^+$ are reported to evaluate these ions as possible internal standards. These $M'O^+$ ions are formed by adding salts containing the metal M′ to aqueous 1% HNO_3. These solutions also contain the analyte element M at an appropriate concentration.

The results are summarized in Figures 3 and 4 and Table 4. Two general types of

behavior are seen. The oxide ion and the analyte ion are suppressed to the same extent in the following cases: $^{63}Cu^+$ and $^{45}Sc^{16}O^+$, $^{103}Rh^+$ and $^{89}Y^{16}O^+$, $^{181}Ta^+$ and $^{169}Tm^{16}O^+$. In the worst case for these three pairs, the relative signal for Cu^+ is different from that for ScO^+ by 11% at a Cs concentration of 2 ppm. This sort of agreement in suppression behavior is similar to that seen when atomic ions of different element are used as internal standards[7, 40]. It is, of course, poorer agreement than that seen for isotope dilution measurements. On the other extreme, Table 4 shows that $^{138}Ba^{16}O^+$ and $^{184}W^{16}O^+$ are suppressed more extensively than $^{159}Tb^+$ and $^{205}Tl^+$, respectively.

Effect of ionization energy on suppression behavior

Ionization energy (IE) for the neutral analogues of most of the ions studied are given in Table 5. For ArO^+ and Ar_2^+, estimates of the total internal energy of the ground state of the ion are given instead, as the neutral molecules ArO and Ar_2 are not stable enough for their IEs to be measured directly.

The observed suppression behavior is related to the IE of the ions involved in the following ways. The ions are arranged in four groups in Table 5. In the first group, the polyatomic ions are either background ions from the plasma (ArO^+, Ar_2^+) or oxides of nonmetallic elements like SO^+ or ClO^+. In these cases, the IE of the polyatomic species is much higher than that of the metal, and both polyatomic ion and metal ion are suppressed similarly by the cesium matrix. The second group consists of the metal oxides ScO^+, YO^+ and TmO^+, which have lower ionization energies than the analyte and are suppressed the same as their respective analytes. The IEs of all these ions are below 8 eV, so they should all be efficiently ionized in the plasma. However, the metal oxides BaO and WO have higher

ionization energies than the analytes, and BaO^+ and WO^+ are suppressed more extensively than the analytes, even though the IE of BaO is only 6.91 eV. This behavior is opposite to that seen for the nonmetal polyatomic ions in the first group (N_2^+, SO^+, etc.), for reasons that are not clear. The last group consists only of $^{16}O_2^+$, which is suppressed much less extensively than $^{24}Mg^+$. In this case, the m/z difference may be too large, and the trajectories of Mg^+ and O_2^+ through the ion lenses may be affected differently by the space charge induced by the matrix ion.[41]

Effect of desolvation

The observation that many oxide ions are suppressed to the same extent as nearby analyte ions is surprising in view of recent studies by Tanner, who showed that oxide ions have kinetic energies that are about 1 eV lower than those of nearby atomic ions. Ions with lower kinetic energy are deflected more extensively by the space charge effect and tend to be lost more severely when matrix ions are present.[42] The lower kinetic energies for $M'O^+$ are attributed to formation of these species mainly in the cool regions surrounding wet droplets.[42] In the present work, the wet aerosol is desolvated, which removes the wet droplets.[43, 44] Injecting the sample as dry aerosol particles could therefore account for the unexpected similarity in the matrix effects for analyte ions and oxide ions.

CONCLUSION

Most of the polyatomic ions studied should serve as reasonable internal standards. Atomic ions from Sc, Y, and Tm are common internal standards, and their oxide ions could be used as well. The most likely scenario for use of ClO^+, SO^+ and SO_2^+ would be for the

analysis of a) aqueous HCl, $HClO_4$ or H_2SO_4 or b) solid samples that require these acids for dissolution. In this latter case, either the original solid should not contain appreciable S or Cl, or the S and Cl content in the sample should be measured separately. Evaluation of the utility of this concept by analysis of standard reference materials is currently underway in our laboratory, as are further studies into the fundamental reasons for the apparent dependence of suppression behavior on the ionization energies of analyte and oxide ions.

ACKNOWLEDGEMENTS

The Perkin-Elmer Graduate Research Fellowship awarded to Xiaoshan Chen is gratefully acknowledged. Ames Laboratory is operated for the U.S. Department of Energy by Iowa State University under Contract No. W-7405-ENG-82. This work was supported by the Office of Basic Energy Sciences, Division of Chemical Sciences.

REFERENCES

1 Houk, R. S., Fassel, V. A., Flesch, G. D., Svec, H. J., Gray, A. L. and Taylor, C. E., *Anal. Chem.*, 1980, **52**, 2283.

2 Date, A. R. and Gray, A. L., *Analyst*, 1981, **106**, 1255.

3 Date, A. R. and Gray, A. L., *Analyst*, 1983, **108**, 159.

4 Gray, A. L. and Date, A. R., *Analyst*, 1983, **108**, 1033.

5 Date, A. R. and Gray, A. L., *Spectrochim. Acta, Part B*, 1983, **38**, 29.

6 Douglas, D. J., Quan, E. S. K. and Smith, R. G., *Spectrochim. Acta, Part B*, 1983, **38**, 39.

7 Thompson, J. J. and Houk, R. S., *Appl. Spectrosc.*, 1987, **41**, 801.

8 Vaughan, M. A. and Horlick, G., *Appl. Spectrosc.*, 1986, **40**, 434.

9 Tan, S. H. and Horlick, G., *Appl. Spectrosc.*, 1986, **40**, 445.

10 Vaughan, M. A. and Horlick, G., *Appl. Spectrosc.*, 1987, **41**, 523.

11 Casetta, B., *At. Spectrosc.*, 1990, **11**, 102.

12 Jarvis, I. and Jarvis, K. E., *Chem. Geol.*, 1992, **95**, 1.

13 Evans, E. H. and Giglio, J. J., *J. Anal. At. Spectrom.*, 1993, **8**, 1.

14 Reed, N. M., Cairns, R. O., Hutton, R. C. and Takaku, Y., *J. Anal. At. Spectrom.*, 1994, **9**, 881.

15 Date, A. R., Cheung, Y. Y. and Stuart, M. E., *Spectrochim. Acta, Part B*, 1987, **42**, 3.

16 Date, A. R., Cheung, Y. Y., Stuart, M. E. and Jin, X. H., *J. Anal. At. Spectrom.*, 1988, **3**, 653.

17 McLaren, J. W., Beauchemin, D. and Berman, S. S., *J. Anal. At. Spectrom.*, 1987, **2**, 277.

18 Alves, L. C., Wiederin, D. R. and Houk, R. S., *Anal. Chem.*, 1992, **64**, 1164.

19 Hutton, R. C. and Eaton, A. N., *J. Anal. At. Spectrom.*, 1987, **2**, 595.

20 Zhu, G. and Browner, R. F., *J. Anal. At. Spectrom.*, 1988, **3**, 781.

21 Bradshaw, N., Hall, E. F. H. and Sanderson, N. E., *J. Anal. At. Spectrom.*, 1989, **4**, 801.

22 Morita, M., Ito, H., Uehiro, T. and Otsuka, K., *Anal. Sci.*, 1989, **5**, 609.

23 Munro, S., Ebdon, L. and McWeeny, D. J., *J. Anal. At. Spectrom.*, 1986, **1**, 211.

24 Ridout, P. S., Jones, H. R. and Williams, J. G., *Analyst*, 1988, **113**, 1383.

25 Beauchemin, D., McLaren, J. W. and Berman, S. S., *Spectrochim. Acta, Part B*, 1987, **42**, 467.

26 Vandecasteele, C., Nagels, M., Vanhoe, H. and Dams, R., *Anal. Chim. Acta*, 1988, **211**, 91.

27 Stotesbury, S. J., Pickering, J. M. and Grifferty, M. A., *J. Anal. At. Spectrom.*, 1989, **4**, 457.

28 Amarasiriwardena, C., J., Gercken, B., Argentine, M. D. and Barnes, R. M., *J. Anal. At. Spectrom.*, 1990, **5**, 457.

29 Vanhaecke, F., Vanhoe, H., Dams, R. and Vandecasteele, C., *Talanta*, 1992, **39**, 737.

30 Hall, G. E. M., Park, C. J. and Pelchat, J. C., *J. Anal. At. Spectrom.*, 1987, **2**, 189.

31 Lichte, F. E., Meier, A. L. and Crock, J. G., *Anal. Chem.*, 1987, **59**, 1150.

32 Doherty, W., *Spectrochim. Acta, Part B*, 1989, **44**, 263.

33 Igarashi, Y., Kawamura, H., Shiraishi, K. and Takaku, Y., *J. Anal. At. Spectrom.*, 1989, **4**, 571.

34 Garbarino, J. R. and Taylor, H. E., *Anal. Chem.*, 1987, **59**, 1568.

35 McLaren, J. W., Beauchemin, D. and Berman, S. S., *Spectrochim. Acta, Part B*, 1988, **43**, 413.

36 Vandecasteele, C., Vanhoe, H. and Dams, R., *J. Anal. At. Spectrom.*, 1993, **8**, 781.

37 Scott, R. H., Fassel, V. A., Kniseley, R. N. and Nixon, D. E., *Anal. Chem.*, 1974, **46**, 76.

38 Tan, S. H. and Horlick, G., *J. Anal. At. Spectrom.*, 1987, **2**, 745.

39 Horlick, G. and Shao, Y., in *Inductively Coupled Plasmas in Analytical Atomic Spectrometry*, eds. Montaser, A. and Golightly, D. W., VCH Publishers, New York, 1992, p. 551.

40 Jarvis, K. E., Gray, A. L. and Houk, R. S., *Handbook of Inductively Coupled Plasma Mass Spectrometry*, Blackie, New York, 1992, p. 165.

41 Tanner, S. D., *Spectrochim. Acta, Part B*, 1992, **47**, 809.

42 Tanner, S. D., *J. Anal. At. Spectrom.*, 1993, **8**, 891.

43 Winge, R. K., Crain, J. S. and Houk, R. S., *J. Anal. At. Spectrom.*, 1991, **6**, 601.

44 Winge, R. K., Chen, X. and Houk, R. S., *J. Anal. At. Spectrom.*, 1995, **10**, in preparation.

45 Lias, S. G., Bartmess, J. E., Liebman, J. F., Holmes, J. L., Levin, R. D. and Mallard, W. G., *J. Phys. Chem. Ref. Data*, 1988, **17, Supplement No. 1**, 1.

46 Flesch, G. D., Nourbaksh, S. and Ng, C.-Y., *J. Chem. Phys.*, 1990, **92**, 3590.

47 Ng, C.-Y., in *State Selected Ion Molecular Reaction Dynamics, Part I: Experiment*, eds. Ng, C.-Y. and Baer, M., *Adv. Chem. Phys. Series*, **82**, 1992, p. 401.

Table 1. ICP-MS operating conditions

Torch	Fassel type[34]
RF power	1.3 kW
Reflected power	≤ 2 W
Plasma gas flow rate	14 L/min
Nebulizer gas flow rate	1.25 L/min
Auxiliary gas flow rate	0.4 L/min
Sampler	Nickel, 1.14 mm orifice diameter
Skimmer	Nickel, 0.89 mm orifice diameter
Sample uptake rate	1.3 ml/min
Nebulizer type	CETAC U-5000 (current setting = 5 Amp)
Heating/Desolvation temperature	140°C/-2°C
Measurement parameters for polyatomic ions	
Resolution mode	High
Number of measurements per peak	17

Table 2. Comparison of signals for analyte metal ions and polyatomic ions as internal standards with cesium as matrix element in HNO_3

Analyte ion	Polyatomic ion	[Cs] ppm	Relative signal	
			Analyte ion	Polyatomic ion
$^{24}Mg^+$	$^{14}N_2^+$	0	100	100
(1.5μM)		2	64	71
		5	40	45
		10	18	16
		50	2.4	2.0
$^{24}Mg^+$	$^{16}O_2^+$	0	100	100
(1.5μM)		2	62	93
		5	39	79
		10	20	54
		50	2.0	3.2
$^{59}Co^+$	$^{40}Ar^{16}O^+$	0	100	100
(1.5μM)		2	87	84
		5	72	70
		10	38	37
		50	7.0	7.0

Table 2. continued.

Analyte ion	Polyatomic ion	[Cs] ppm	Relative signal	
			Analyte ion	Polyatomic ion
$^{75}As^{+}$	$^{40}Ar_2^{+}$	0	100	100
(1.5μM)		2	78	79
		5	74	77
		10	37	38
		50	10	12

Table 3. Comparison of signals for analyte metal ions and polyatomic ions as internal standards with cesium as matrix element in H_2SO_4 or HCl

Analyte ion	Polyatomic ion	[Cs] ppm	Relative signal	
			Analyte ion	Polyatomic ion
$^{45}Sc^+$	$^{32}S^{16}O^+$	0	100	100
(1.5μM)		2	81	80
		5	69	64
		10	39	39
		50	8.7	8.0
$^{63}Cu^+$	$^{32}S^{16}O_2^+$, $^{32}S_2^+$ [a]	0	100	100
(1.5μM)		2	77	83
		5	63	68
		10	35	37
		50	5.0	5.3
$^{55}Mn^+$	$^{35}Cl^{16}O^+$	0	100	100
(1.5μM)		2	72	60
		5	57	49
		10	30	24
		50	2.5	2.0

[a] High resolution measurements indicate both these ions are significant from H_2SO_4 at m/z=64.

Table 4. Comparison of signals for analyte metal ions and metal monoxide ions as internal standards with cesium as matrix element in HNO_3

M^+	$M'O^+$	[Cs] ppm	Relative signal	
			M^+	$M'O^+$
$^{63}Cu^+$	$^{45}Sc^{16}O^+$	0	100	100
(0.2μM)	(Sc 200ppb)	2	80	87
		5	60	67
		10	30	33
		20	10	11
		50	1.4	1.5
$^{103}Rh^+$	$^{89}Y^{16}O^+$	0	100	100
(0.2μM)	(Y 200ppb)	2	85	85
		5	63	61
		10	31	28
		20	8.3	7.9
		50	0.7	0.7
$^{159}Tb^+$	$^{138}Ba^{16}O^+$	0	100	100
(1.0μM)	(Ba 4 ppm)	2	88	75
		5	77	50
		10	46	27

Table 4. Continued.

M^+	$M'O^+$	[Cs] ppm	Relative signal	
			M^+	$M'O^+$
$^{159}Tb^+$	$^{138}Ba^{16}O^+$	20	12	5.8
		50	0.4	0.1
$^{181}Ta^+$	$^{169}Tm^{16}O^+$	0	100	100
(0.6μM)	(Tm 1ppm)	2	66	71
		5	49	51
		10	20	23
		20	8	9
		50	0.6	0.6
$^{205}Tl^+$	$^{184}W^{16}O^+$	0	100	100
(2.0μM)	(W 4ppm)	2	88	70
		5	74	52
		10	39	29
		20	15	12
		50	1.3	1.2

Table 5. Ionization energies of metal atoms and neutral polyatomic molecules studied[41-43]

Metal Species	IE (eV) (eV)	Polyatomic Species	IE (eV)	Suppressed the Same?
Mg	7.65	N_2	15.58	yes
Sc	6.54	SO	10.3	yes
Mn	7.44	ClO	11.1	yes
Co	7.86	ArO	~13 [a]	yes
Cu	7.73	SO_2	12.32	yes
		S_2	9.36	yes
As	9.81	Ar_2	14.7 [a]	yes
Cu	7.73	ScO	6.6	yes
Rh	7.46	YO	5.85	yes
Ta	7.40	TmO	6.44	yes
Tb	5.86	BaO	6.91	no
Tl	6.11	WO	9.1	no
Mg	7.65	O_2	12.06	no

[a] The values listed are the estimated total internal energies for Ar_2^+ and ArO^+.[42, 43]

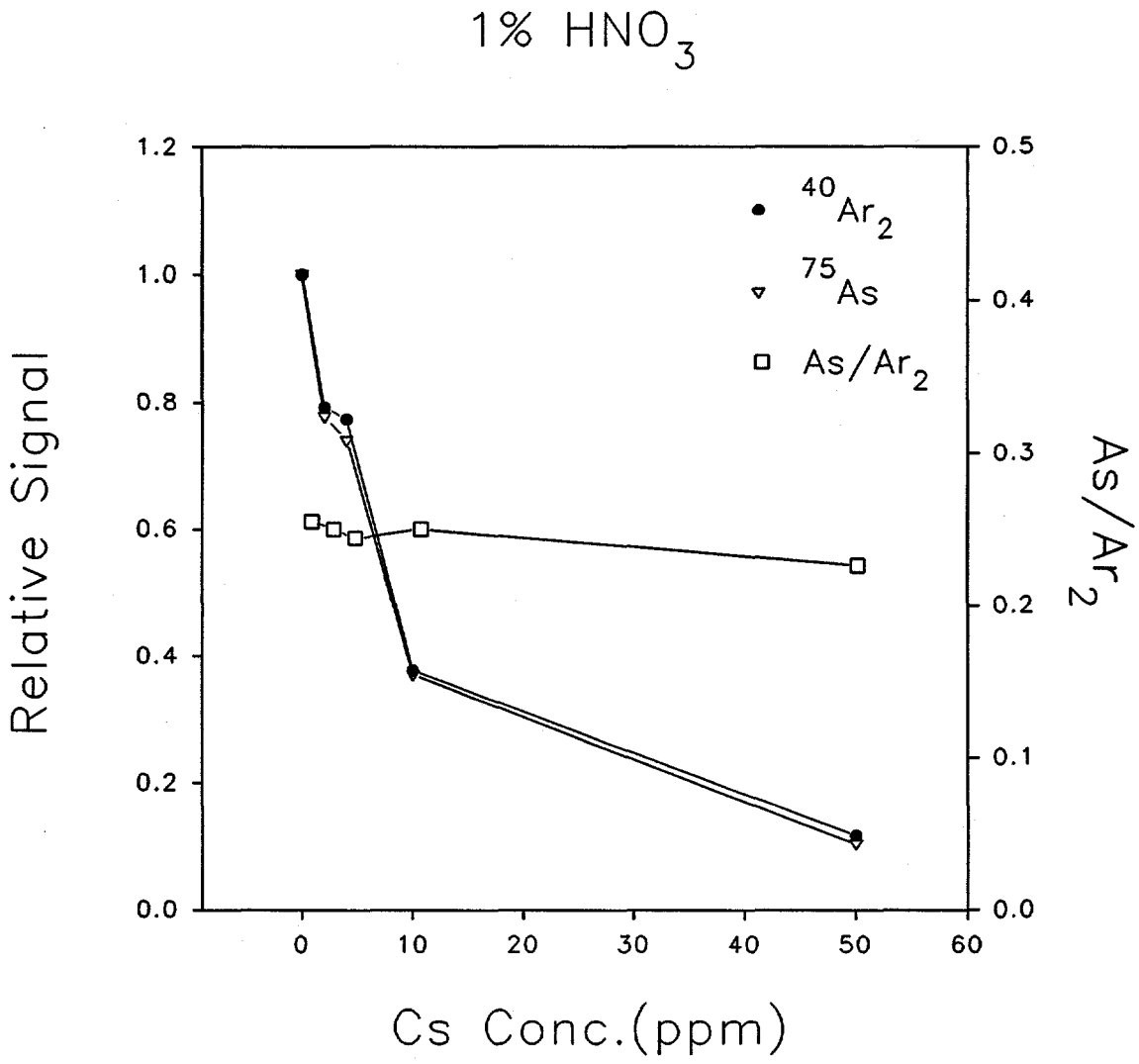

Figure 1. $^{40}Ar_2^+$ as internal standard for $^{75}As^+$.

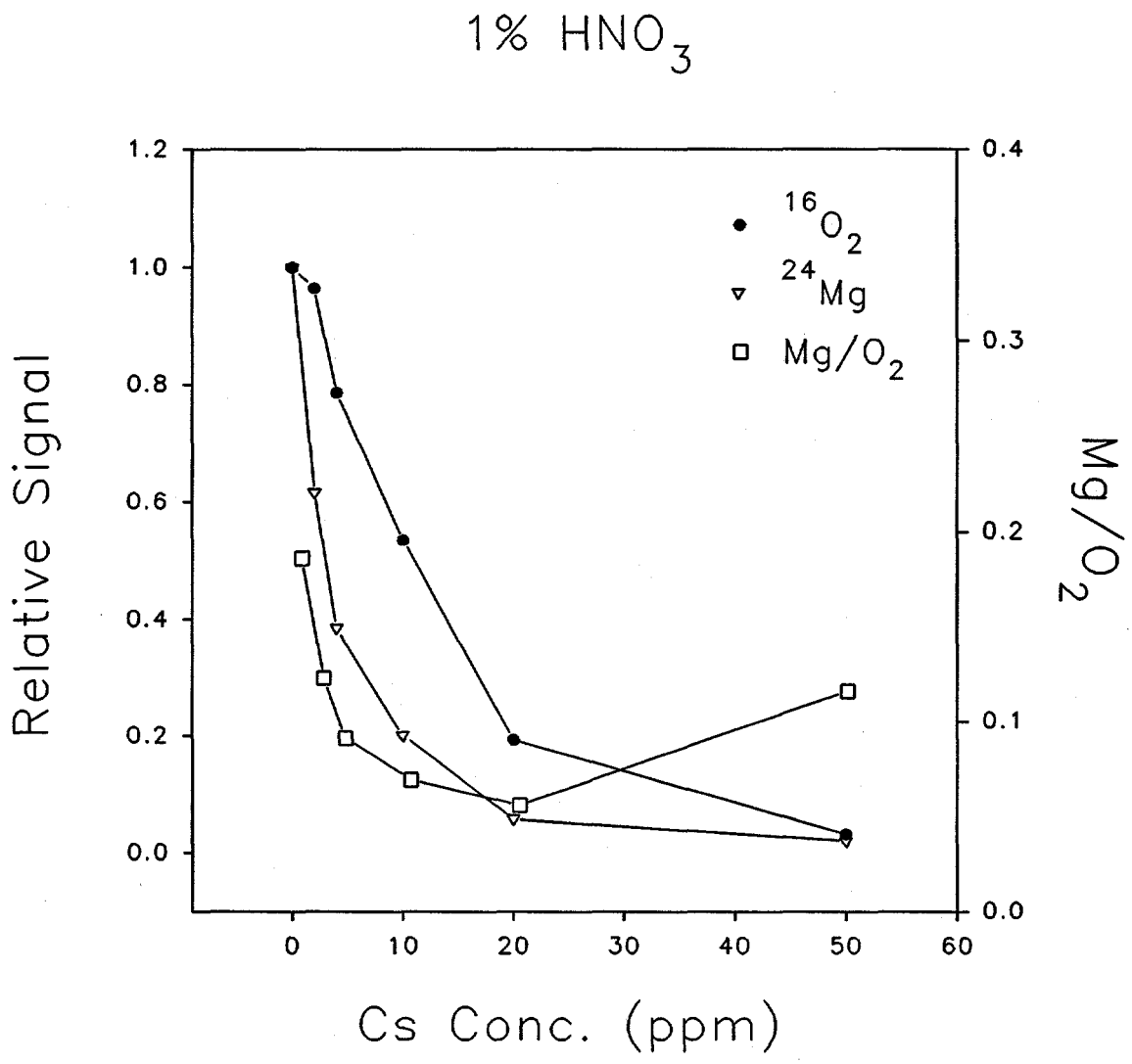

Figure 2. $^{16}O_2^+$ as internal standard for $^{24}Mg^+$.

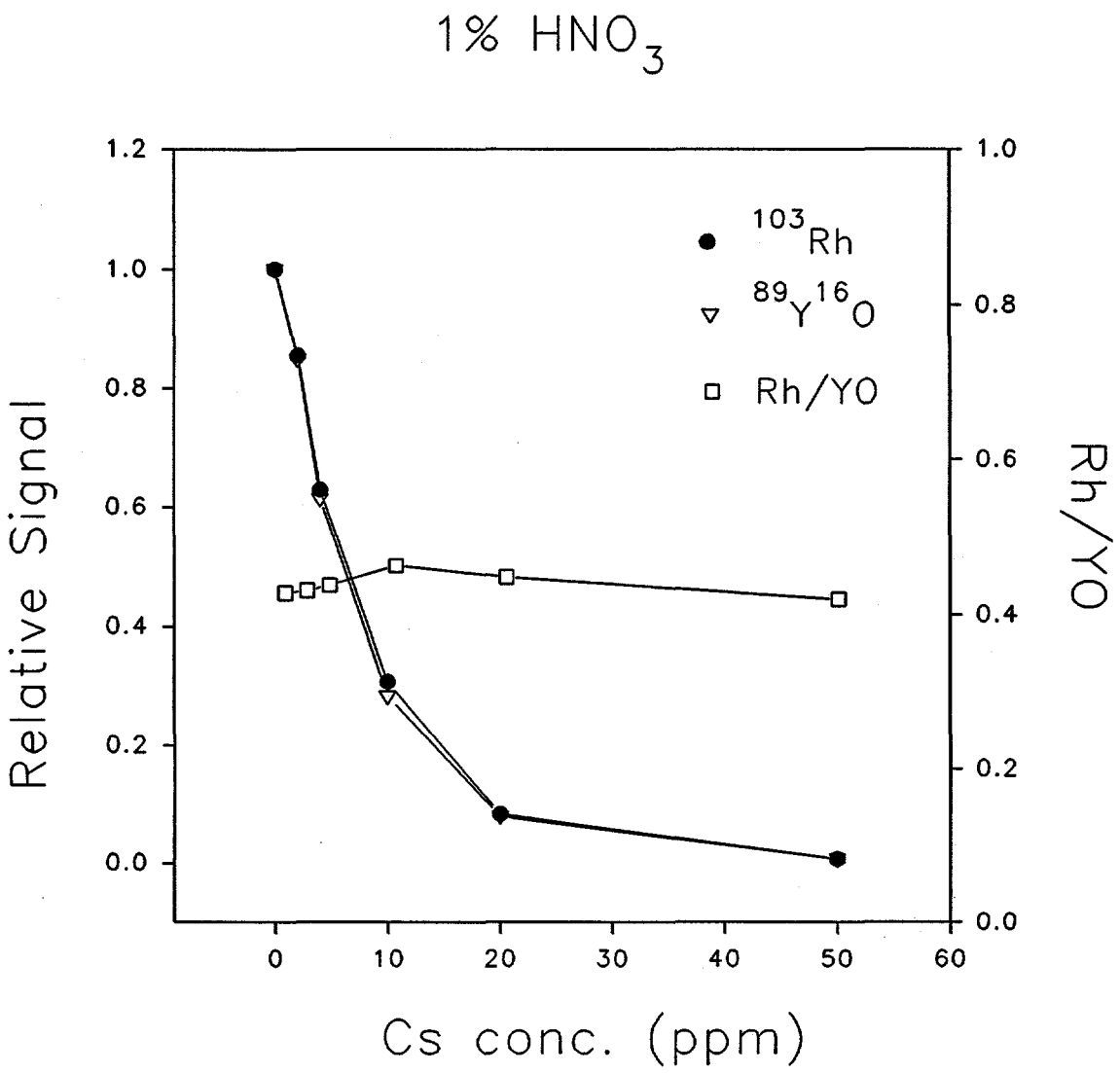

Figure 3. $^{89}Y^{16}O^{+}$ as internal standard for $^{103}Rh^{+}$.

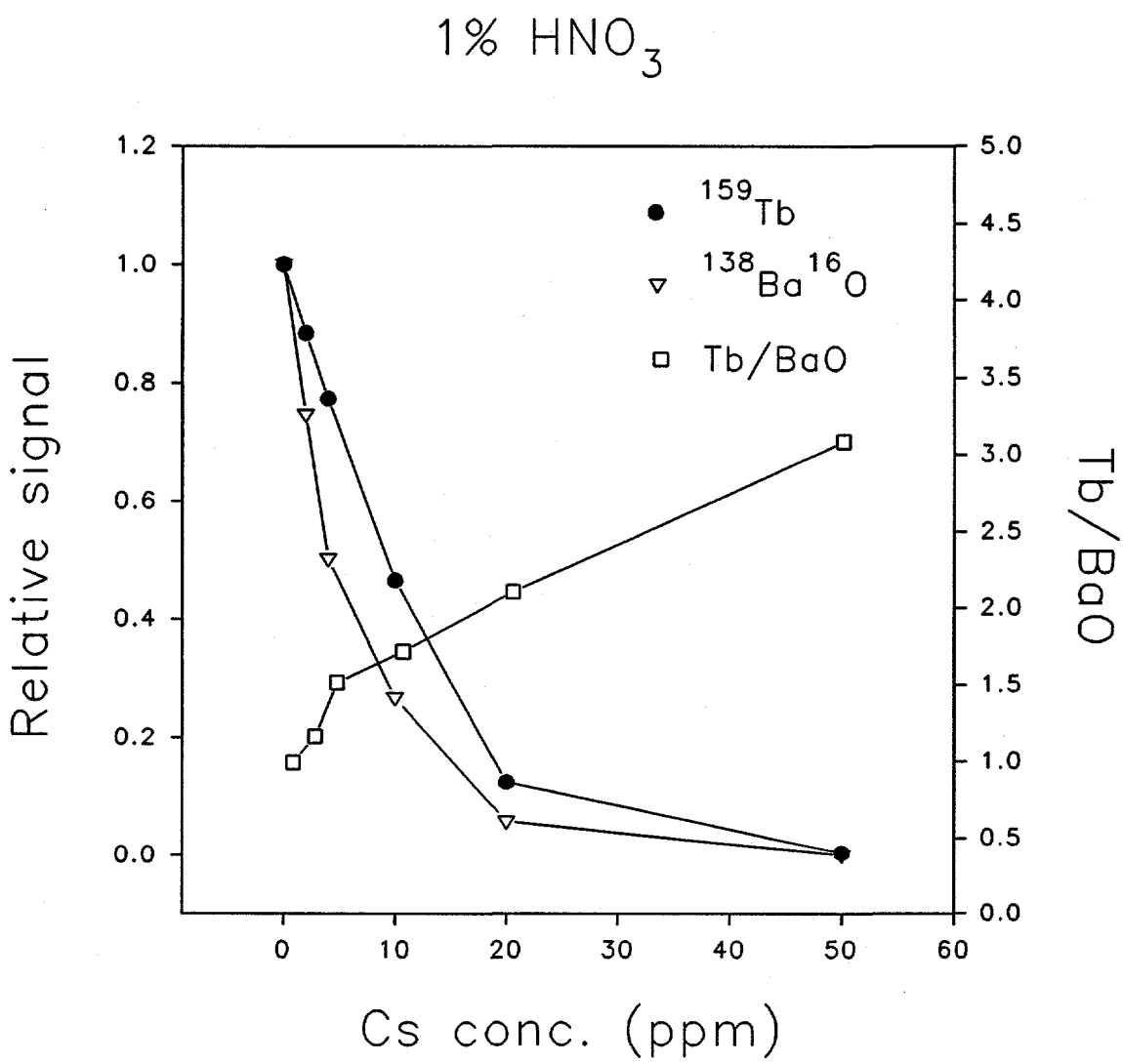

Figure 4. $^{138}Ba^{16}O^{+}$ as internal standard for $^{159}Tb^{+}$.

3. SPATIALLY RESOLVED MEASUREMENTS OF ION DENSITY BEHIND THE SKIMMER OF AN INDUCTIVELY COUPLED PLASMA MASS SPECTROMETER

A paper submitted to Spectrochimica Acta

Xiaoshan Chen and R. S. Houk

ABSTRACT

Ions are extracted from the ICP through a conventional sampler and skimmer and then deposited on an array of graphite targets at the exit of a set of electrostatic ion lenses. Scandium ion signal is enhanced by choosing appropriate potentials on the ion lenses. The Sc^+ ion signal is suppressed by the presence of concomitant Cs ions at high concentrations. Comparisons of grounded ion lenses and two different ion lens potential settings were made. The signal is enhanced more extensively by the ion lenses when there are no concentrated concomitant ions. This study indicates that matrix effects in ICP-MS could possibly be alleviated by choosing ion lens potentials such that the ions enter the ion optics with a relatively broad beam cross section; the beam then focused to a smaller size. A photon stop inside the ion lens stack reduces ion transmission and changes the shape of the beam profile from conical to bimodal.

1. INTRODUCTION

The detection limits of ICP-MS based on quadrupole instruments are no better than 1×10^6 atoms[1]. It is believed that the ions are lost in the ion extraction process in the sampling interface of the ICP-MS, as well as to the ion lenses and the quadrupole analyzer. In addition, analyte signals are suppressed when solutions containing highly concentrated matrices are nebulized[2-42], especially for light analyte ions and heavy matrix ions. In general, the sensitivity of ICP-MS is poorer for light analytes (e.g., Li^+) than for heavy ones such as U^+. This mass bias problem complicates internal standardization and general calibration of sensitivity for a variety of elements using standards for only a few.

These matrix interferences are generally attributed largely to space charge effects[17], which probably also contribute to mass bias and low overall ion transmission. The free charge in a particle beam is called space charge since it exists in free space. Space charge forces have been described[43] as mutual electrostatic repulsion among particles of like charge, if particles of the opposite charge are not present in approximately equal concentrations. Therefore, the space charge effect in a neutral plasma is not significant. Olivares and Houk [44] first pointed out that space charge effects may be an important factor in ion extraction in ICP-MS. They and Gillson *et al*[17] postulated that the ion beam behind the skimmer is space charge limited, i.e. it reaches an ion density so high that mutual repulsion defocuses the ions. The space charge problem also accounts for the observed dependence of matrix effects on the atomic weights of the analyte and the matrix elements.

The expansion of the plasma through the ICP-MS interface has been described by two models. Douglas and French[45] proposed that the process is like a neutral gas expansion,

where the maximum beam angle sampled through the skimmer is defined by the diameter of the skimmer orifice and the sampler-skimmer spacing. Another model by Chambers and Hieftje[27-29] states that significant charge separation occurs between the sampler and the skimmer. In this case, the ion entry angle would be much larger than predicted for the neutral beam. Tanner and co-workers[41, 46] have recently reported that comparable sensitivity, less mass bias and matrix effects can be achieved by adding a third aperture behind the skimmer to reduce the total ion current by a factor of about 600.

A spatially-resolved profile of the density of specific ions behind the skimmer could provide direct information about space charge effects. In this study, such information is provided by spatially-resolved ion deposition, in which ions are accelerated and implanted into a solid. Ion deposition is used to introduce impurities into solids in a uniform and reliable way to change the properties of the solid material. It is a widespread surface modification technique in semiconductor technology[47-49]. Thin films of refractory materials have been made using an ICP combined with an extraction device like that used in ICP-MS[50]. Preliminary aspects of the present work have been described previously[51, 52], as have similar experiments by Farnsworth's group[53]. First, we describe the salient aspects of ion extraction to provide the reader with some basic information for evaluation of the results presented later.

2. ION SAMPLING PROCESS

2.1 Gas and Ion Flow Behind the Skimmer

The Ar atom number density in the central channel of an atmospheric pressure ICP is approximately 1.5×10^{18} cm^{-3} at 1 atm and 5000 K. At the usual sampling position, the electron density is about 1.5×10^{15} cm^{-3}, and so is the total ion density. We assume the sampler diameter is 1.14 mm, the skimmer diameter is 0.89 mm, and the sampler-skimmer separation is 7.0 mm, which are typical parameters for an ELAN ICP-MS. Under these conditions, the gas flow rate through the skimmer at 152 K is about 1×10^{19} atoms s^{-1} or 1×10^{16} Ar^+ s^{-1}, which is about 2.6% of the central flow in the ICP[45]. Theoretically, the total ion current through the skimmer should then be about 1.5 mA. However, the measured total ion current at the base of the skimmer[17] is only about 6 μA. This measured ion current corresponds to loss of over 99% of the ions during the extraction process[17, 27-29, 35, 41, 46].

The loss of analyte ions can also be estimated by a similar line of reasoning. For a 1 ppm Y solution with uptake rate of 1 ml/min and aerosol gas flow rate of 1 l min^{-1}, assuming 2% nebulization and transport efficiency (for a typical pneumatic nebulizer) and 100% atomization-ionization efficiency, the Y^+ density in the central channel is 8×10^9 Y^+ ions cm^{-3}[3], which is 5.4 ppm of the total ion density in the ICP. Assuming the ratio (n_{Y+}/n_{Ar+}) remains constant in the flow through the sampler and the skimmer, theoretically there should be 5.2×10^{10} Y^+ ions s^{-1} leaving the skimmer for the 1 ppm Y solution. Taking the sensitivity of an ICP-MS of about 1×10^7 ions s^{-1} ppm^{-1}, the ion transmission efficiency from the skimmer to the detector of an ICP-MS is about 0.02%. Considering the skimmer

passes only 2.6% of the central flow of the ICP, the overall efficiency of the ICP-MS is about 5×10^{-6}. In other words, for every 10^6 analyte ions in the central channel of the ICP, only 5 ions reach the detector of the ICP-MS. This estimate is in good agreement with other studies[1, 54].

It is crucial therefore to understand how the ions are lost in the ion extraction process before the ion transmission efficiency can be increased. Tanner *et al*[46] recently reported a modified three-aperture ICP-MS interface with normal ion optics and quadrupole mass analyzer. The transmission efficiency from the reducer to the detector is about 7%, which includes the ion optics, the mass analyzer and the detector. This 7% value can be viewed as an efficiency factor that reflects the ion transmission through the ion optics in the third chamber and mass analyzer to the detector. Since the plasma gas flow is reduced to the order of the space-charge-limited flow, the transmission through the ion optics and thereafter can be evaluated separately.

The 7% transmission value seen for the three-aperture device is much better than the 0.02% value calculated above for a conventional two-aperture ICP-MS device. This comparison shows that many ions are lost between the skimmer tip and the ion optics, or inside the ion optics in the second vacuum chamber. As has been pointed out by Tanner *et al*[41, 46], the plasma flow through the sampler and the skimmer is still neutral, and the flux (atoms s^{-1} cm^{-2}) through the skimmer decreases as the square of the distance downstream from the sampler tip. Therefore, the gas flux f_2 at position Z_2 downstream from the sampler is:

$$f_2 = f_1 \frac{Z_1^2}{Z_2^2} \quad (1)$$

where f_1 is the gas flux at position Z_1. Taking the flow rate at the tip of the skimmer to be 1×10^{19} s^{-1}, the corresponding ion current of 1500 μA, the first ion lens position at 50 mm downstream from the skimmer tip (57 mm downstream of the sampler), the flux at the entrance of the ion lens becomes only 1.5% of that at the skimmer tip. Therefore, the loss of ions behind the skimmer is first of all due to the rarefaction of the beam as it travels farther from the skimmer tip.

It has been shown that the ion signals increase when the entrance to the ion optics is positioned closer to the skimmer[55]. For example, the shallow, sharply pointed skimmers in recent use in several devices can provide substantial improvements in ion signals by allowing the first lens to be inserted close to the skimmer tip[56]. It is therefore crucial that the distance between the skimmer tip and the ion optics be minimized in order to increase the ion transmission efficiency for the stage between the skimmer and the ion optics.

After the ions pass through the skimmer, there are two factors that can induce the charge separation and affect the ion transmission. Langmuir probe measurements of the electron temperature and electron density show that with no voltages applied to the ion optics, the Debye length λ_D can be as large as 2 mm[57] when the beam reaches 40 mm behind the skimmer tip. This value of λ_D is significant compared to the overall size of the beam and the dimensions of the lens, so the electrons tend to diffuse from the beam, and a net positive charge density remains along the centerline of the beam. Thus, significant charge

separation can occur in the beam, even when the ion lenses are kept at ground potential. Tanner *et al*[41, 46] recently reported that λ_D at the skimmer was 3×10^{-3} mm, while at the tip of the reducer, which was positioned at about 1/3 of the skimmer length, λ_D was 6×10^{-3}mm. This is also an indication of the rapid increase in Debye length as ions leave the skimmer tip. Usually, the voltage applied to the first ion lens is negative, so this lens also repels electrons and attracts ions. Thus, the lens directly separates different charges. Once the neutrality of the beam is destroyed, the flow of ions is governed by the space-charge-limited flow.

2.2 Space-Charge-Limited Flow

The positive charge carried by the particles in a positive ion beam causes the space charge force in the beam. There are three important effects caused by the space charge force in such an ion beam[58, 59]: a) depression of the potential in the beam; b) beam spreading; and c) limitation to the maximum current.

The significance of the space charge in a particle beam can be described quantitatively using the perveance, P, which is defined as follows:

$$P = \frac{I}{V^{3/2}} \tag{2}$$

where I is the total current in amps and V is the accelerating potential in volts. Perveance P is characteristic of an ion extraction system and as will be seen in Eq. 6, it depends only on the geometry of the extractor (D/L) and the type of the particle (m_{ion})[60]. For a beam of singly charged positive ions with negligible space charge effect, the quantity P must satisfy the relation[59]:

$$P < 10^{-8} \left\{ \frac{m_{ion}}{m_e} \right\}^{-\frac{1}{2}} \quad (3)$$

For Ar ions, the maximum perveance without significant space charge effect is 3.7×10^{-11}. In the second stage of an ICP-MS device, an ion beam with total current of 6 μA and -10 V potential gives a P value of 1.9×10^{-7}, which exceeds the maximum perveance by a factor of over 5000.

The space-charge-limited maximum electron current that can be focused through a tube with diameter D and length L is:

$$I_{e,\,max}(A) = 38.6\times10^{-6}\, V^{\frac{3}{2}} \left\{ \frac{D}{L} \right\}^2 \quad (4)$$

where V is the accelerating voltage, D the tube diameter and L the tube length. The maximum ion current is related to the maximum electron current in the following way[60]:

$$\frac{I_{ion}}{I_e} = \left\{ \frac{m_e}{m_{ion}} \right\}^{\frac{1}{2}} = 0.0234 \left\{ \frac{z}{m_{ion}} \right\}^{\frac{1}{2}} \quad (5)$$

where z = charge on ion (+1, +2,..., or -1,...). Therefore the space-charge-limited current flow through a tube is:

$$I_{ion,\,max}(A) = 9.04\times10^{-7} \left\{ \frac{z}{m_{ion}} \right\}^{\frac{1}{2}} V^{\frac{3}{2}} \left\{ \frac{D}{L} \right\}^2 \quad (6)$$

If the ion beam is 10 mm in diameter (measured beam width at the target) and 27 mm long (i. e., the overall length of the ion lenses), the D/L ratio is 0.37. Using an average ion lens

potential of -50 V, Eq. 6 gives the Y ion current of about 4.6 μA at the target, which agrees well with the measured ion current. Thus, the ion beam extracted through the lenses is space charge limited.

There is an error in Gillson's paper[17] in Equation 6 where $(m/z)^{1/2}$ was used instead of $(z/m)^{1/2}$. The error has been quoted in some other papers, including our own[61]. For an ion energy of 3 eV for Ar, and the D/L ratio of 0.5 for the skimmer, the calculated Ar^+ ion current should have been 0.18 μA, rather than the 6 μA measured at the base of the skimmer.

In summary, beam spreading due to the increase in Debye radius, preferential loss of electrons and the subsequent buildup of space charge under the influence of the ion optics causes the loss of ions in this stage. The remainder of this paper describes experimental efforts to measure some of these effects.

3. EXPERIMENTAL SECTION

3.1 Instrumentation

The ion deposition experiment was performed using a commercial ICP RF generator (Model HFS 3000D, Plasma-Therm, Inc, now RF Plasma Products, Kresson, NJ). The ICP torch was turned to the horizontal orientation usual in ICP-MS. The load coil was grounded at the turn farthest downstream, as shown in Figure 2X of ref. 62. The elements to be deposited were introduced into the ICP by a concentric nebulizer (Meinhard TR30-C3) with a Scott type spray chamber[63] and desolvation system[64]. The plasma operating conditions are listed in Table 1. The power, aerosol gas flow rate, and sampling position approximate

those used for analysis if this device were configured as a mass spectrometer. The skimmer orifice was enlarged to 1.59 mm diam. to increase the ion transmission[55].

The vacuum chamber, including the sampler and skimmer interface, has been described[65] and is illustrated in Figure 1. The chamber is pumped by a diffusion pump with a cryotrap (Models VHS-6 and 362-6, Varian Vacuum Products, Lexington, MA). The interface is pumped by a mechanical pump (Model 1397 DUO-SEAL, W. M. Welch Manufacturing Company, Chicago, IL).

3.2 Targets for Ion Deposition

A variety of target materials were tested for ion deposition. Compared to metal electrodes, high density graphite ones were inexpensive, available in sufficient purity, and most importantly, insoluble in aqueous HNO_3. The diameter of the electrodes was also a consideration. Electrodes with larger diameters were more readily available and had larger cross sections for deposition but provided poorer spatial resolution for a small ion beam. We found that 1.59 mm (1/16 in.) diameter electrodes gave adequate spatial resolution with sufficient cross section. The flat top graphite electrodes (Ultra Carbon Corp., Bay City, MI) used were of high density SPK grade and high "F" purity. They were mounted horizontally on a stainless steel clamp (Fig. 1), which was water cooled and extended through an electrical feedthrough to a high voltage power supply. These graphite electrodes were packed in an array immediately next to each other so that little ion signal was lost to the gaps between the electrodes. Between the graphite electrode and the ion optics there was a stainless steel grid (304 stainless steel, mesh 24, 67% transparent) to shield the ions inside the lens from the high voltage on the targets. The grid was connected to the last ion lens to

provide a uniform electrical potential for the exiting ions.

Yttrium ions were also deposited on a Ni grid as an alternative target. The grid was a piece of pure Ni wire cloth (Newark Wire Cloth, Newark, NJ), with diameter of 25.4 mm, 33.6% transparency and grid size of 0.127 mm. The deposition process was the same as for the graphite target. The deposits were then analyzed with a scanning electron microscope (Model JSM-840A, JEOL, Japan) and an energy dispersive X-ray analyzer (Model Delta V, Kevex X-ray Inc., Scott Valley, CA). These results are also discussed in the following section.

3.3 Procedure

The sampling position and aerosol gas flow rate were chosen so that the sampler was ~1 mm downstream from the initial radiation zone (IRZ)[66] when a concentrated yttrium solution was introduced into the plasma. This position mimicked the sampling position that usually provides maximum ion signal in ICP-MS. The ions passed through the sampler, skimmer, the ion lenses and the grid and were then deposited onto the graphite electrodes at a kinetic energy of ~1000 eV. The electrodes were exposed to the ion beam for 60 minutes in each run. Then the vacuum chamber was vented and opened and the targets were removed from the back. The ICP was kept on and in position up against the sampler so that the plasma conditions and the sampling position remained the same. A new array of targets was inserted and the chamber was evacuated again in preparation for a new deposition experiment. Keeping the plasma on while the targets were changed improved reproducibility and reliability and allowed comparison of results between successive deposition experiments.

Meanwhile, each exposed graphite electrode was removed and placed overnight in a

separate polyethylene bottle containing 5 ml of aqueous 1% HNO_3. Only the end containing the deposit was exposed to the acid. This procedure yielded a set of solutions of the deposited metal at various concentrations related to the total amount deposited on each target.

The deposited metals in the resulting solutions were measured with a different ICP-MS (ELAN 250, Perkin-Elmer SCIEX, Thornhill, ON, Canada) with Fassel-type torch [63], upgraded ion optics, electronics and ELAN 5000 software. The nebulizer gas flow rate was regulated by a mass flow controller (Model 8200, Matheson Scientific, East Rutherford, NJ). The sample was introduced using an ultrasonic nebulizer (Model U-5000, CETAC Technologies, Omaha, NE). The deposited ion signals were then plotted against the radial distance from the central axis through the sampler and skimmer. Each point represents a separate measurement on an individual electrode. The total ion current collected on the target was measured with a picoammeter (Model 485, Keithley Instruments, Cleveland, OH). Matrix effects from co-deposited Cs in the solutions were not severe because the Cs count rates on the ELAN ICP-MS device were only $\sim 10^4$ counts s^{-1} from the solutions produced when 1000 ppm Cs was used in the deposition step. Several of the electrodes were treated a second time with aqueous 1%HNO_3. No additional Sc or Y was present in these second batches of solution, so the recovery of the deposited metal was complete after one dissolution treatment.

3.4 Reagents

The HNO_3 was Ultrex II Ultrapure acid from J. T. Baker (Phillipsburg, NJ). The $CsNO_3$ was a Specpure ICP standard from Alfa Johnson Matthey (Columbus, OH). Other reagents used were from PLASMACHEM Associates, Inc (Armingdale, NJ). The samples

were diluted with high purity water (18 MΩ-cm resistivity) from a 5-stage Milli-Q Plus Water System (Millipore Corporation, Bedford, MA). Scandium and yttrium were chosen to avoid contamination, since they are not common impurity elements, and they were absent originally in the graphite electrodes.

4. RESULTS AND DISCUSSION

4.1 Ion Trajectory Simulations

Ion trajectories were simulated with SIMION PC 4.02 (Idaho National Engineering Laboratory, Idaho Falls, ID). The simulation gives the ion trajectories inside the vacuum chamber under the influence of an electrostatic field provided by the ion optics without considering mutual repulsions between the ions. Trajectory simulations without such space charge effects still provide some guidance for the optimal ion lens settings to focus the ion beam. The ICP-MS interface and ion lenses used in the simulation closely resemble the corresponding components used for the experimental studies.

Ion trajectories with the optimal ion lens potential settings are shown in Figures 2 - 6. Voltages corresponding to three different lens settings are given in Table 2. The ion initial kinetic energy in these simulations was set at 4.6 eV, which simulated the measured kinetic energy of Y^+ for a similar plasma and interface[55]. Scandium ion has a slightly lower kinetic energy (4.0 eV) and slightly different ion trajectories. The divergence angle was stepped between 0° and 4°, which was based on the sampling orifice-skimmer orifice separation and the skimmer orifice diameter.

Figure 2 shows the ion trajectories when all the ion lenses and the grid were set at

ground potential. In the absence of space charge, the ions should travel linearly through such a field-free region, just as expected from a free jet expansion. In this case, the ions should reach the target electrodes in a beam ~15 mm wide. Figure 3 is a side view version of the simulation in Figure 2. If the beam leaving the lens is broad, some of the ions may be deposited on the sides of the graphite targets, rather than onto the ends of the targets. This phenomenon could affect the spatial resolution of the deposition experiment, since the ions measured on any single target could come from a relatively wide area of the beam. Therefore, the spatial profiles described subsequently should be considered to be only laterally resolved, not radially resolved.

The ion trajectories for three different sets of lens voltages were also simulated. The voltages used are described by Setting 1, 2, or 3 in Table 2 and are selected to resemble voltages that allow reasonable ion transmission through the lens, based on our experience with similar ICP-MS instruments. We should point out that adjusting the lens voltages to maximize ion transmission is difficult in this experiment, because there is no mass spectrometer to monitor the ion beam in real time. Thus, we did not optimize the lens voltages to actually maximize ion deposition on the targets, as such a procedure would require too many separate deposition experiments. We did adjust plasma conditions (i.e., aerosol gas flow rate and sampling position) such that the tip of the initial radiation zone for yttrium was ~ 1 mm upstream from the sampler, which generally yields maximum ion signal in most ICP-MS devices.

Figure 4 shows the simulated trajectories when the ion lenses were set at -110 V, -40 V and -50 V. The ion beam should now be focused tightly and should strike only the center

electrode. Figure 5 shows the simulation when the ion lenses were set at 2 V, -50 V and -60 V. The ion beam with this lens setting has a different pattern from the one in Figure 4. The ion beam is not tightly focused in the beginning, resulting in an expansion-contraction trajectory. The beam then reaches the target with a small cross section. Figure 6 shows the ion trajectory with a photon stop in the center of the second ion lens. The potentials on the ion lenses were chosen to maximize transmission of ions around the photon stop while still focussing the beam to a central point at the target array.

4.2 Ion Deposition Results

4.2.1 Ion Intensity and Ion Beam Profile. In this study Li, Sc, Y, and Cs were deposited separately on the graphite electrodes. Analysis of the targets shows that the deposition efficiency varies among different ions. Only trace amounts of lithium are found on the targets. The transmission and sensitivity for Li^+ are poor in most ICP-MS devices[67]. Cesium is deposited at higher concentrations than Li but with much less efficiency and a much broader spatial distribution than is the case for Sc or Y. Perhaps the target is hot enough to vaporize Cs even with water cooling. Scandium and yttrium are therefore used as analytes in subsequent experiments.

First, we investigated the possibility of depositing unvaporized solid particles from the plasma. For a 60 minute deposition of 50 ppm Sc solution with the targets grounded, the deposited Sc is negligible. Therefore, neutral solid particles do not contribute to the deposition process. The bulk of the deposited scandium probably comes from atomic Sc^+ ions. However, positively charged solid particulates that are not fully vaporized by the plasma could also be deposited under the conditions used. These charged particulates cannot

be distinguish easily from atomic Sc^+ by changing the target voltage. The desolvation process should have removed wet droplets[68].

First, we describe some general features of the deposition results. First, as can be seen in Figure 7, when the ion lenses are grounded the ion beam profile is similar to that predicted by SIMION (Figure 2). If the ions travel linearly from the center point at the sampler tip through the skimmer until they hit the grid, the beam width should be 15 mm at the targets, while the measured beam widths are 10 to 13 mm. The smaller measured values for beam width could simply mean there are too few ions in the outer fringes of the beam to be detected readily. Secondly, the ion beam is only moderately narrower when the potentials on the ion lenses are applied, and the different lens settings do not change the beam width appreciably. It is unclear whether the ion beam never reaches the focal point or the ion beam starts diverging from the focal point before reaching the targets. Another possibility is that a shock wave forms when the neutral beam hits the targets[35, 41, 46]. Such a shock wave would spread the ions among various targets. The targets, however, are some 90 mm behind the skimmer tip, and any shock wave so far from the skimmer would be weak and diffuse [69].

The effects of ion lens potentials on the transmission efficiency of Sc^+ ions are also shown in Figure 7. When nonzero potentials are applied to the ion lenses for either ion lens setting 1 or 2, the ion beam intensity is greater than when the lenses are grounded by a factor of two. Obviously, the electric field on the ion lenses extracts the Sc^+ ions and enhances the Sc^+ ion transmission through the ion optics. This observation indicates that the ion lens does help ion transmission, in contrast to the results described by Ross *et al.*[31].

Note that ions are transmitted with the first lens either strongly negative (-110 V, Setting 1) or slightly positive (+2 V, Setting 2), with the other lens voltages adjusted accordingly. This duality of possible voltages for the first lens has a close commonality with ICP-MS practice. Setting 1 (i.e., the first lens is negative) is analogous to the lens settings traditionally used with quadrupole ICP-MS devices, while Setting 2 is similar to that used in the new ELAN 6000 instrument from Perkin-Elmer SCIEX [70] and also in our device with an offset ion lens [37].

4.2.2 **Recovery of Ions.** As calculated earlier, the theoretical ion flow through the skimmer of a Sciex ICP-MS is 5.2×10^{10} Y^+ ions s^{-1} per ppm Y in the ICP. Correcting this number for our larger skimmer orifice and bigger sampler-skimmer spacing, the ion flow should be 9.1×10^{10} Y^+ ions s^{-1} per ppm Y. The gas flow is estimated to be 4.5% of the central flow of the plasma.

Therefore, 2.4 μg of Y should be collected on all the electrodes for a 60 minute deposition. Actually, a total of only 0.3 to 0.4 μg of Y is present in the solutions (see Figure 13), corresponding to an Y^+ ion current of 0.1-0.13 μA and a recovery of about 14% of the Y^+ leaving the skimmer. The total current measured is about 4 μA, so the Y^+ ion current is 2.5% of the total current passing the ion optics, which is much bigger than the Y^+/Ar^+ ion ratio in the plasma. This enrichment of analyte ions relative to Ar^+ and other background ions has been noted previously[3] and may be caused by the Auger neutralization process described by Koppenaal *et al*[71]. Ions like Ar^+, whose neutral analogs have high ionization energies, can be neutralized preferentially as they pass near a metal surface. This process could occur inside either the sampler or skimmer, or both. Alternatively, Tanner suggests

that Ar^+ ions can be lost preferentially by resonant charge transfer reactions with neutral Ar atoms behind the skimmer or inside the ion lens. The resulting product Ar^+ ions have different kinetic energies than the original Ar^+ and are scattered out of the beam, are not transmitted efficiently by the lens, and/or simply stay within a potential well inside the lens [69].

4.2.3 Effect of Cs Matrix Figure 8 shows that addition of Cs matrix suppresses the Sc ion signal deposited onto the graphite electrodes with ion lens setting 1 where the potentials applied to the lenses are such that the ion beam is focused tightly on the axis. The beam width is about the same when the two peaks are normalized. It is interesting to note that this matrix suppression effect can be alleviated with a different ion lens setting. Figure 9 shows that if a slight positive potential is applied to the first lens (setting 2), the effect of Cs matrix on deposition of Sc^+ is minimal. This method of reducing matrix effects was also observed by other experimental studies in this laboratory[37] and by Denoyer et al. [70].

These results suggest that if the ions are brought into the ion optics as a relatively broad beam, the reduced ion flux with less space charge may alleviate matrix effects. For Sc samples with a Cs matrix added, the ion lenses enhance the ion transmission compared to that obtained for the grounded ion lenses. Figure 10 shows the effect of ion lens potential when the matrix is present. Ion lens setting 2 yields better ion beam intensity than setting 1 or simply grounding the lenses.

4.2.4 Effect of Photon Stop A photon stop (or a stop lens) is normally used to block the photons emitted by the ICP. Such a photon stop is normally charged as a part

of the ion lens setting to facilitate the ion flow. Because the photon stop is in the center of the ion path, it is expected to play a critical role on the ion transmission through the ion optics.

Figure 11 shows that when the photon stop is in place, applying the voltages corresponding to lens setting 3 (see Table 2) enhances the ion transmission by about 30% compared to the transmission when all the lenses were grounded. When a Cs matrix is added (Fig. 12), applying a nonzero voltage to the photon stop and lens enhances the transmission of Sc^+ only moderately. This observation suggests that matrix effects are more severe when the photon stop is in place, and the potential on the ion lenses including the photon stop may have to be changed accordingly to alleviate the matrix effects[72].

Apparently, the photon stop has three major effects on the ion extraction process. First, it blocks the central flow of the ions. Only the off-axis ions can pass the ion lens, which can be seen from the dip in the center of the ion profile in Figures 11 and 12. Similar observations were reported in the ion trajectory simulations of Vaughan and Horlick[73]. Secondly, the photon stop reduces the overall ion intensity, in this experiment, by a few hundred fold. Thirdly, the photon stop plays an important and complex role in the space charge effects and matrix interferences in ICP-MS.

4.2.5 Deposition of Yttrium Oddly, the deposition behavior of Y differed in several ways from that of Sc. Ion lens settings 1 and 2 reduce the transmission of Y^+ slightly (see Figure 13); setting 1 transmits more ions than setting 2. Nevertheless, ion lens settings 1 and 2 still yield slightly higher ion signals than do the grounded lenses for a solution of Y with Cs matrix (Figure 14). Deposition of Y with Cs as a matrix element produces some

strange results. The addition of Cs increases the amount of Y deposited in the targets compared to that from the Y solution only (Figures 15 and 16). The blank Cs standard solution was analyzed and contained very little Y, not nearly enough to account for the obtained increase in Y signal. We also tried Cs standards from three different vendors and the results were about the same. This enhancement was also confirmed by repeated experiments and by depositing Y on a Ni grid. Scanning electron microscopy shows a broader image of deposited ions when Cs is added to the solution compared to the deposition of Y solution alone, and energy dispersive X-ray spectrometry shows that the Y concentration on the Ni grid increases as the Cs matrix is added. Perhaps there is some codeposition process with Cs that enhances the deposition efficiency for Y.

5. CONCLUSION

Ion deposition provides some experimental information about the ion beam profile in the second stage of an ICP-MS device. The lens focuses the beam, but not nearly as tightly as SIMION would predict. Unexpectedly, the suppression of Sc^+ corresponds more to loss of total Sc^+ than to broadening of the Sc^+ beam, in general agreement with the fluorescence measurements of matrix effects on Sr^+ by Hobbs and Olesik[74]. Applying appropriate potentials to the ion lens can alleviate the matrix effect. The same lens settings that enhance Sc^+ signal are not as effective in enhancing the Y^+ signal, although they do alleviate the matrix effect to a smaller extent. The photon stop in the ICP-MS significantly reduces the ion signal intensity and changes the shape of the spatial distribution of ions from conical to bimodal.

ACKNOWLEDGEMENTS

The Perkin-Elmer Graduate Research Fellowship awarded to Xiaoshan Chen is gratefully acknowledged. Ames Laboratory is operated for the U.S. Department of Energy by Iowa State University under Contract No. W-7405-ENG-82. This work was supported by the Office of Basic Energy Sciences, Division of Chemical Sciences.

REFERENCES

[1] H. Falk, *J. Anal. At. Spectrom.* **7**, 255 (1992).

[2] R. S. Houk, *Anal. Chem.* **58**, 97 (1986).

[3] J. A. Olivares and R. S. Houk, *Anal. Chem.* **58**, 20 (1986).

[4] D. W. Boomer and M. J. Powell, *Canad. J. Spectrosc.* **31**, 104 (1986).

[5] C. J. Pickford and R. M. Brown, *Spectrochim. Acta, Part B* **41**, 183 (1986).

[6] D. Beauchemin, J. W. McLaren and S. S. Berman, *Spectrochim. Acta, Part B* **42**, 467 (1987).

[7] D. C. Gregoire, *Appl. Spectrosc.* **41**, 897 (1987).

[8] D. C. Gregoire, *Spectrochim. Acta, Part B* **42**, 895 (1987).

[9] H. Kawaguchi, T. Tanaka, T. Nakamura, M. Morishita and A. Mizuike, *Anal. Sci.* **3**, 305 (1987).

[10] S. H. Tan and G. Horlick, *J. Anal. At. Spectrom.* **2**, 745 (1987).

[11] J. J. Thompson and R. S. Houk, *Appl. Spectrosc.* **41**, 801 (1987).

[12] B. T. G. Ting and M. Janghorbani, *Spectrochim. Acta, Part B* **42**, 21 (1987).

[13] D. A. Wilson, G. H. Vickers and G. M. Hieftje, *J. Anal. At. Spectrom.* **2**, 365 (1987).

[14] D. Beauchemin, J. W. McLaren and S. S. Berman, *J. Anal. At. Spectrom.* **3**, 775 (1988).

[15] J. R. Dean, L. Ebdon, H. M. Crews and R. C. Massey, *J. Anal. At. Spectrom.* **3**, 349 (1988).

[16] D. J. Douglas and L. Kerr, *J. Anal. At. Spectrom.* **3**, 749 (1988).

[17] G. R. Gillson, D. J. Douglas, J. E. Fulford, K. W. Halligan and S. D. Tanner, *Anal. Chem.* **60**, 1472 (1988).

[18] R. C. Hutton and A. N. Eaton, *J. Anal. At. Spectrom.* **3**, 547 (1988).

[19] J. W. McLaren, D. Beauchemin and S. S. Berman, *Spectrochim. Acta, Part B* **43**, 413 (1988).

[20] R. D. Satzger, *Anal. Chem.* **60**, 2500 (1988).

[21] J. G. Williams and A. L. Gray, *Anal. Proc.* **25**, 385 (1988).

[22] J. S. Crain, R. S. Houk and F. G. Smith, *Spectrochim. Acta, Part B* **44**, 1355 (1989).

[23] W. Doherty, *Spectrochim. Acta, Part B* **44**, 263 (1989).

[24] Y. S. Kim, H. Kawaguchi, T. Tanaka and A. Mizuiki, *Spectrochim. Acta, Part B* **45**, 333 (1990).

[25] J. R. Pretty, E. H. Evans, E. A. Blubaugh, W. L. Shen and J. A. Caruso, *J. Anal. At. Spectrom.* **5**, 437 (1990).

[26] J. Wang, W. L. Shen, B. S. Sheppard, E. H. Evans, J. A. Caruso and F. L. Fricke, *J. Anal. At. Spectrom.* **5**, 445 (1990).

[27] D. M. Chambers and G. M. Hieftje, *Spectrochim. Acta, Part B* **46**, 761 (1991).

[28] D. M. Chambers, J. Poehlman, P. Yang and G. M. Hieftje, *Spectrochim. Acta, Part B* **46**, 741 (1991).

[29] D. M. Chambers, B. S. Ross and G. M. Hieftje, *Spectrochim. Acta, Part B* **46**, 785 (1991).

[30] Y. Igarashi, H. Kawamura, K. Shiraishi and Y. Takaku, *J. Anal. At. Spectrom.* **4**, 571 (1991).

[31] B. S. Ross and G. M. Hieftje, *Spectrochim. Acta, Part B* **46**, 1263 (1991).

[32] D. M. Templeton and M. Vaughan, in *Applications of Plasma Source Mass Spectrometry*, G. Holland and A. N. Eaton, Eds., The Royal Society of Chemistry, Cambridge, p. 101 (1991).

[33] P. J. Turner, in *Applications of Plasma Source Mass Spectrometry*, G. Holland and A. N. Eaton, Eds., The Royal Society of Chemistry, Cambridge, p. 70 (1991).

[34] E. H. Evans and J. A. Caruso, *Spectrochim. Acta, Part B* **47B**, 1001 (1992).

[35] S. D. Tanner, *Spectrochim. Acta, Part B* **47**, 809 (1992).

[36] F. Vanhaecke, H. Vanhoe, R. Dams and C. Vandecasteele, *Talanta* **39**, 737 (1992).

[37] K. Hu and R. S. Houk, *J. Am. Soc. Mass Spectrom.* **4**, 28 (1993).

[38] P. Richner, *J. Anal. At. Spectrom.* **8**, 927 (1993).

[39] F. Vanhaecke, R. Dams and C. Vandecasteele, *J. Anal. At. Spectrom.* **8**, 433 (1993).

[40] M. J. Bloxham, S. J. Hill and P. J. Worsfold, *J. Anal. At. Spectrom.* **9**, 935 (1994).

[41] S. D. Tanner, L. M. Cousins and D. J. Douglas, *Appl. Spectrosc.* **48**, 1367 (1994).

[42] G. Xiao and D. Beauchemin, *J. Anal. At. Spectrom.* **9**, 509 (1994).

[43] E. W. McDaniel, *Collision Phenomena in Ionized Gases*, John Wiley & Sons, New York (1964).

[44] J. A. Olivares and R. S. Houk, *Anal. Chem.* **57**, 2674 (1985).

[45] D. J. Douglas and J. B. French, *J. Anal. At. Spectrom.* **3**, 743 (1988).

[46] S. D. Tanner, D. J. Douglas and J. B. French, *Appl. Spectrosc.* **48**, 1373 (1994).

[47] J. F. Ziegler, *Ion Implantation, Science and Technology*, Academic Press, New York (1988).

[48] J. S. Williams and J. M. Poate, *Ion Implantation and Beam Processing*, Academic Press, Australia (1984).

[49] H. Ryssel and I. Ruge, *Ion Implantation*, John Wiley & Sons (1986).

[50] B. D. Merkle, R. N. Kniseley and F. A. Schmidt, *J. Appl. Phys.* **62**, 1017 (1987).

[51] X. Chen, R. S. Houk and J. Hoekstra, *42nd Conference on Mass Spectrometry and Allied Topics*, American Society for Mass Spectrometry, Chicago, Il, **Paper No. 271**, (May 1994).

[52] X. Chen and R. S. Houk, *Pittsburgh Conference on Anal. Chem. and Appl. Spectrosc.*, New Orleans, LA, **Paper No. 768**, (March 1995).

[53] P. B. Farnsworth, Y. Chen and M. Wu, XXI *FACSS Conference, St. Louis, MO*, **Paper No. 773**, (September 1994).

[54] R. S. Houk, S. C. K. Shum and D. R. Wiederin, *Anal. Chim. Acta* **250**, 61 (1991).

[55] K. Hu, P. S. Clemons and R. S. Houk, *J. Am. Soc. Mass Spectrom.* **4**, 16 (1993).

[56] R. C. Hutton and D. Gregson, *private communications* (1992).

[57] H. Niu and R. S. Houk, *Spectrochim. Acta, Part B* **49**, 1283 (1994).

[58] G. A. Nagy and M. Szilagyi, *Introduction to the Theory of Space-Charge Optics*, Halsted Press, New York, Macmillan and London (1974).

[59] M. Szilagyi, *Electron and Ion Optics*, p. 313, Plenum Press, New York (1988).

[60] S. Humphries, *Charged Particle Beams*, p. 834, John Wiley & Sons, New York (1990).

[61] K. Hu and R. S. Houk, *J. Am. Soc. Mass Spectrom.* **4**, 733 (1993).

[62] A. L. Gray, R. S. Houk and J. G. Williams, *J. Anal. At. Spectrom.* **2**, 13 (1987).

[63] R. H. Scott, V. A. Fassel, R. N. Kniseley and D. E. Nixon, *Anal. Chem.* **46**, 76 (1974).

[64] V. A. Fassel and B. R. Bear, *Spectrochim. Acta, Part B* **41**, 1089 (1986).

[65] H. S. Niu, K. Hu and R. S. Houk, *Spectrochim. Acta, Part B* **46**, 805 (1991).

[66] S. R. Koirtyohann, J. S. Jones and D. A. Yates, *Anal. Chem.* **52**, 1965 (1980).

[67] K. E. Jarvis, A. L. Gray and R. S. Houk, *Handbook of ICP-MS*, Blackie, London, p. 36 (1992).

[68] R. K. Winge, X. Chen and R. S. Houk, *J. Anal. At. Spectrom.* **10**, in preparation (1995).

[69] S. D. Tanner, personal communication (1995).

[70] E. R. Denoyer, D. Jacques, E. Debrah and S. D. Tanner, *Atomic Spectrosc.* **16**, 1 (1995).

[71] D. W. Koppenaal, C. J. Barinaga and M. R. Smith, *J. Anal. At. Spectrom.* **9**, 1053 (1994).

[72] B. S. Sheppard, W. L. Shen and J. A. Caruso, *J. Am. Soc. Mass Spectrom.* **2**, 355 (1991).

[73] M. A. Vaughan and G. Horlick, *Spectrochim. Acta, Part B* **45**, 1301 (1990).

[74] S. E. Hobbs and J. W. Olesik, *Appl. Spectrosc.* **45**, 1395 (1991).

Table 1. Ion deposition conditions

Plasma gas flow rate	14 L/min
Nebulizer gas flow rate	1.05 L/min
Auxiliary gas flow rate	0.4 L/min
RF Power	1000 W
Nebulizer type	Meinhard TR30-C3
Sampler orifice diameter	1.0 mm
Skimmer orifice diameter	1.59 mm
Sampling position	7 mm from load coil, on center
Sampler-skimmer separation	9 mm
Skimmer tip-target separation	94 mm
Electrode material	"F" purity graphite, SPK grade, high density
Electrode diameter	1.59 mm (1/16 inch)
Diameter of ion lens	22.6 mm, stainless steel
Graphite target potential	-1000 V
Ion deposition time	60 min.
Target-grid separation	10 mm
Diffusion pump speed	2,400 L/s air
First stage pressure	2 torr
Second stage pressure	1.0×10^{-4} torr
Shielding screen	Stainless steel 304, mesh 24, 67% transparent

Table 2. Voltages corresponding to different ion lens settings (in volts). Letter (a)-(c) denote the individual lenses, as shown in Fig. 1.

Settings	First Lens (a)	Second Lens (b)	Photon Stop (c)	Plate Lens (d)
All grounded	0	0	-	0
Setting 1	-110	-40	-	-50
Setting 2	2	-50	-	-60
Setting 3 (With photon stop)	2	7	0	-15

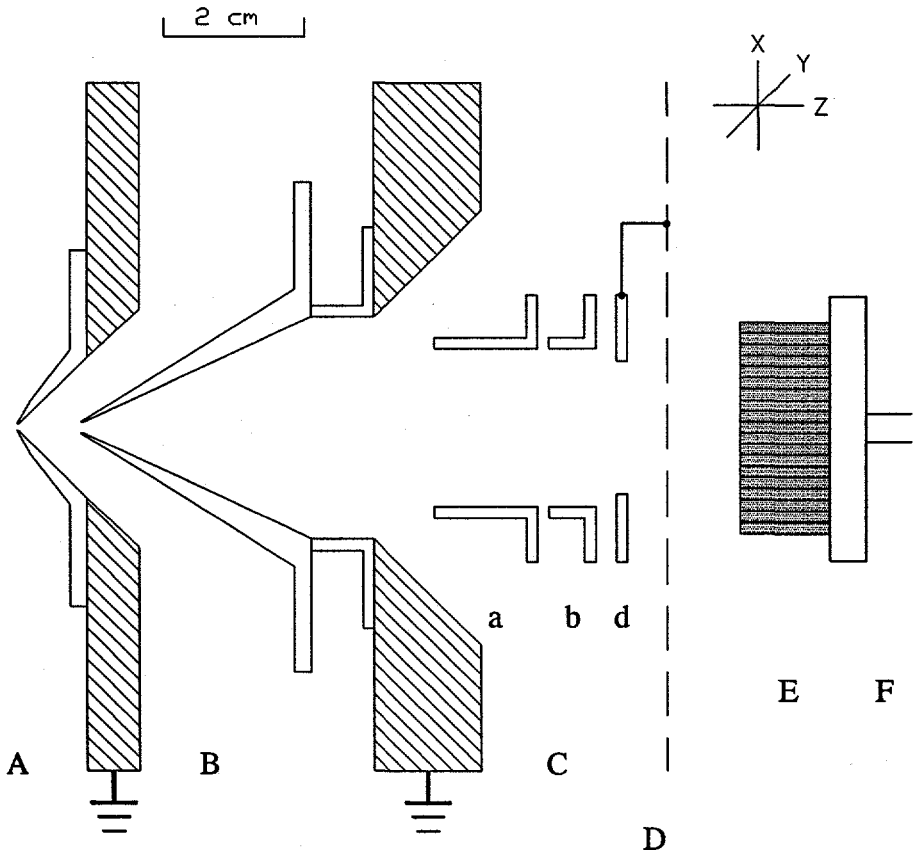

Figure 1. Top view of deposition apparatus. The targets were oriented horizontally. A: sampler. B: skimmer. C: ion optics, including the following elements: a: first cylindrical ion lens, b: second cylindrical ion lens, c: photon stop (not shown here, see Figure 6), d: plate ion lens. D: grid. E: graphite targets. F: water cooled mounting clamp and stand off, potential of -1000 V was provided by an electric feedthrough connected to a high voltage power supply.

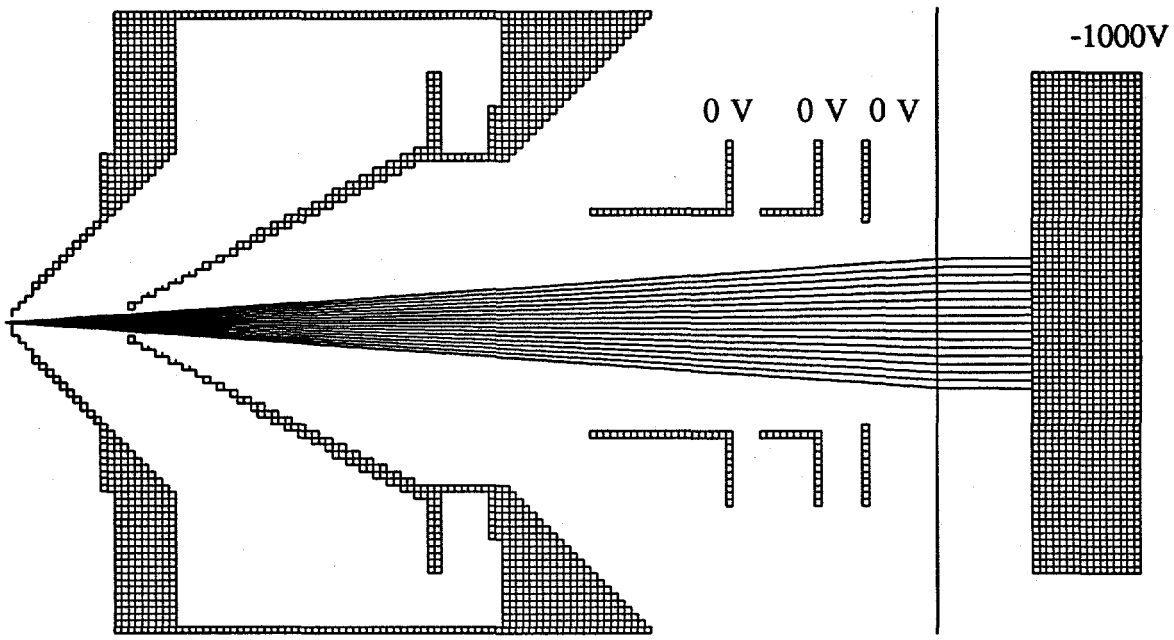

Figure 2. Top view of the SIMION ion trajectory simulation with all the ion lenses set at ground potential. This is the X-Z plane shown in Figure 1. The grids at the right represent the deposition targets. Each grid is 0.94 mm wide in this and Figs. 3-6.

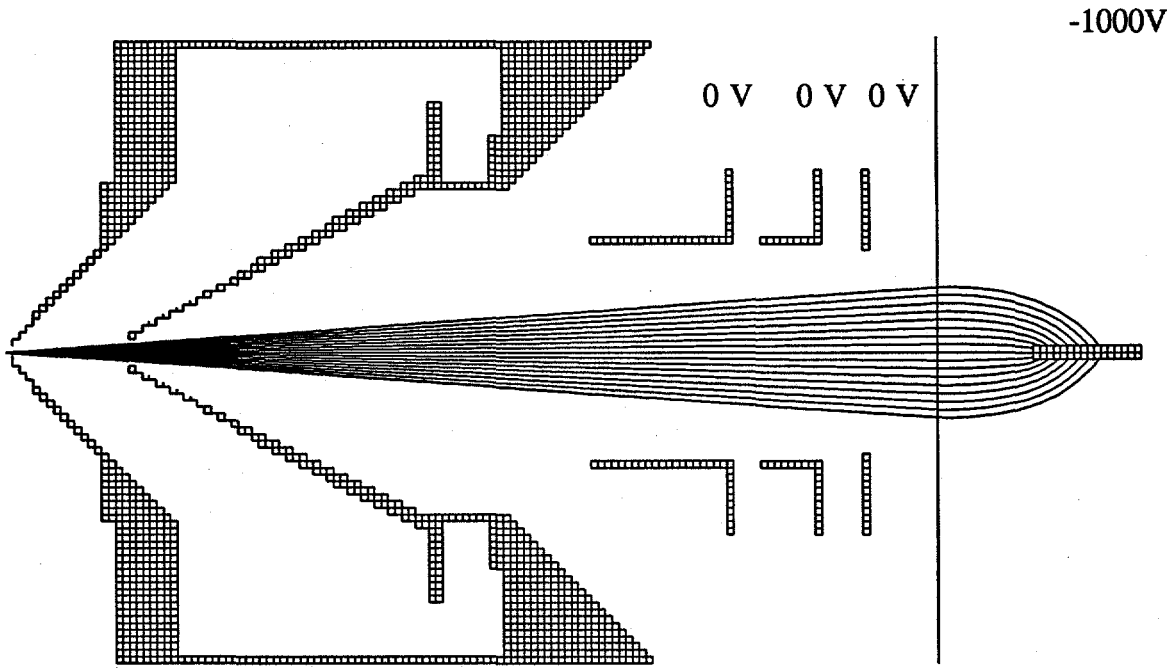

Figure 3. SIMION ion trajectory simulation with all the ion lenses set at ground potential. This is a side view of Figure 2, i.e., the Y-Z plane from Figure 1. The two grids at the right represent the thickness of one of the target electrodes.

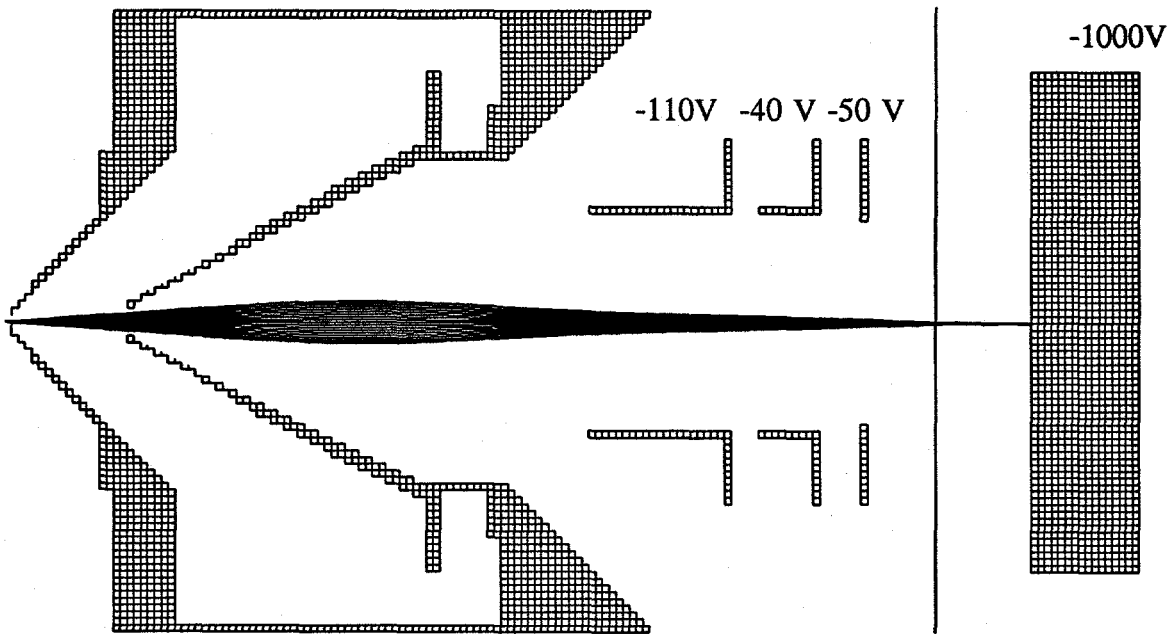

Figure 4. SIMION ion trajectories for ion lens setting 1.

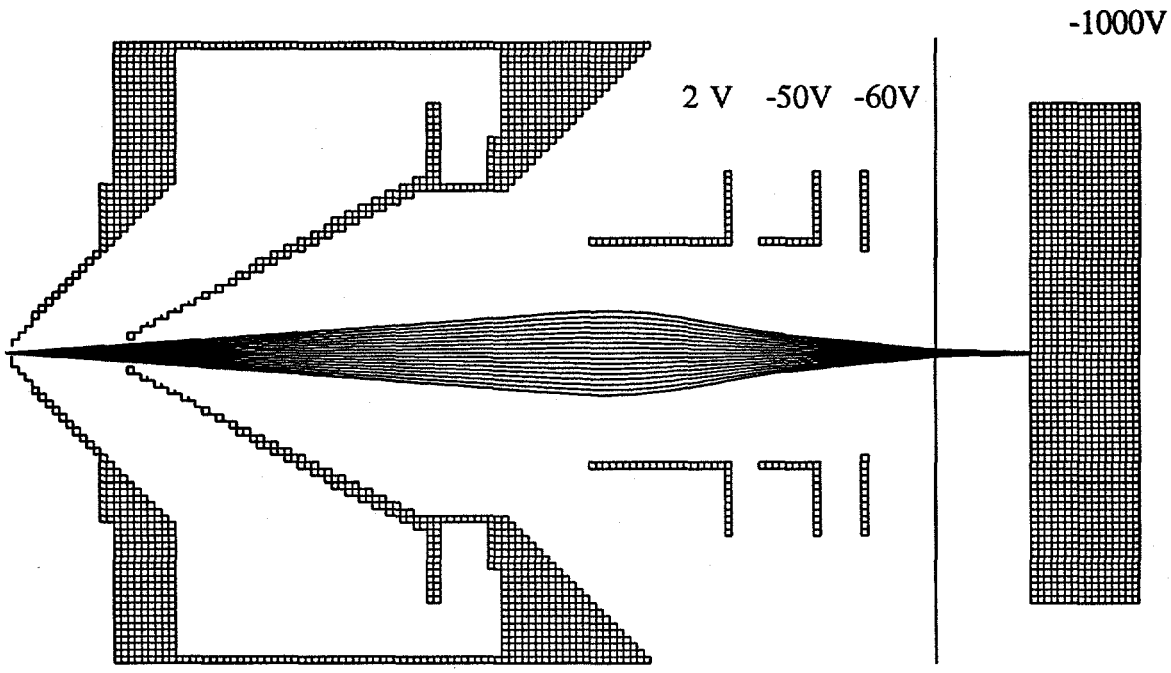

Figure 5. SIMION ion trajectories for ion lens setting 2.

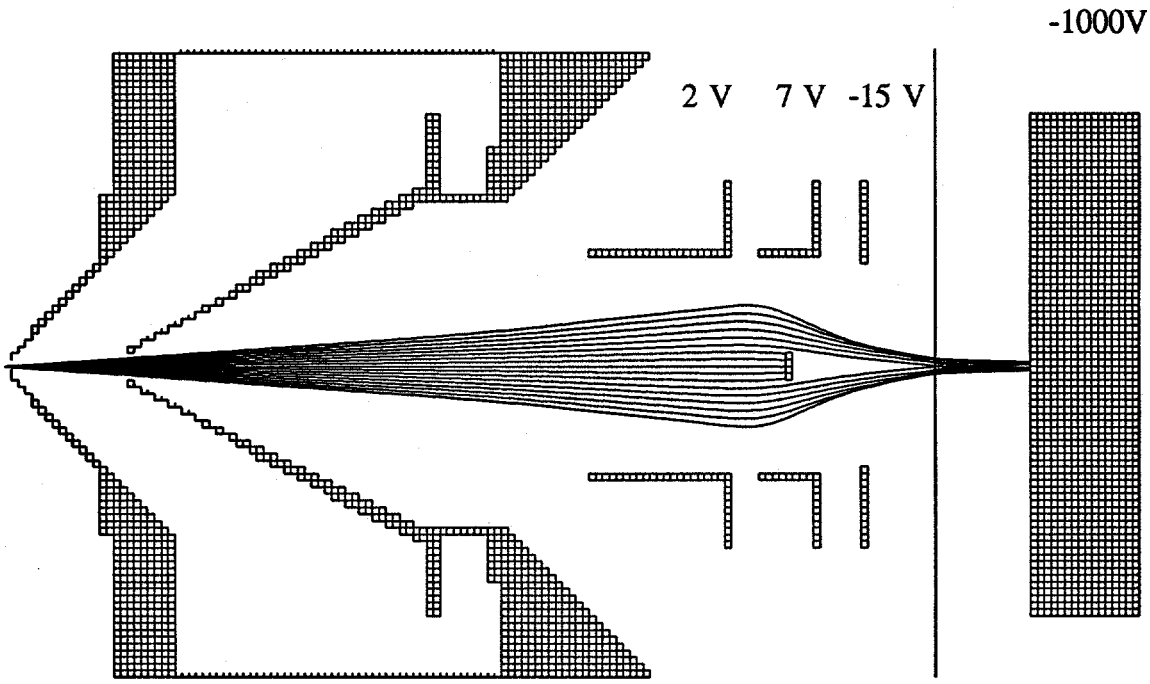

Figure 6. SIMION ion trajectories for ion lens setting 3 where a photon stop is present.

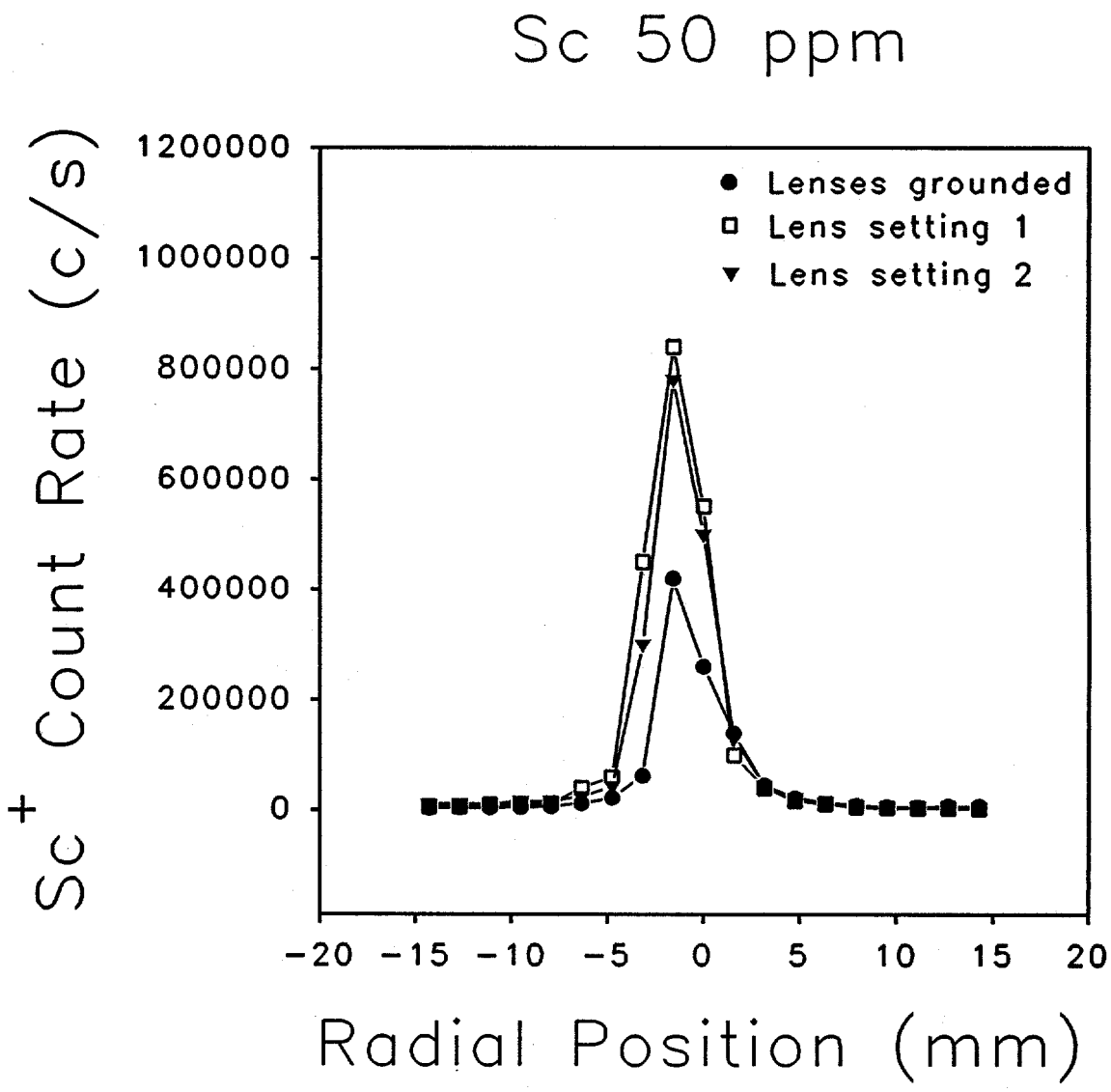

Figure 7. Deposition profile for Sc at 50 mg L^{-1}.

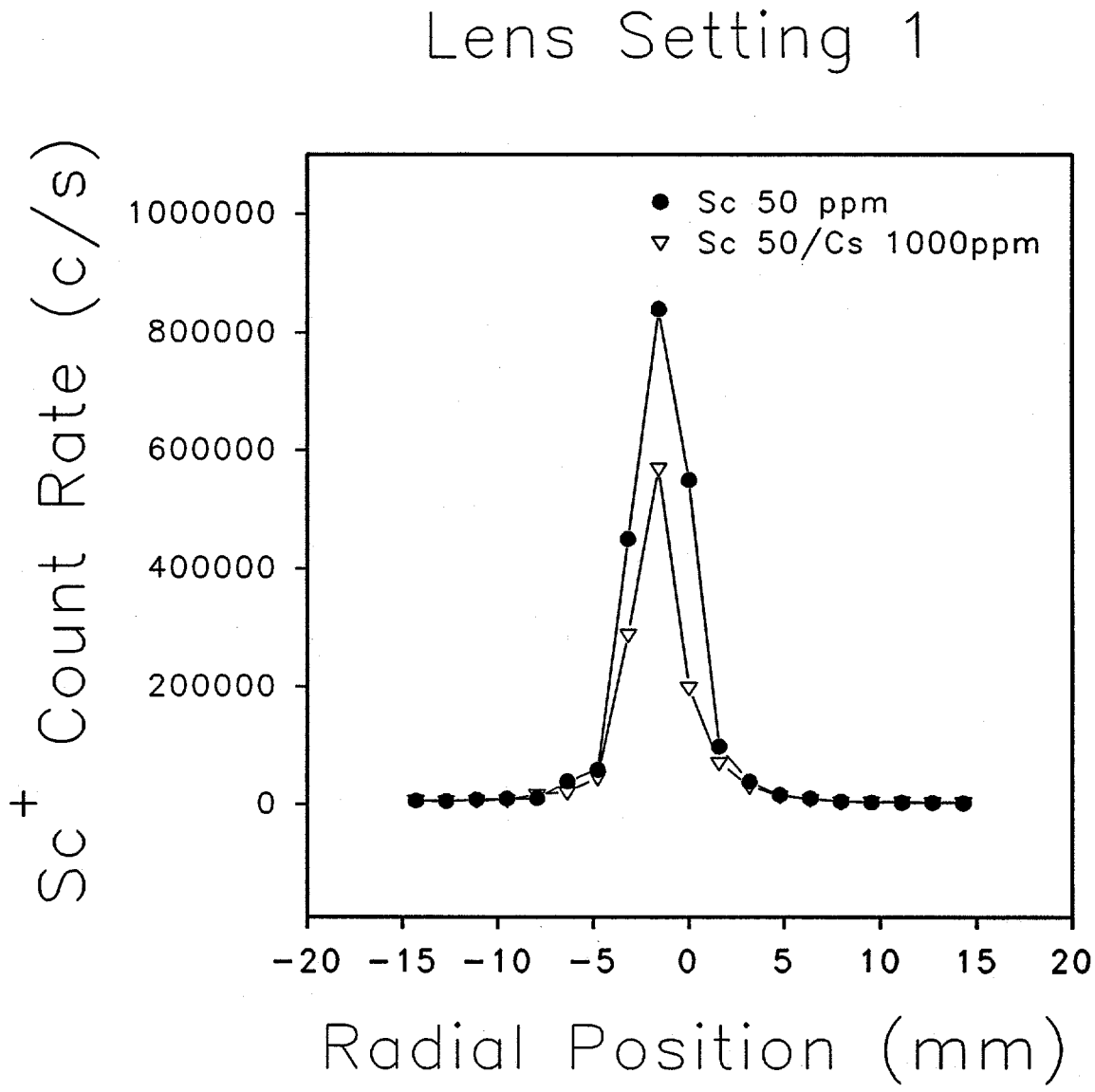

Figure 8. Effect of Cs matrix (1000 mg L^{-1}) on Sc beam profile, lens setting 1.

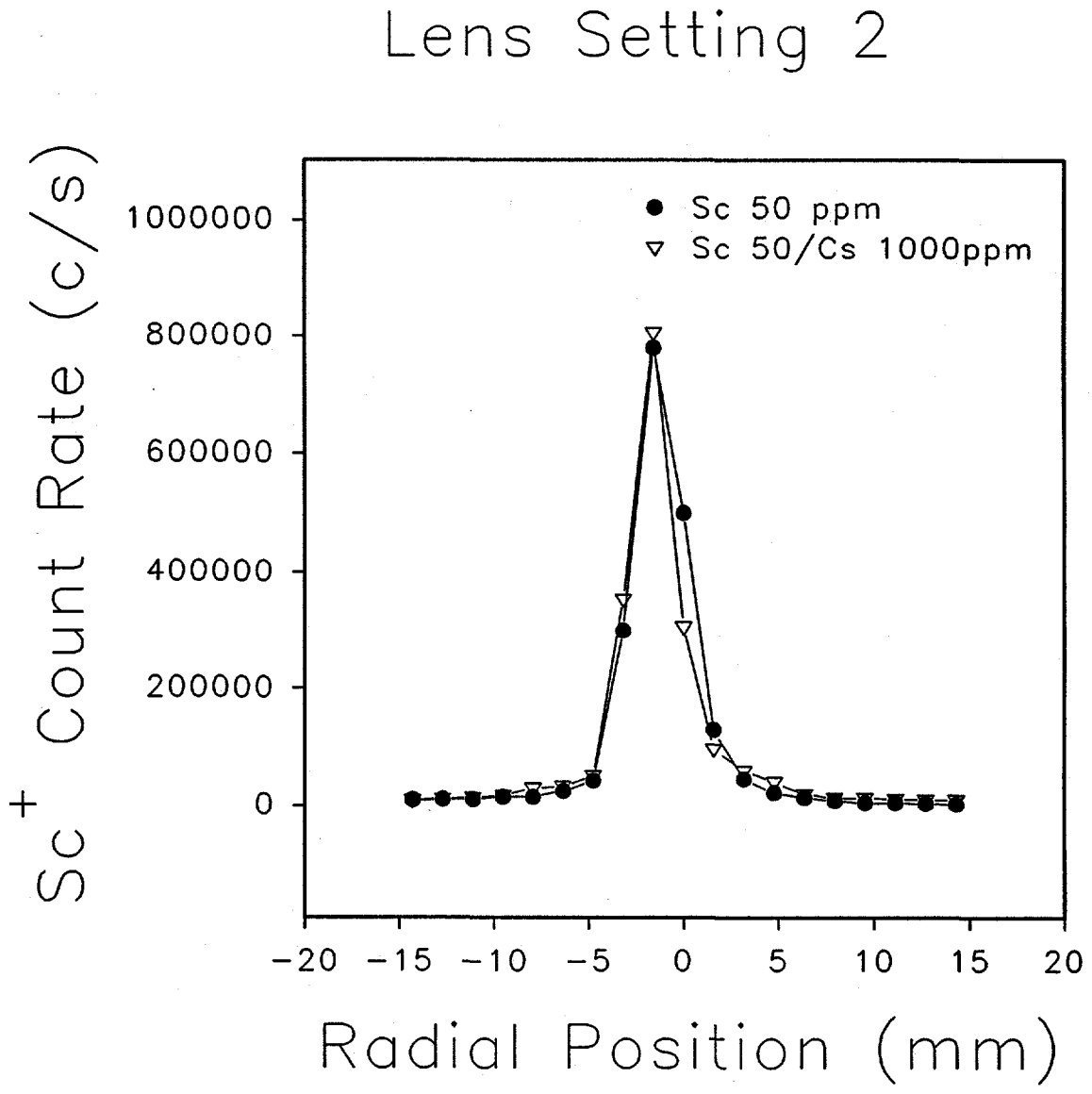

Figure 9. Effect of Cs matrix (1000 mg L^{-1}) on Sc beam profile, lens setting 2.

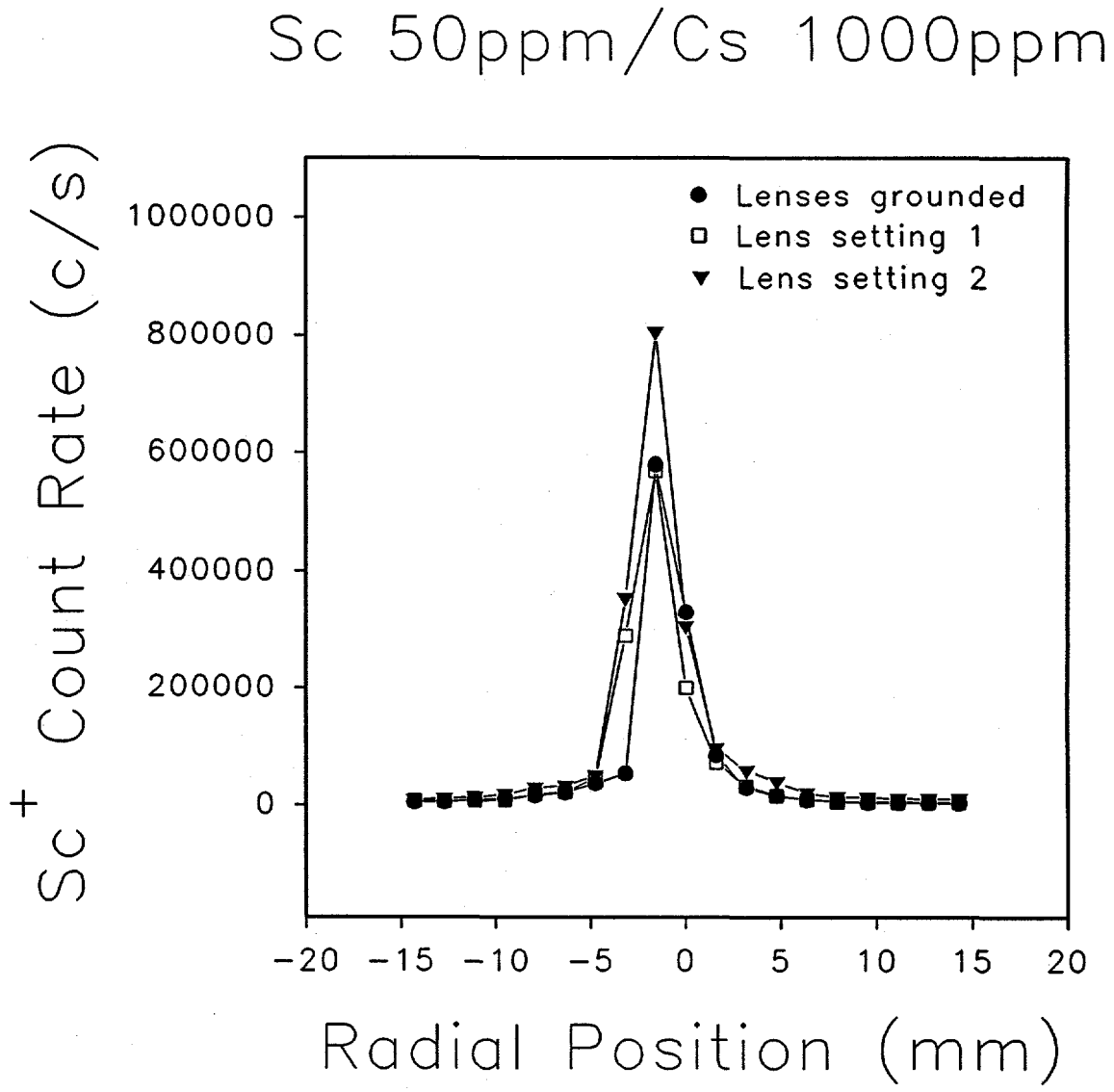

Figure 10. Effect of lens settings on Sc beam profile, with Cs matrix at 1000 mg L^{-1}.

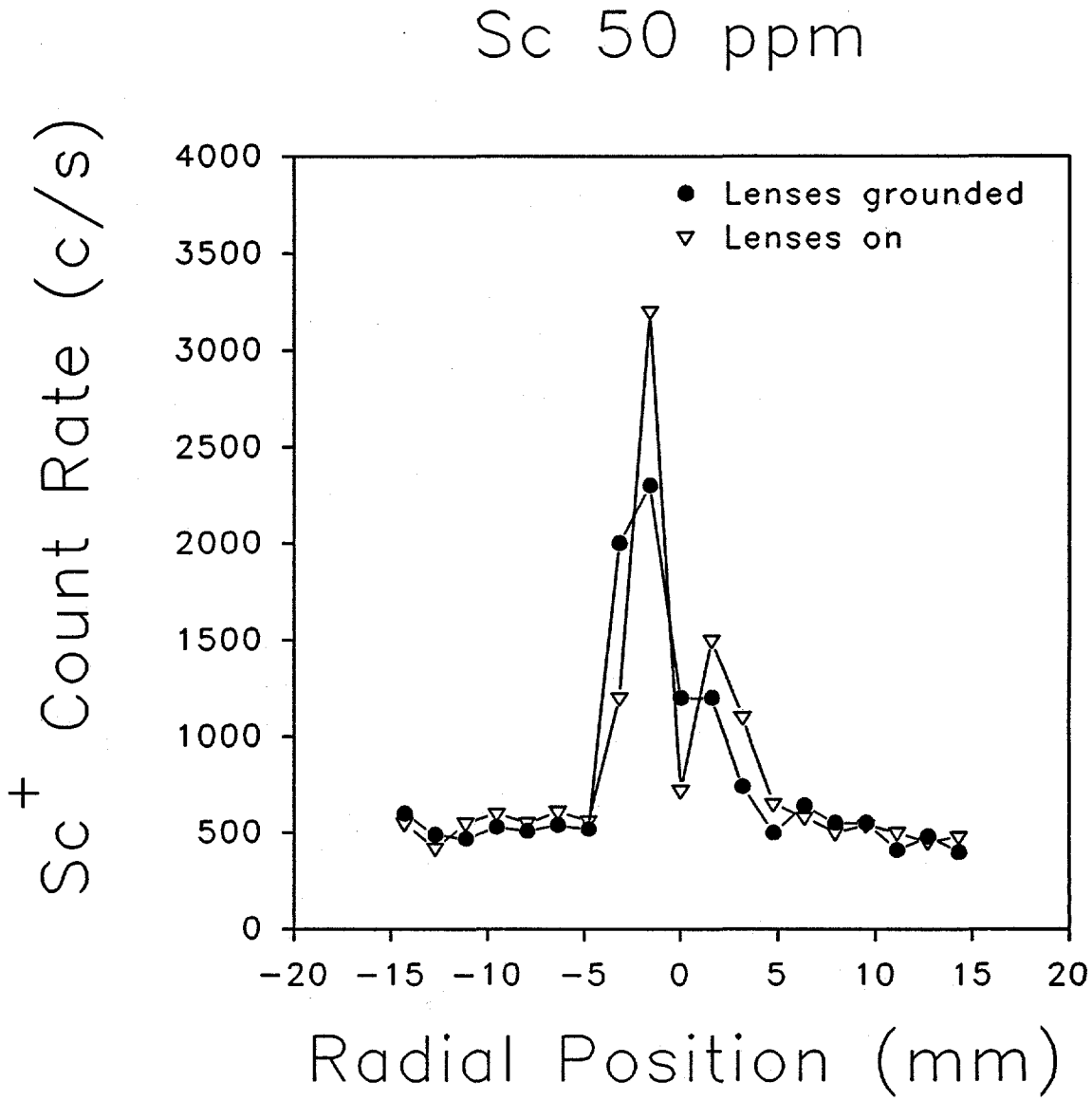

Figure 11. Beam profile for Sc at 50 mg L^{-1} with a photon stop. There is less of a dip in the center with the lenses grounded.

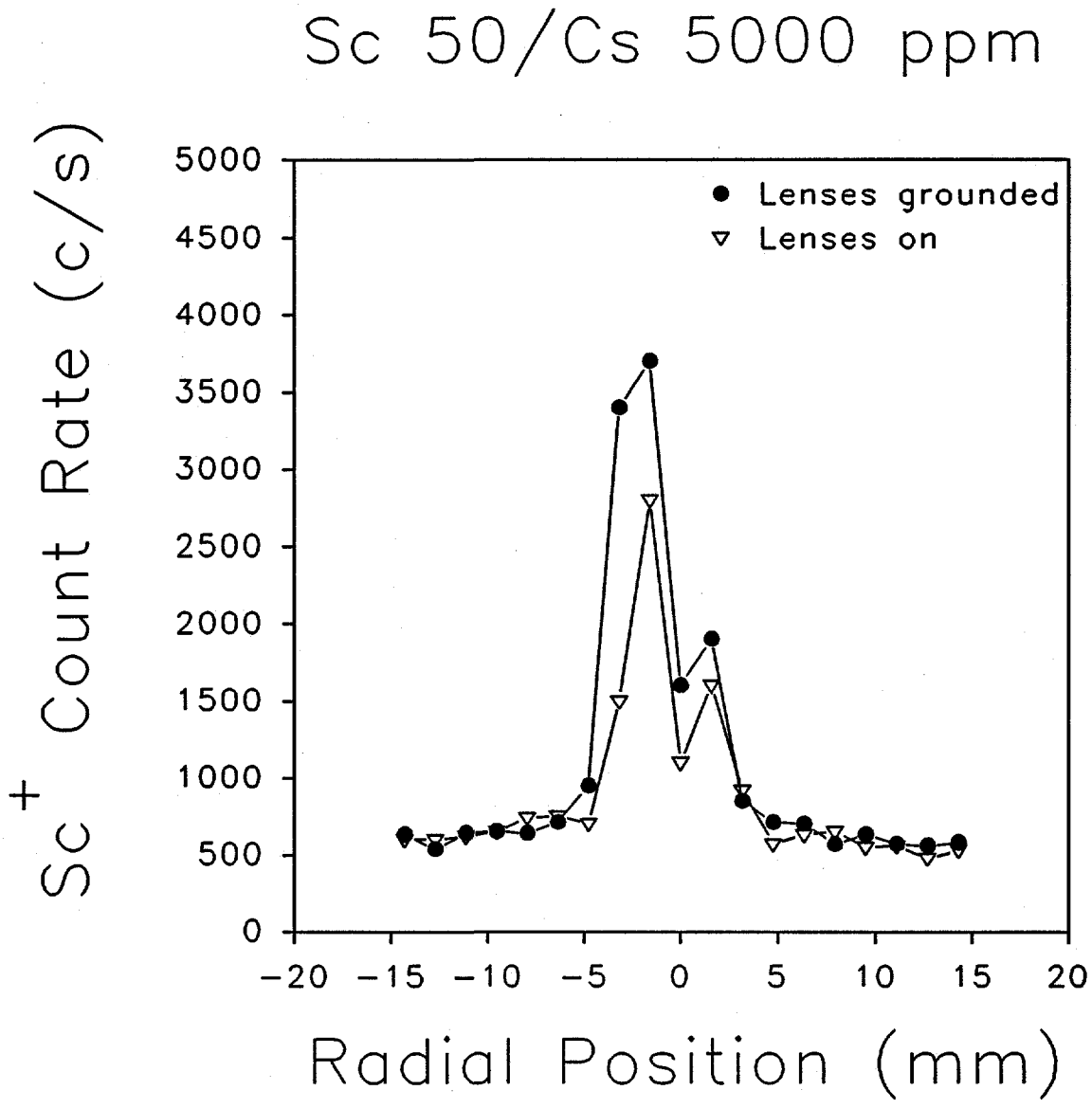

Figure 12. Beam profile for Sc at 50 mg L^{-1} with Cs matrix at 5000 mg L^{-1} and a photon stop. With matrix element present, grounding the lenses gives moderately higher signals than biasing them.

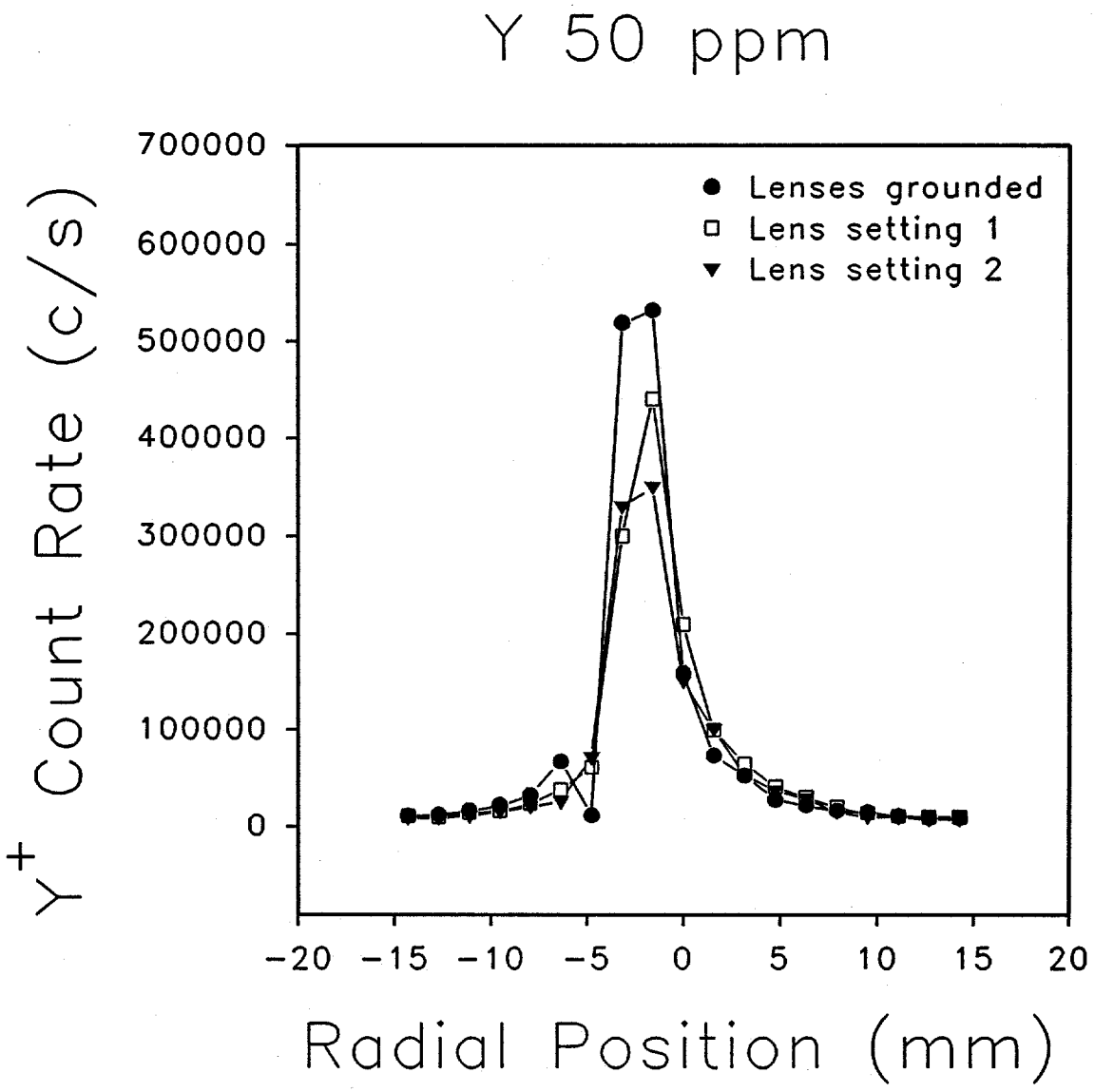

Figure 13. Effect of lens settings on Y beam profile.

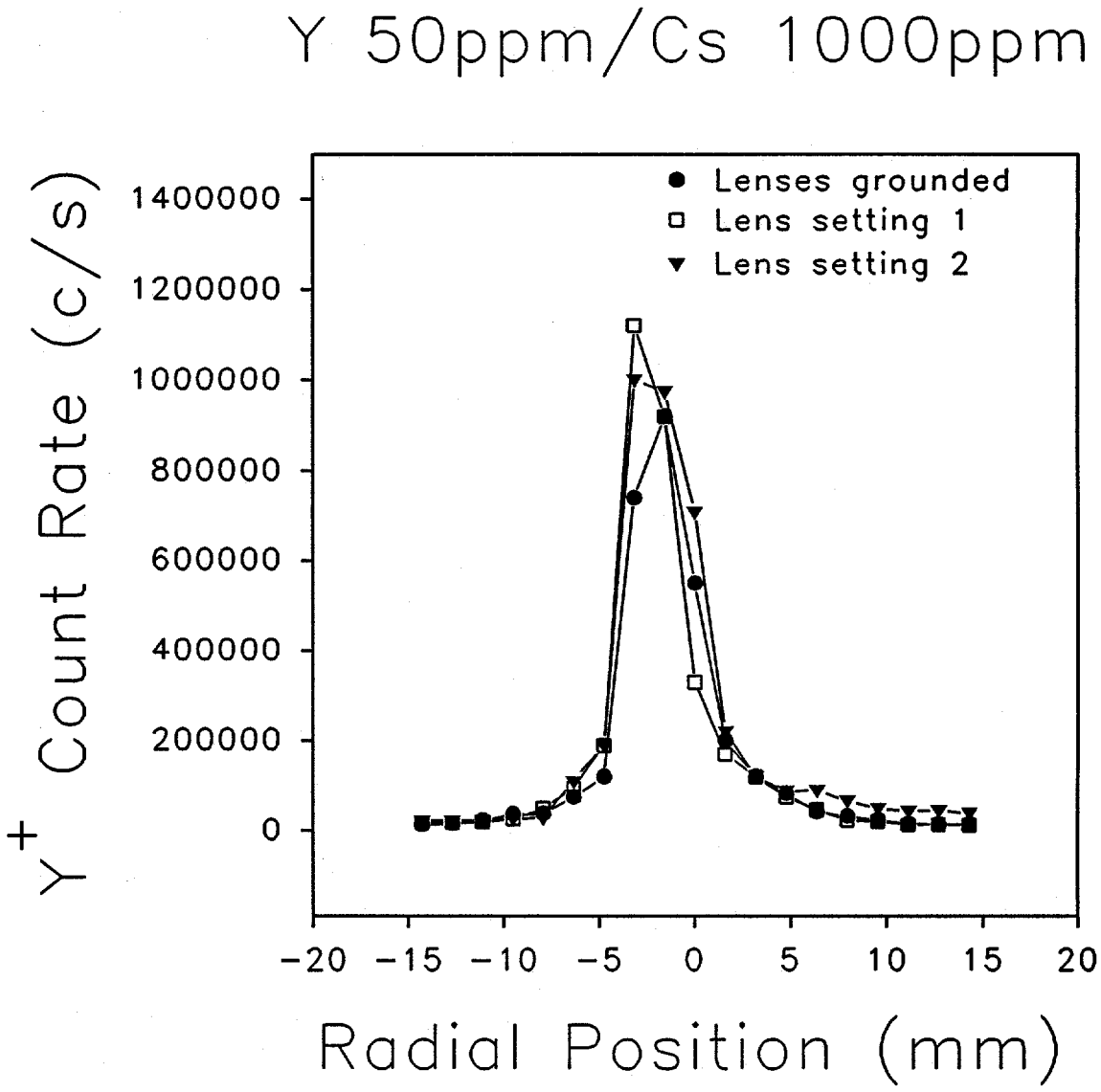

Figure 14. Effect of lens settings on Y beam profile, with Cs matrix at 1000 ppm.

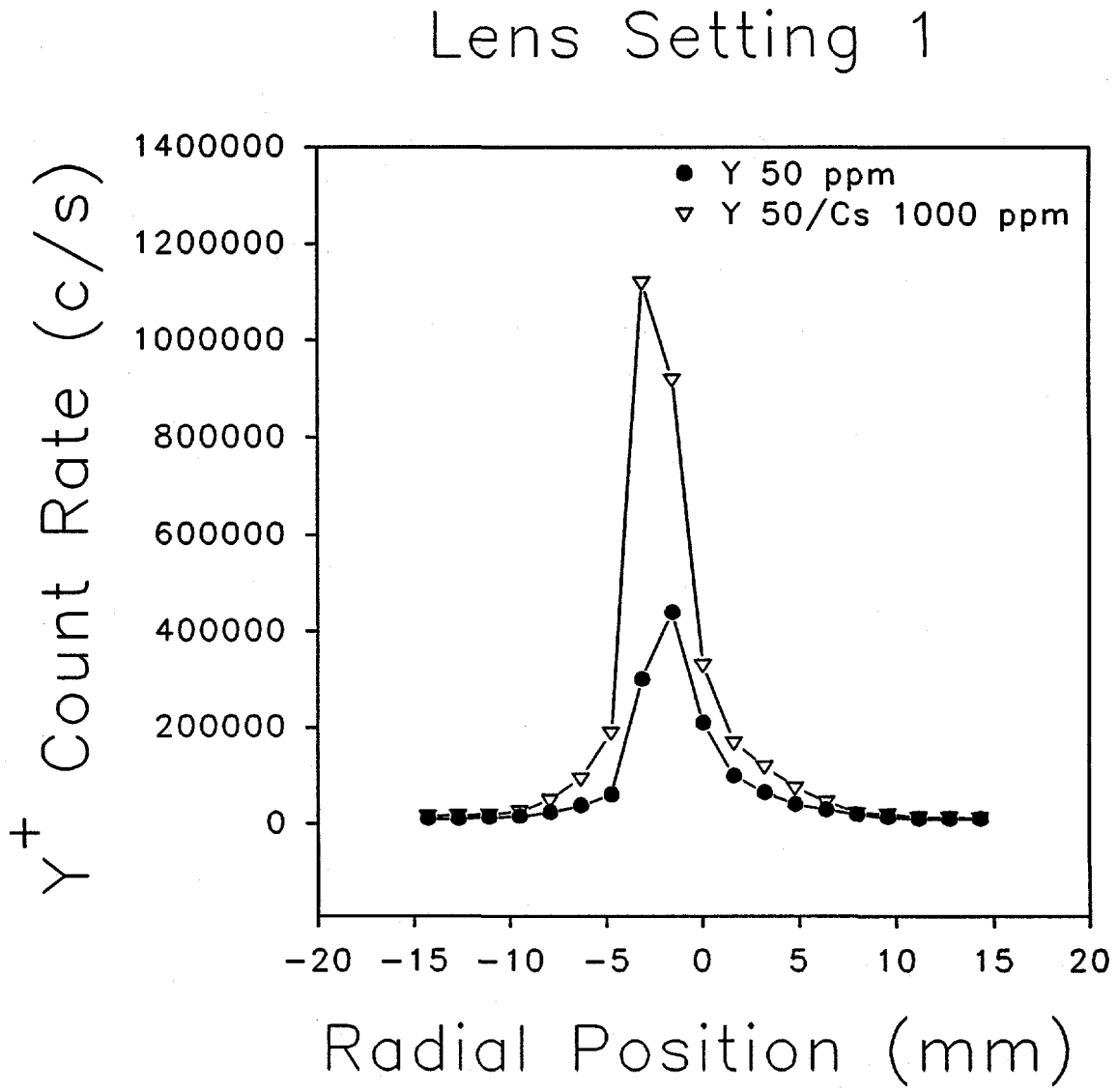

Figure 15. Effect of Cs matrix (1000 mg L^{-1}) on Sc beam profile, lens setting 1.

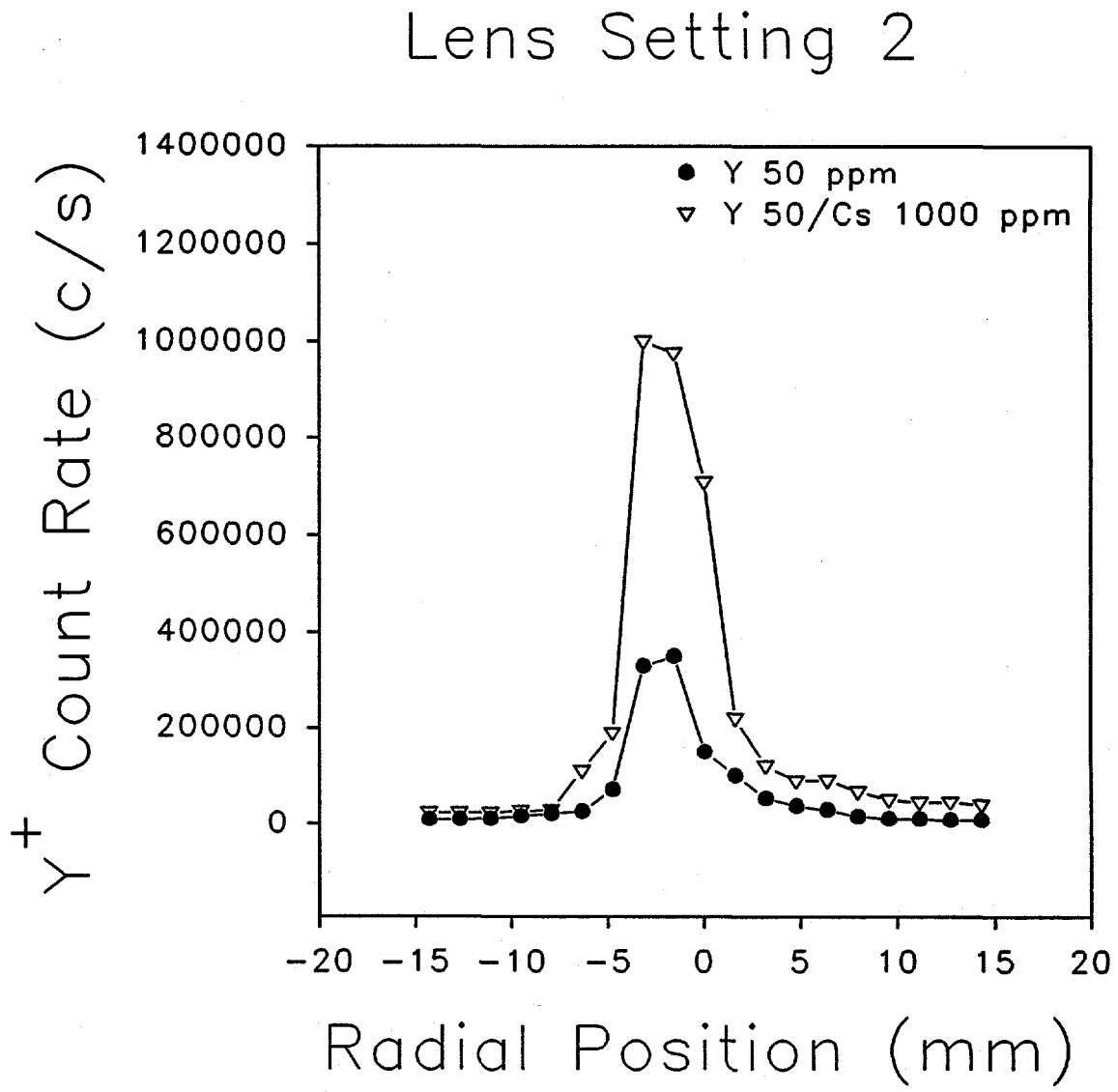

Figure 16. Effect of Cs matrix (1000 mg L^{-1}) on Sc beam profile, lens setting 2.

4. AN INDUCTIVELY COUPLED PLASMA MASS SPECTROMETER WITH A MOVABLE QUADRUPOLE MASS DETECTOR

A paper to be submitted to Journal of American Society of Mass Spectrometry

Xiaoshan Chen and R. S. Houk

ABSTRACT

Currently available ICP-MS devices can not provide angular ion intensity and composition information, which are necessary to further understand the ion extraction process, the space charge effects and ion loss mechanisms in the second stage of the ICP-MS. In order to increase the ion transmission efficiency in an ICP-MS device, a new ICP-MS device is designed and constructed which can be used to reveal the spatial distribution of the ion beam leaving the skimmer. The detector chamber moves inside a larger outer chamber such that the inner chamber can pivot away from the central line of the ion beam while detecting ions.

INTRODUCTION

An ICP-MS device consists of an inductively coupled plasma, an interface, and a mass spectrometer. The ICP part of the device in this design is a commercial ICP RF generator with a matching box (Model HFS 3000D, Plasma-Therm, Inc, now RF Plasma Products, Kresson, NJ), and it will not be discussed further. The interface of the ICP-MS,

as shown in Figure 1, is used to extract the ions produced in the central channel of the ICP. The mass spectrometer part of an ICP-MS device is very similar to any other quadrupole mass spectrometer except that the ionization source is replaced by the ICP and the interface. Figure 2 shows the layout of the quadrupole mass spectrometer in the Perkin-Elmer SCIEX ELAN 250 ICP-MS.

The overall efficiency of the ICP-MS is about 5×10^{-6}. Therefore, for every 10^6 analyte ions in the central channel of the ICP, only 5 ions reach the mass detector of the ICP-MS[1, 2]. The rest of the ions are believed to be lost in the skimmer, ion optics and quadrupole mass analyzer. A majority of ions are lost in between the skimmer and the first ion lens. Theoretical calculations predict the total current passing through the skimmer is 1.5 mA whereas the measured total ion current at the base of the skimmer is only 6 μA. There are two established factors that affect the recovery of the ions that pass the skimmer orifice. The first factor is the rarefaction of the beam as it travels downstream from the skimmer tip. As stated in the previous chapter, the beam entering the skimmer orifice is considered a continuation of the supersonic expansion, and the beam entering the skimmer is still considered quasineutral in nature. For the same area the flow at the entrance of the ion lens 50 mm downstream of the skimmer tip becomes only 1.5% of the flow at the skimmer tip, and the current through the same area is reduced from 1.5 mA at the skimmer tip to 22 μA at 50 mm downstream from the tip, simply due to the expanding nature of the beam and the need for low pressure. Therefore, the ion flow through the skimmer cannot be completely recovered. The second factor is the space-charge-limited current flow. As has been established in the previous chapter, the perveance corresponding to the measured 6 μA in

the ICP-MS already exceeds the maximum perveance without space charge effect by a factor of over 5000. thus the current flow in the ion optics is space-charge-limited. It is then reasonable to believe that between the skimmer tip and the first ion optics the ion flow is in the transition between plasma flow and space-charge-limited flow. It should be noticed that a current collecting electrode is always negatively charged, therefore when placing an electrode at the base of the skimmer to measure the current flow, the space charge induced by the potential at the electrode is comparable to the effect of the ion optics. The theoretical 1.5 mA probably would never be measured.

In summary, the beam spreading due to the increase in Debye radius and subsequently the space charge buildup under the influence of the ion optics causes the loss of ions in this stage. Therefore there is interest to investigate how the ion beam spreads behind the skimmer, i.e., the angular ion composition and intensity distribution, and how this spread changes with respect to the change in the composition and mass of sample matrix, in order to further understand the ion extraction process, the space charge effects and ion loss mechanisms in this stage, so that the ion transmission efficiency in an ICP-MS device can be increased. Currently available ICP-MS devices can not provide such angular information.

The purpose of the current study is to design and construct an inductively coupled plasma mass spectrometer, as shown in Figure 3 in a side section view, which can be used to reveal the spatially resolved ion distribution of the ion beam leaving the skimmer to provide information about the composition and intensity of the beam by incorporating a movable inner chamber inside a larger outer chamber. The inner chamber can pivot away from the central line of the ion beam while detecting ions. The rest of this section describes

the general features of this new ICP-MS device, and the detailed design is given in the experimental section.

The ICP-MS device is designed to operate in one of the three modes:

1) regular mode. The ICP-MS runs the same way as other similar devices, when the central line of the inner chamber is aligned with the central line of the interface and with the inner chamber at the full forward position.

2) pivoting mode. The inner chamber moves away from the central line of the interface and collects the ions as it is pushed by a lateral motion feedthrough (Y-axis) at the base of the ball bearing plate. The pivoting center is at the tip of the sampler, and the maximum pivoting angle is 20° (see Figure 4).

3) linear motion (X-axis) mode. In this mode, the central line of the inner chamber is aligned with the central line of the interface during the motion, while the distance between the inner chamber and the interface changes by turning the X-axis positioner at the base of the inner chamber connected to an axial motion feedthrough through the outer chamber (see Figures 5 and 6).

In addition, a laser beam can be introduced through the viewing port directly, or through an optical fiber mounted through the viewing ports, at the front of the extraction tip of the inner chamber (see Figure 3). Thus, experiments such as laser dissociation and laser ionization of polyatomic species coupled with mass spectrometry can be done.

EXPERIMENTAL SECTION AND DISCUSSION

Outer Chamber Design

The outer chamber (see Figures 7, 9 and 10) consists of the interface assembly, the chamber body, the turbomolecular pump port, a few electrical feedthrough ports, the diffusion pump port, the UV-vis viewing ports, a Bayard & Alpert type ionization gauge tube port, and the back flange assembly. The outer chamber design will be divided into two parts for discussion: the interface assembly and the outer chamber assembly.

Interface Assembly The interface design (shown in Figure 8 and Figure 9) is similar to other ICP-MS devices constructed in this laboratory[1, 3-7]. It consists of a sampling flange, a sampler, an interface chamber, a skimmer flange and a skimmer. The copper sampling flange and the skimmer flange all have a 6.35 mm O.D. (1/4 in.) copper cooling water line embedded and soldered on it. The water cooling tubes of the sampler flange and the skimmer flange are designed such that they can be easily connected in series so that they need only one cooling water outlet.

Sampler and Skimmer The sampler is made of either nickel or copper. The sampler tip has a 1.0 mm diameter orifice and the base inner diameter is 20.3 mm (0.8 in.). The skimmer is made of stainless steel with tip orifice of 0.7 mm in diameter and the base inner diameter is 31.8 mm (1 1/4 in.). Both the sampler and the skimmer orifice size are the same as the ones used in the ICP-MS device by VG Instruments, Inc. but smaller than the ELAN ICP-MS devices (1.14 mm and 0.89 mm respectively).

Interface Chamber The interface chamber is stainless steel with a port that connects to a 33.86 mm (1 1/3 in.) rotatable CF flange for a convectron vacuum gauge (Model 275,

Granville-Phillips Company, Boulder, CO), and another port that goes to a Kwik-Flange (25.4 mm (1 in.) tube O.D.) for the roughing pump. The direction of the flange tubes are such that the lengths of the connecting tubes are minimized and yet they do not interfere with other attachments. Because the inner chamber has to be able to pivot 20° away from the interface central line, the central line of the interface is shifted off the center of symmetry of the outer chamber, as shown in Figure 9.

Mach Disk Position The adiabatic expansion of plasma gas into the first stage of an ICP-MS device through a small orifice forms a free jet expansion. This jet is supersonic because the gas kinetic temperature decreases rapidly and the gas flow speed exceeds that of the local speed of sound. The center of the free expansion region is called the "zone of silence" and is surrounded by a concentric barrel shock. The expansion terminates downstream in a perpendicular shock wave known as the Mach disk. The position of the Mach disk is given as follows:[8, 9]

$$x_m = 0.67 D_0 \left(\frac{P_0}{P_1}\right)^{1/2} \quad (1)$$

where x_m is the distance between the sampler tip and the Mach disk, D_0 is the sampler orifice diameter, P_0 is atmospheric pressure, and P_1 is the pressure in the first stage. In the Mach disk the jet is disturbed by collisions with the background gas, the density and the temperature of the gas increases, and the flow stagnates and becomes sub-sonic. Thus the position of the skimmer tip should be in front of the Mach disk. If skimmer tip is right at the position of the Mach disk, the ion signal is far from maximum, the polyatomic ion signal may increase, and the skimmer tip gets too hot and degrades easily. Therefore it is important

in ICP-MS instrumentation to calculate the position of the Mach disk, and to choose the optimal position for the skimmer to maximize the ion signal in ICP-MS. Assuming D_0 is 1.0 mm, P_0 is 760 torr and P_1 is 1.5 torr, the onset of the Mach disk is at 15 mm downstream of the sampler tip.

Sampler-Skimmer Separation The optimal separation between the sampler and the skimmer is based on the following equation that gives the best neutral beam intensity:[8,9]

$$x_{s,m} = D_0 C_1 [K_{n0}^{-1} (\frac{P_0}{P_1})]^{1/3} \quad (2)$$

where $x_{s,m}$ is the optimal sampler-skimmer separation, C_1 is equal to 0.125, K_{n0} is the Knudsen number at the sampler orifice. The Knudsen number can be used to characterize the flow regimes of a gas beam:[10]

$0 < K_n < 0.01$	continuum flow (gas-gas collisions dominate)
$0.01 < K_n < 0.1$	slip flow
$0.1 < K_n < 10$	transition flow
$10 < K_n$	free-molecular flow (gas-surface collisions dominate)

The Knudsen number is given by the following equation:[10]

$$K_{n0} = \frac{\lambda_{visc}}{D_0} \quad (3)$$

where the λ_{visc} is the viscosity based mean free path, given by the following equation:[10]

$$\lambda_{visc} = \frac{1}{\sqrt{2} n_0 Q_{visc}} \tag{4}$$

Q_{visc} is called the viscosity based, hard sphere type total cross section:[10]

$$Q_{visc} = \frac{5[2\pi MkT]^{1/2}}{16\eta[2N_0]^{1/2}} \tag{5}$$

where M is the gas molecular weight in a.m.u., and η is the viscosity in poise. Although Q_{visc} equals 41 $Å^2$ at 293 K and people have used this value for calculations at other temperatures, the viscosity is a function of temperature. According to the *CRC Handbook of Chemistry and Physics*, the viscosity is linear at temperatures between 273 K and 1100 K. Extrapolating the data to 5000 K, η is 2255×10^{-6} poise (compared to 234.4×10^{-6} poise at 293 K), which gives Q_{visc} = 16.6 $Å^2$, and λ_{visc} = 2.9×10^{-4} cm. For a sampler diameter of 1.0 mm, K_{n0} is 2.9×10^{-3}. This means that at the tip of the sampler the flow is continuum and the gas-gas collisions dominate the flow. Assuming at the skimmer tip the temperature is 152 K[9], and the skimmer orifice diameter is 0.89 mm (a typical ELAN device value), a similar calculation indicates that K_n = 0.26, so the flow at the skimmer tip is in the transition flow regime, where there are still some collisions between gas molecules. Assuming the same D_0, P_0 and P_1 values as above, the optimal sampler-skimmer separation is 7 mm. Therefore we choose 7 mm as our sampler-skimmer separation, which is similar to a typical ICP-MS device such as the SCIEX ELAN 250.

Outer Chamber Assembly The diameter of the outer chamber is determined by the maximum pivoting width of the inner chamber (see Figure 4).

Ports There are three viewing ports welded on the outer chamber near the skimmer flange, one on each side and one on the top (see Figures 7, 8 and 9). The viewing ports have sapphire windows, and they can transmit UV-vis laser beams. The three viewing ports are placed such that a laser can be shot directly at the front of the extraction tip (see Figure 3), or the laser beam can be introduced using an optical fiber which can be mounted close to the tip of the extraction cone and moved together with the inner chamber. The top viewing port can be used to view the resulting scattering or fluorescent signal directly, or it can be used to mount an optical detector, such as a photodiode array or a CCD, directly in the chamber. Therefore laser dissociation of polyatomic ion experiment can be done in this fashion. The outer chamber pressure is measured through a port for a Bayard & Alpert type ionization gauge (shown in Figures 7 and 9). The bottom port in Figure 9 is to be connected to a cryotrap, and the side port in Figure 9 is the turbomolecular pump assembly that provides a pumping path through the metal bellows (Model 60285-7, Senior Flexonics, Inc., Metal Bellows Division, Sharon, MA) to the inner chamber (see Figure 6 or Figure 13). The metal bellows is made of stainless steel with 8.9 cm (3.5 in.) I.D., and it is extendable (extended length 20 cm) and compressible (compressed length 5.9 cm). The connections at the ends of the metal bellows are made with Kwik-Flanges for easy assembly. The details of the pumps will be discussed in the pump system design section. The top port is the electrical feedthrough port that provides all the electrical connections to the inner chamber and the pre-amplifier. The details of the electrical signals will be discussed in the quadrupole control and data acquisition section.

Back Flange The back flange of the outer chamber is hinged to provide

convenience in operation due to its size and weight (see Figures 10 and 6). There is an axial translational feedthrough assembly built on the back flange to carry out the third mode of operation (shown in Figures 3 and 5). The axial feedthrough is mounted on the back flange using a CF flange through which the feedthrough is inserted into the outer chamber. The shaft of the feedthrough is designed such that it can be pushed linearly in the vacuum chamber until it strikes the micrometer of the X-axis positioner. Then the feedthrough can be turned to move the inner chamber in the X-axis direction, while the pivoting angle is 0°. In this way, the inner chamber can be used to detect ions at different locations along the ion beam axis. The information obtained then reveals the ion intensity changes as a function of the distance behind the skimmer.

Inner Chamber Design

Inner Chamber The inner chamber, shown in Figure 11, consists of the extraction cone, the front chamber cone, the chamber body, the mass analyzer assembly, the X-Y-Z axis positioners, the radial swing mechanism assembly, a pumping port to the turbomolecular pump through a stainless metal bellows, a supporting cradle that houses the quadrupole mass analyzer and the detector and back flange. An extraction cone is necessary because it makes replacing a damaged orifice easier without having to replace the whole front chamber cone. The extraction cone is made of stainless steel with a 1.6 mm diameter orifice. There is no photon stop in this device (if necessary it can be added in the ion lens stage) since the inner chamber can be easily pivoted to a small angle to keep the photons out of the ion path. The extraction cone can be charged to conduct the ions into the inner chamber. The front chamber cone can be insulated by inserting a Vyton washer in between

the front chamber cone and the inner chamber body, and using Nylon socket head screws to join them. In order to maximize the pumping efficiency, there should be no protrusion on the front surface of the inner chamber. To achieve this the extraction cone is designed to have no flanges or screws on the surface, and the junction between the extraction cone and the front chamber cone is smooth, too. It does however have a pair of small holes that are designed to be able to use a specially designed tool to remove or mount it onto the front chamber cone. The outer angle of the extraction cone and the front chamber cone is 60°, which enables the inner chamber to be placed close to the skimmer while still providing enough space for pumping.

X-Y-Z Stage There is an X-Y-Z translational stage underneath the inner chamber, shown in Figures 11 and 12, which is mounted on a movable mechanism that allows the quadrupole mass analyzer to sample the ions in a supersonic beam in a range of 0-20° away from the central line of the beam. The X-Y-Z translational stage consists of the following components (from top down). The Z-axis plate provides some adjustment in the vertical axis (Z-axis) through four screws at the each corner, and the Z-plate is in turn mounted on a ball bearing stage (Model 4418-P1, CMA, Minneapolis, MN) as the Y-axis stage, and another ball bearing stage (Model 4413-P1, CMA, Minneapolis, MN) as the X-axis stage, which is mounted on the motion mechanism. The X-Y-Z translational positioner adjusts the sampling position of the mass analyzer in all three dimensions relative to the center line of the ion beam and corrects for any possible misalignment in the manufacturing process. The support base of the swing mechanism is welded inside the outer chamber.

Flanges All the ion lens system, the entrance mass filter, the quadrupole mass

analyzer and the detector are mounted on the inner chamber back flange through the cradle and can be removed from the back of the inner chamber for servicing. The detector is mounted on a separate detector flange which can be easily taken out from the rest of the inner chamber without removing the quadrupole. Contrary to some other ICP-MS devices including some commercial ones, this design makes it easy to access and dismount the detector and quadrupole assembly. At the center of the detector flange there is a viewing port for laser alignment of the interface orifices, extraction orifice, the quadrupole inlet/outlet, and the detector (see Figure 12). All the electrical connections to the quadrupole assembly are made through the quadrupole flange at the back (shown in Figure 12). Welded in the quadrupole flange are two RF feedthroughs for the quadrupoles, and a multi-pin connector for the ion lenses. The RF feedthrough and the multi-pin connector are of the hermetically sealed and pressure tight type (W.W. Fischer Inc., Atlanta, GA).

Motion Mechanism The design of the motion mechanism for the inner chamber is the key component of the project. Design considerations include the following. 1) The inner chamber hangs from the top of the outer chamber through an O-ring sealed port. Movement of the inner chamber is driven from outside the outer chamber. The flange moves only in a given curve. 2) The inner chamber is pumped through a metal bellows inside the outer chamber and is built on a circular motion guide that slides on a curved rail shaft. The final design uses a ball bearing plate that contains a set of three ball bearings positioned in a triangle. Two of them roll on a V-shaped swing groove carved on top of the swing plate to provide the motion and a set of two ball bearings beneath the swing plate through a spring to pull the top ball bearings down into the groove (see Figures 5 and 12).

This assembly allows the mass analyzer to pivot by up to 20° around the tip of the sampler of the ICP-MS by pushing the ball bearing plate through the lateral motion feedthrough (shown in Figure 4).

Pumping Considerations The inner chamber is pumped through the metal bellows which is connected to the turbopump. To maximize the pumping of the inner chamber, neither the conductance of the inner chamber nor the conductance of the metal bellows should become the limiting factor for pumping. Under the molecular flow conditions ($P \leq 10^{-4}$ torr), the conductance of a tube with diameter D (cm) and length L (cm) is given as:

$$C\ (l/s) = 12\frac{D^3\ (cm^3)}{L\ (cm)} \tag{6}$$

the pumping speed of the vessel is given as:

$$\frac{1}{S_{ves}} = \sum \frac{1}{C_i} + \frac{1}{S_{pump}} \tag{7}$$

It can be calculated that the conductance of the inner chamber is 2138 l/s (the tapered cone portion is ignored), and the conductance of the metal bellows is 572 l/s. The pumping speed of the turbopump is 145 l/s. Thus the conductance of the vessel is 110 l/s, which is 76% of the turbopump pumping power. Therefore turbopump is not too limited by the conductance of the inner chamber.

Ion Lenses and Mass Analyzer

The key component of the whole instrument is the quadrupole mass analyzer assembly, which is contained in the inner chamber. The mass analyzer consists of the ion lens assembly, the RF only entrance quadrupole mass filter, the quadrupole mass analyzer,

the quadrupole supporting cradle, the mass detector assembly and its flange.

Ion lenses As shown in Figure 11, the ion lens assembly consists of three ion lenses: the first one is a cylindrical extraction lens with small holes in the cylinder to increase the pumping efficiency, the second and the third are plate lenses. There is a exit ion lens at the end of the main quadrupole, and the electrical lead goes through a small hole in the cradle. All the ion lens are powered through the multi-pin connector at the quadrupole flange. It has been proposed in the previous chapter and verified in this laboratory[1, 4] that the extraction lens should be charged with a slight positive potential to alleviate the matrix effect and to improve the sensitivity. The potentials on the other plate lenses need to be charged negatively and optimized experimentally to maximize the ion signals.

RF Only Rods The mass analyzer consists of two sets of quadrupole rods. The first one is a short (19 mm long) RF only quadrupole to facilitate the transmission of all the ions passing through the lenses. The RF only rods are round stainless steel tubes and are built in the Ames Lab Machine Shop. They are mounted in a Macor ceramic support in a stainless extension tube which is fitted in front of the main quadrupole housing tube. The extension tube is made such that the gap between the two quadrupoles is minimal but not in touch and the rods are aligned with each other.

Main Quadrupole The main mass analyzer is a 9.5 mm (3/8 in.) quadrupole (Model 162-8) from Extranuclear Laboratories, Inc. (now Extrel Mass Spectrometry, Millipore Corporation, Pittsburgh, PA). The mass filter housing is supported in a cradle that is welded onto the quadrupole flange. The cradle serves two roles. 1) It houses and supports the quadrupole housing, the orientation of which can be adjusted slightly by turning three

screws on the top and each side of the cradle, and one screw in front bottom. 2) The cradle also houses the detector.

Wiring and Connections If possible, all the unshielded electrical connections inside the vacuum chamber should be made of bare stainless wire insulated with ceramic beads to ensure easy degassing and durability. But plastic insulated wires are acceptable if necessary (e.g. ELAN 250). The shielded connections (e.g., signal) can be made with normal shielded BNC connectors and compatible wires. The RF power is connected to the quadrupoles in the following way (see Ke Hu's Ph.D. thesis, Figure 3, p.158). The RF power is connected to the main quadrupole. The electrical connection between the RF rods and the main rods is made through a pair of capacitors (50 pF, 7.5 KDCV, ceramic) to block out the DC component from the power supply (thus it's RF only). A separate DC power supply is connected through a pair of 1 MΩ resistor to the RF only rods to provide the bias potential, which is a parameter in the optimization.

Pumping System Design

The pumping system consists of three mechanical pumps, a diffusion pump, a turbomolecular pump, a sliding gate valve and a cryotrap (only the turbomolecular pump is shown in the figures).

Roughing Pumps The mechanical pump can start to function from atmosphere. The minimum pressure that can be achieved by the mechanical pumps is about 10^{-3} torr. The first mechanical pump pumps the interface chamber (the space between the sampler and the skimmer). The pump provides a pressure of $1 \sim 2$ torr at the interface region during operation. The second mechanical pump is used for rough pumping the outer chamber and

to evacuate the foreline of the diffusion pump through a valve. The third mechanical pump is used to rough the inner chamber and to support the turbomolecular pump through a mechanism in the turbopump flange and a valve.

Diffusion Pump The diffusion pump (Model VHS-6, Varian Vacuum Products, Lexington, MA) has pumping speed of 2400 L s^{-1} for air. The minimum pressure can be reached by the diffusion pump is 5×10^{-9} torr. The sliding gate valve is used to isolate the diffusion pump and the chamber. The diffusion pump will not function when it is exposed to high pressure. Therefore the gate valve should only be opened when the pressure in the outer chamber reaches 10^{-3} torr or lower. The cryotrap (Model 362-6, Varian Vacuum Products, Lexington, MA) uses liquid nitrogen as the cooling medium and when filled (capacity 10 l) can last 8 hours in the summer (or 10 hours in the winter) before refill.

Turbopump The TURBOVAC turbomolecular pump (Model TMP 151, Leybold Vacuum Products, Export, PA), with pumping speed rated at 145 l/s for N_2, is grease-lubricated with ceramic ball bearings and therefore can be mounted in any orientation. It comes with a CF-100 flange for a 15.2 cm O.D. pumping tube. The turbopump is powered and controlled by a TURBOTRONIK NT 150/360 frequency converter. The frequency converter converts the single-phase AC voltage into a three-phase AC voltage suitable for driving the three-phase asynchronous motor of the TURBOVAC. It also performs automatic monitoring functions. The turbomolecular pumping port assembly contains a roughing mechanism that is to be used for roughing the inner chamber to $\sim10^{-2}$ torr before the turbomolecular pump starts. When the diffusion pump and the turbopump are ready to function, the valves that are used to rough the chambers need to be closed, and the

mechanical pumps are now only used to evacuate the foreline of the diffusion pump or the turbopump.

Safety Considerations The diffusion pump and the turbopump are cooled by chilled water. The cooling water needs to be running at all times. Should a power outage occur when the diffusion pump is functioning, the sliding gate valve and the valve between the diffusion pump and its support pump need to be closed immediately, otherwise the oil in the diffusion pump will backstream into the vacuum chamber.

Quadrupole Control and Data Acquisition System Design

Figure 14 shows a diagram of the quadrupole control and data acquisition system. From the hardware point of view, the quadrupole control system and the data acquisition systems are two separate systems, and they normally are purchased separately, too. They become an integral part of a system through the computer.

Quadrupole Control System The quadrupole control system of the ICP-MS device consists of the mass spectrometer quadrupole control, the radio frequency power source, the high-Q head, a digital to analog converter, and a personal computer with appropriate software. The quadrupole control, the RF power source and the high-Q head are from Extranuclear Laboratories, Inc. (now Extrel Mass Spectrometry, Millipore Corporation, Pittsburgh, PA).

Control Process The computer sends out a digital signal to the D/A converter, which is usually an interface board or a part of such a board inserted in the ISA bus of the computer, to be converted into a voltage signal. The analog signal goes to the SWEEP IN connector in the quadrupole control. The way the voltages are sent determines the way the

quadrupole functions. In the peak hopping mode, a set of discrete voltages are sent in sequence; in the scanning mode, a ramping voltage is sent continuously. The voltage signal is in the 0 to +10 V range, corresponding to m/z= 0 to 300. For a normal quadrupole device the resolution is $\Delta M = 0.1$ a.m.u., therefore the D/A converter should be able to produce at least $300/0.1 = 3000$ different voltage levels in order to match the resolution. Therefore, the digital resolution is the most important characteristics for the D/A converter. The digital resolution is expressed in number of bits. A 12 bit D/A converter is capable of outputing 4096 different voltage levels, which is normally enough. However, a 16 bit D/A converter with 65536 ramping level can provide better than $\Delta M = 0.01$ a.m.u. capability, to fully take advantage of the maximum resolution of the quadrupole mass analyzer. After the quadrupole control receives the ramping signal, it controls the radio frequency power source, which in turn sends the signal to the high-Q head, and finally the RF and the DC bias signal are sent to the quadrupole to pass the ions at given mass range and resolution.

Synchronization Immediately after each control signal is sent, the data acquisition system starts to collect the signal from the detector for a given period of time (dwell time). Because the control step (signal out) and the data collection step (signal in) must be synchronized, attention must be paid before purchasing a data acquisition software. Unless specially written for an MS application, a general purpose data acquisition software does not usually include an analog output controlling part, and synchronization of controlling the mass spectrometer and collecting the data can be a problem. However, some data acquisition software does allow incorporation of other control software if it does not contain one. Other choices include writing one's own program, or buying a complete MS application

package.

Data Acquisition System The data acquisition system of an ICP-MS is usually a single channel counting system, which consists of a channel electron multiplier (the detector) with a high voltage power supply, a preamplifier, an amplifier, a discriminator, a counter with the IEEE-488 communication option, and a computer with the IEEE-488 board (shown in Figure 14). The discriminator is often built into either the amplifier or the preamplifier unit. In this section the general design of data acquisition for the ICP-MS system is discussed, and two such data acquisition systems available are compared. the first, the PRM-100 Systems (referred to the PRM system, from Advanced Research Instruments Corp., Boulder, CO), which is available as a complete system, and the second and more expensive system (EG&G ORTEC, Oak Ridge, TN), which needs to be bought as separate components and assembled, as has been used for the twin-quadrupole mass spectrometer in our lab.

1) Detector Electron multipliers have been used as detectors in mass spectrometers for over thirty years. Channel electron multipliers (CEM) are made from a specially formulated lead silicate glass and coated with lead oxide, which produces the conductivity and secondary emissive characteristics. The count rate limits of the CEMs determine the frequency requirement of the preamplifier, the amplifier and the counter. Earlier CEMs were limited to about 10^6 counts per second maximum. The newer devices can be operated in excess of 10^7 cps. The Channeltron 4830 device (Galileo Electro-Optics Corp., Sturbridge, MA) is capable of 10^7 cps counting rate, so it is adapted in this ICP-MS device, as has been used in our labs as the detector for our ICP-MS devices. To avoid alias sampling, this count rate mandates a counting frequency of 100 MHz (10 times the maximum

count rate) for the subsequent devices.

2) CEM Power Supply The gain of the CEM is dependent on the applied voltages. Although the CEMs are generally used near saturation, a quiet, stable power supply is desirable to minimize the flicker noise from the detector. There is a low noise power supply for the PRM system, whose features include less than 100 μV peak-to-peak noise level, 100 ppm stability. The EG&G provides a 5-kV detector bias supply with less than 10 mV peak-to-peak noise level, better than 1000 ppm hr^{-1} stability.

3) Preamplifier The preamplifiers used for mass spectrometers are fast, current-sensitive preamplifiers that convert fast current pulses to voltage pulses. The timing resolution is the key characteristic of such a device. The pulse pair resolution should be 10 ns or better (i.e., the inverse of 100 MHz). The PRM system has two options: the F-100E (ECL logic standard, discussed later in this section) preamplifier has pulse pair resolution of 5 ns, the F-100T (TTL logic standard) has 10 ns resolution. The EG&G has rise time of < 1 ns (no pulse pair resolution data). All are fast enough for our needs.

The signal from the CEM goes directly to the input of the preamplifier. A long cable connection between the detector and the preamplifier adds input capacity, and also makes the electronics more susceptible to RF interference noise from the ICP or the quadrupole power supply. Both effects can degrade the signal resolution and timing. Therefore the connection between the CEM and the preamplifier must be minimized in order to improve the signal to noise ratio. In order to minimize the cable length, the preamplifier is mounted inside the vacuum chamber right next to the outlet of the CEM. There is a clamp near the end of the inner chamber to fasten the preamplifier. The cable used should be also a high quality one,

not just any BNC cable, which may have defects in its shielding. The best choice for this connection is the Belden RG-58/U 9223 low triboelectric coaxial cable, designed for audio, communication and instrumentation, and is available as free samples in short lengths.(!)

4) Amplifier The amplifier is used to amplify the voltage pulses produced by the preamplifier, and it has to be able to handle 100 MHz signal rates. For the PRM system, the amplifier is part of the rate counting system. For the EG&G system, the amplifier (9302 Amplifier/Discriminator) has a gain of either 20 or 200.

5) Discriminator The discriminator removes the dark current pulses from the signals. Most of the dark current pulses are lower in magnitude than the signal pulses. A discriminator produces an output logic pulse when the input signal crosses a fixed threshold level. Any pulse lower than the threshold is ignored. The discriminator is usually built after the amplifier. In the PRM system, the discriminator level is adjustable from 200 mV up to 2.5 V and is built into the amplifier. There is a noise discriminator built in the preamplifier to reduce the noise, and the threshold is continuously adjustable with a potentiometer. The discriminator in the EG&G system is built inside the amplifier unit (after the amplification stage to be exact). The discriminator range is from 50 mV to 1 V, which may not be enough in some cases.

6) Counter The counter is the only module in the data acquisition system that communicates with the computer. It counts the rate of the logic pulses produced by the amplifier in a given time period specified by the computer and sends these data to the computer through the IEEE-488 interface. The counter should be able to handle the 100 MHz signal rates. The PRM system has a counter-timer system (PRM-100 Precision Rate

Meter). The advantages of the system include a) an LED display shows the count rate; b) the dwell time base is variable (4 ms to 32 s) and is computer controllable with IEEE-488 option; c) the counter is compatible with NIM, ECL and TTL logic standards. The EG&G provides a counter (997 CCNIM Counter) with 100 MHz capability, LED display, IEEE-488 option, and compatibility with NIM-positive and NIM-negative logic.

7) Logic Signal Standards Each data acquisition system and their components are compatible only with certain logic standard. Attention should be paid to the compatibility of these signal standards when choosing the components. There are four options in the data acquisition system: NIM-standard positive, NIM-standard negative, ECL, and TTL. Each of these standards has certain frequency limits, and requires using different impedance matching cables and terminators for connections. If the module at the receiving end has a high input impedance, a tee and a impedance matching terminator is needed at the module input to properly terminate the cable to eliminate the reflection. The NIM-standard, positive logic, the default setting in the EG&G system, is used for repetition rates from DC to 20 MHz, which it not fast enough for ICP-MS data acquisition. The NIM-standard, fast negative logic and the ECL logic can handle counting rates up to 100 MHz. The NIM negative standard requires 50-Ω cables terminated in 50-Ω at the receiving end. The connections of the ECL are usually made using either a ribbon cable or a pair of 100-Ω twisted cables. If the module at the receiving end has a high impedance, a 100-Ω resistor must be connected between the pair of wires at the receiving end. TTL logic can handle maximum of 50 MHz logic signals, which is faster than NIM-standard positive logic signal, but still not the best choice for our purposes. The TTL signal standard is designed such that it is often compatible

with NIM-standard positive logic levels, although there is no guarantee. For TTL logic signals, 50-Ω cables terminated in 50-Ω at the receiving end must be used.

ACKNOWLEDGMENTS

The Perkin-Elmer Graduate Research Fellowship awarded to Xiaoshan Chen is gratefully acknowledged. Ames Laboratory is operated for the U.S. Department of Energy by Iowa State University under Contract No. W-7405-ENG-82. This work was supported by the Office of Basic Energy Sciences, Division of Chemical Sciences. The authors wish to thank Terry Herman of Engineering Services, Ames Laboratory for helping us in the design and making the final drawings.

REFERENCES

1. Chen, X. and Houk, R. S. *Spectrochim. Acta, Part B* **1995**, submitted.
2. Falk, H. *J. Anal. At. Spectrom.* **1992**, *7*, 255.
3. Hu, K.; Clemons, P. S. and Houk, R. S. *J. Am. Soc. Mass Spectrom.* **1993**, *4*, 16.
4. Hu, K. and Houk, R. S. *J. Am. Soc. Mass Spectrom.* **1993**, *4*, 28.
5. Niu, H. S.; Hu, K. and Houk, R. S. *Spectrochim. Acta, Part B* **1991**, *46*, 805.
6. Warren, A. R.; Allen, L. A.; Pang, H. M.; Houk, R. S. and Janghorbani, M. *Appl. Spectrosc.* **1994**, *48*, 1360.
7. Niu, H. and Houk, R. S. *Spectrochim. Acta, Part B* **1994**, *49*, 1283.
8. Campargue, R. In *Proceedings of the 6th International Symposium on Rarefied Gas Dynamics*; Academic Press: New York, 1969; p 1003.

9. Douglas, D. J. and French, J. B. *J. Anal. At. Spectrom.* **1988**, *3*, 743.

10. French, J. B. In *Molecular Beams for Rarefied Gasdynamic Research*, Vol. 112; Nelson, W. C., Ed.; NATO-AGARD Fluid Dynamics Panel: Paris, 1966; p 96.

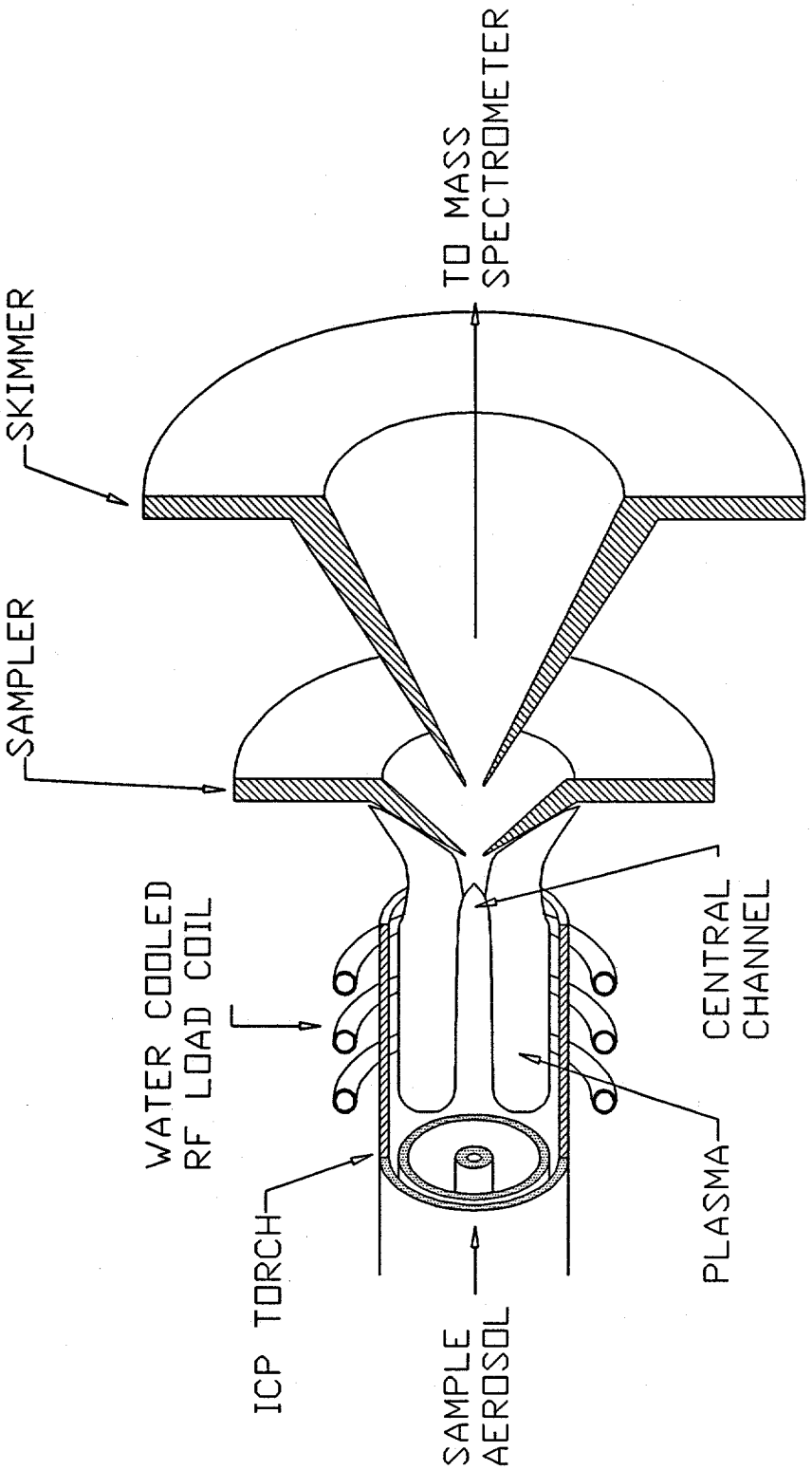

Figure 1. Illustration of an ICP torch and ICP-MS interface.

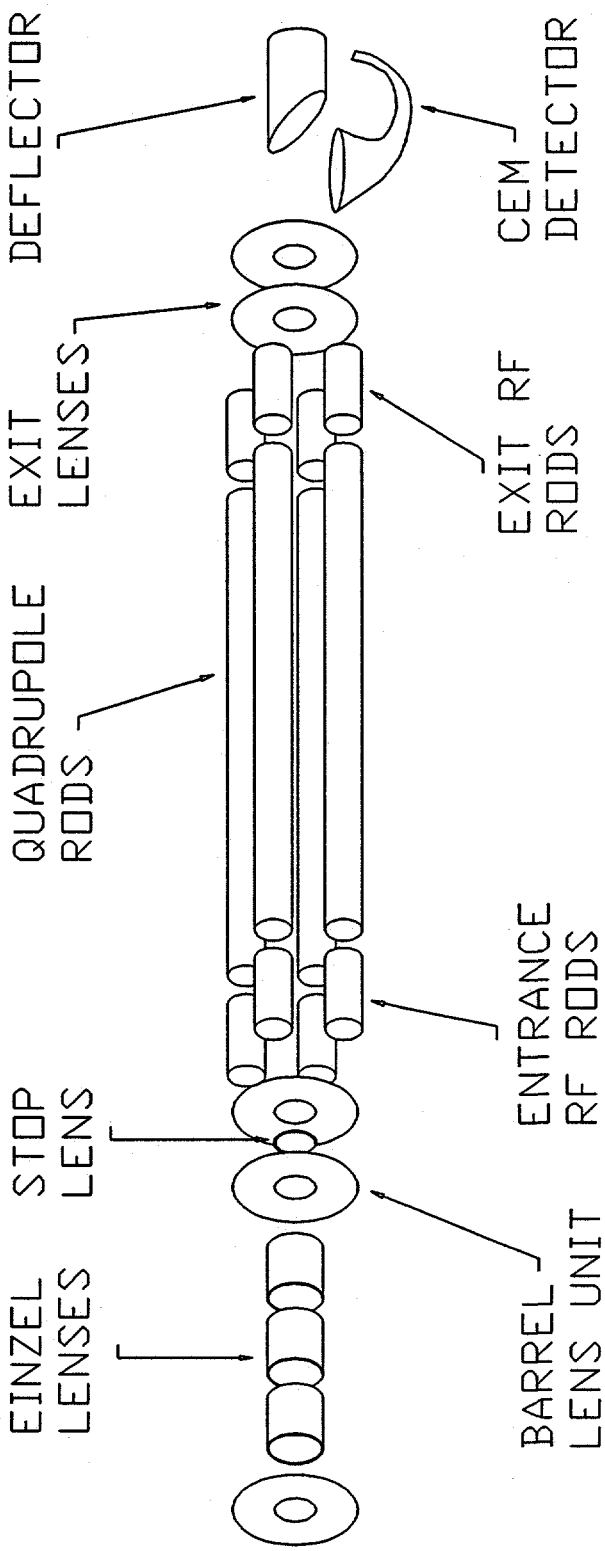

Figure 2. Illustration of a mass spectrometer in ICP-MS.

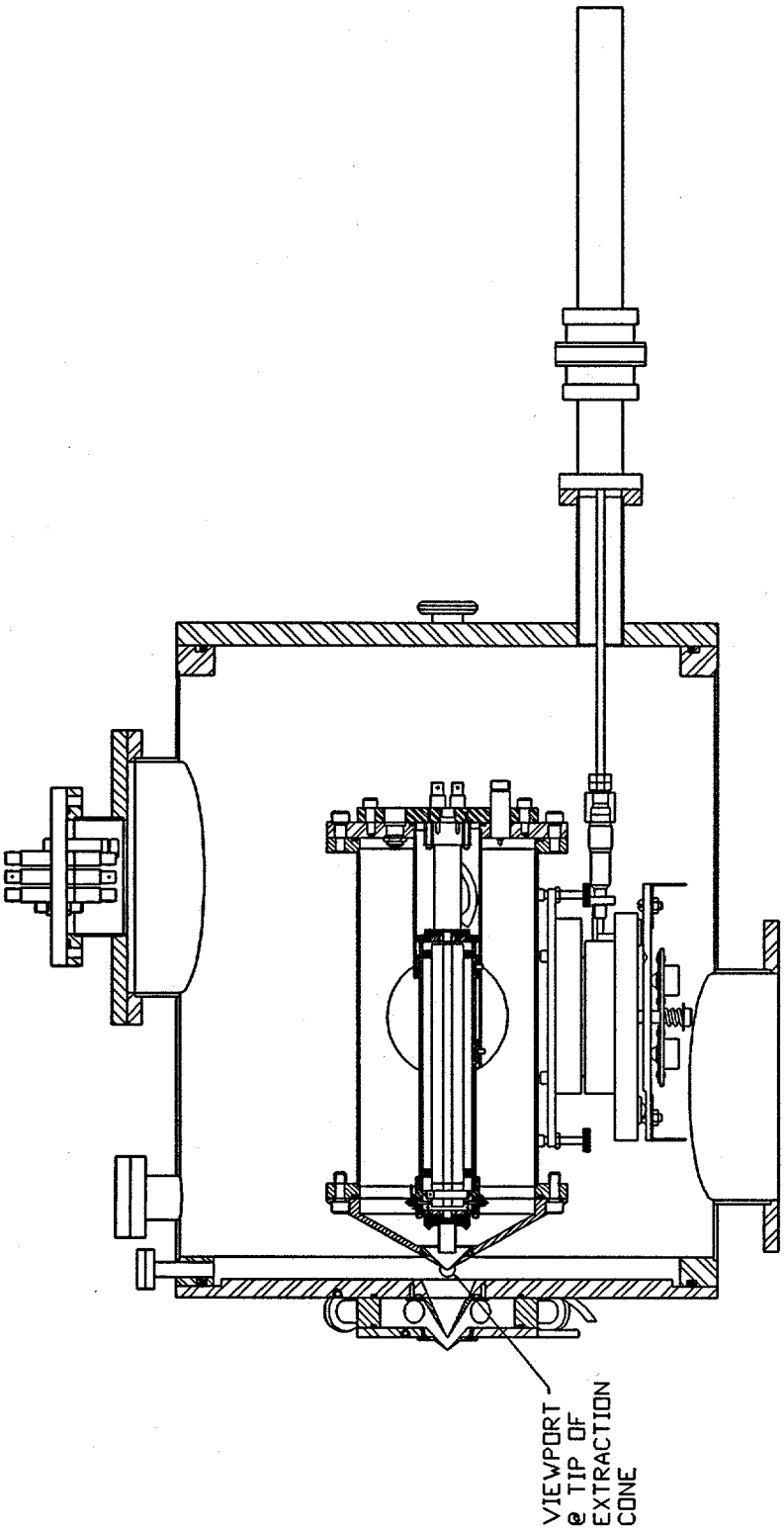

Figure 3. Section view of the ICP-MS device.

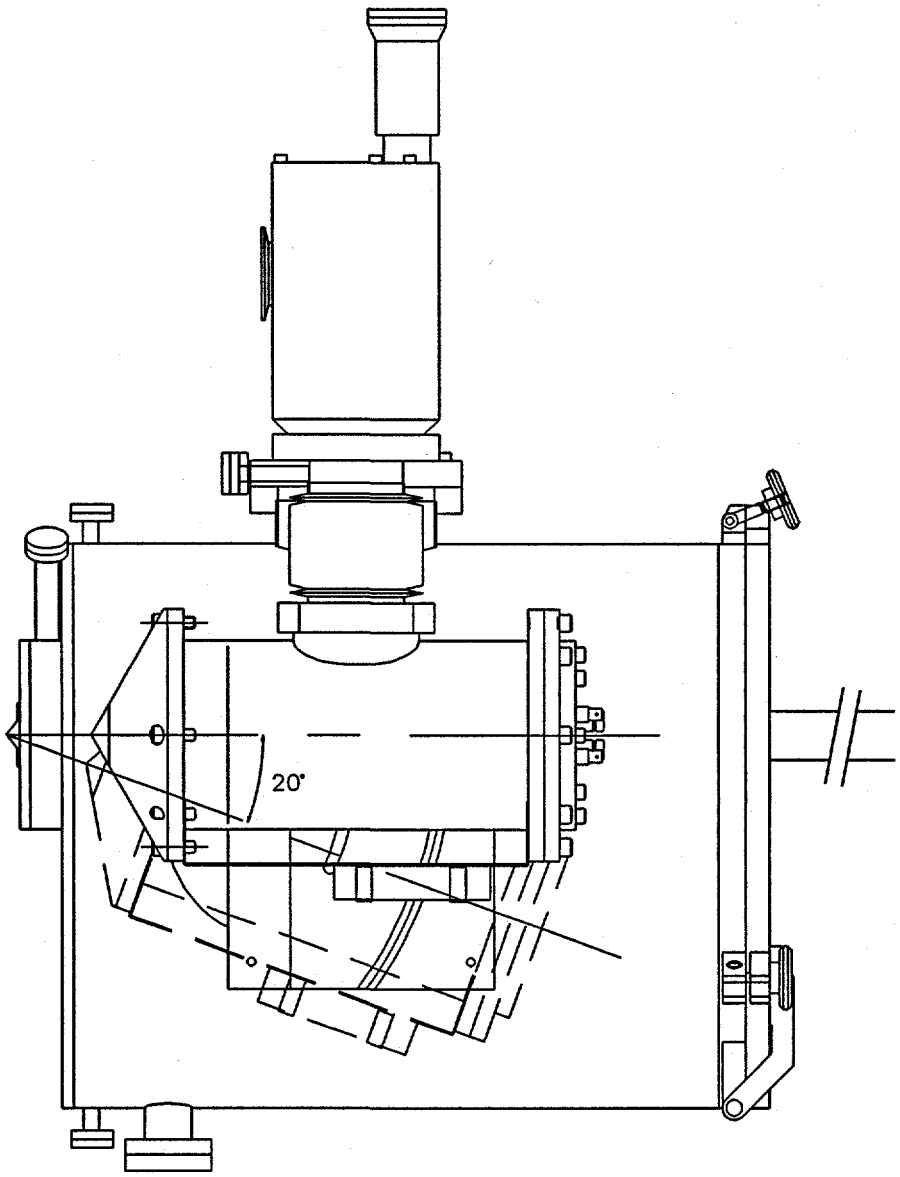

Figure 4. Lateral motion of the inner chamber. The maximum pivoting angle is 20°.

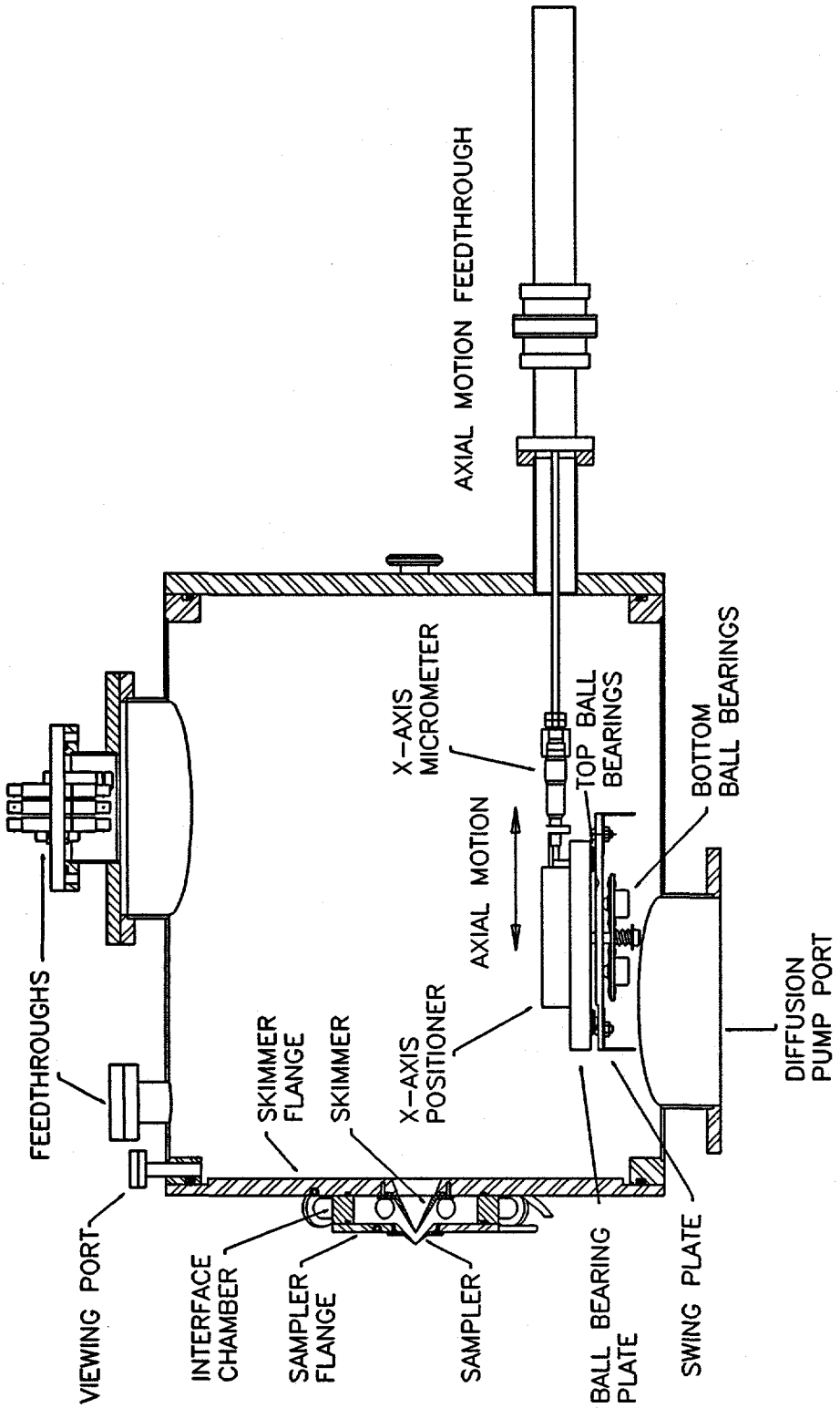

Figure 5. Section view of the ICP-MS device. Axial motion is provided by the axial motion feedthrough.

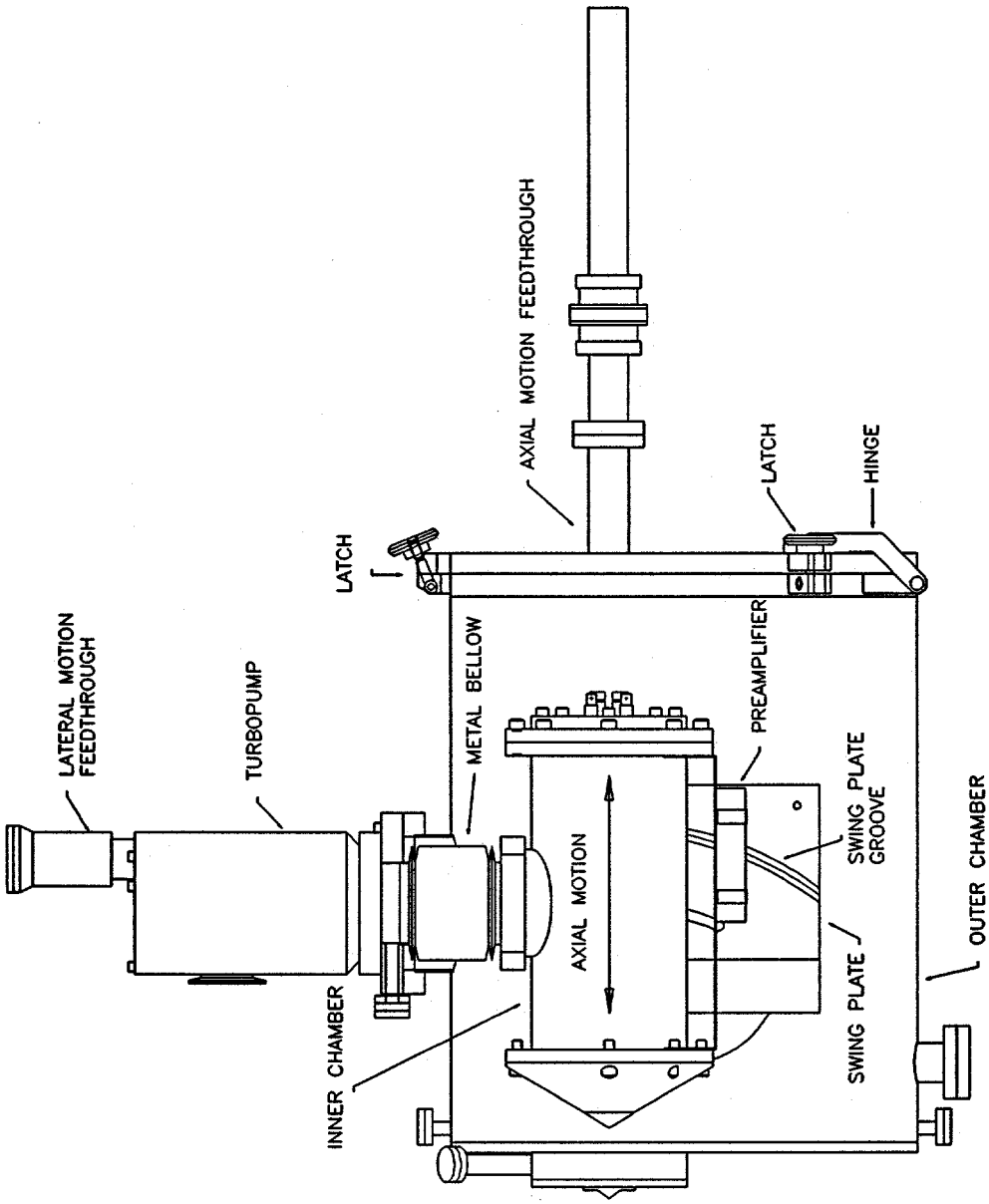

Figure 6. Top view showing axial motion of the inner chamber.

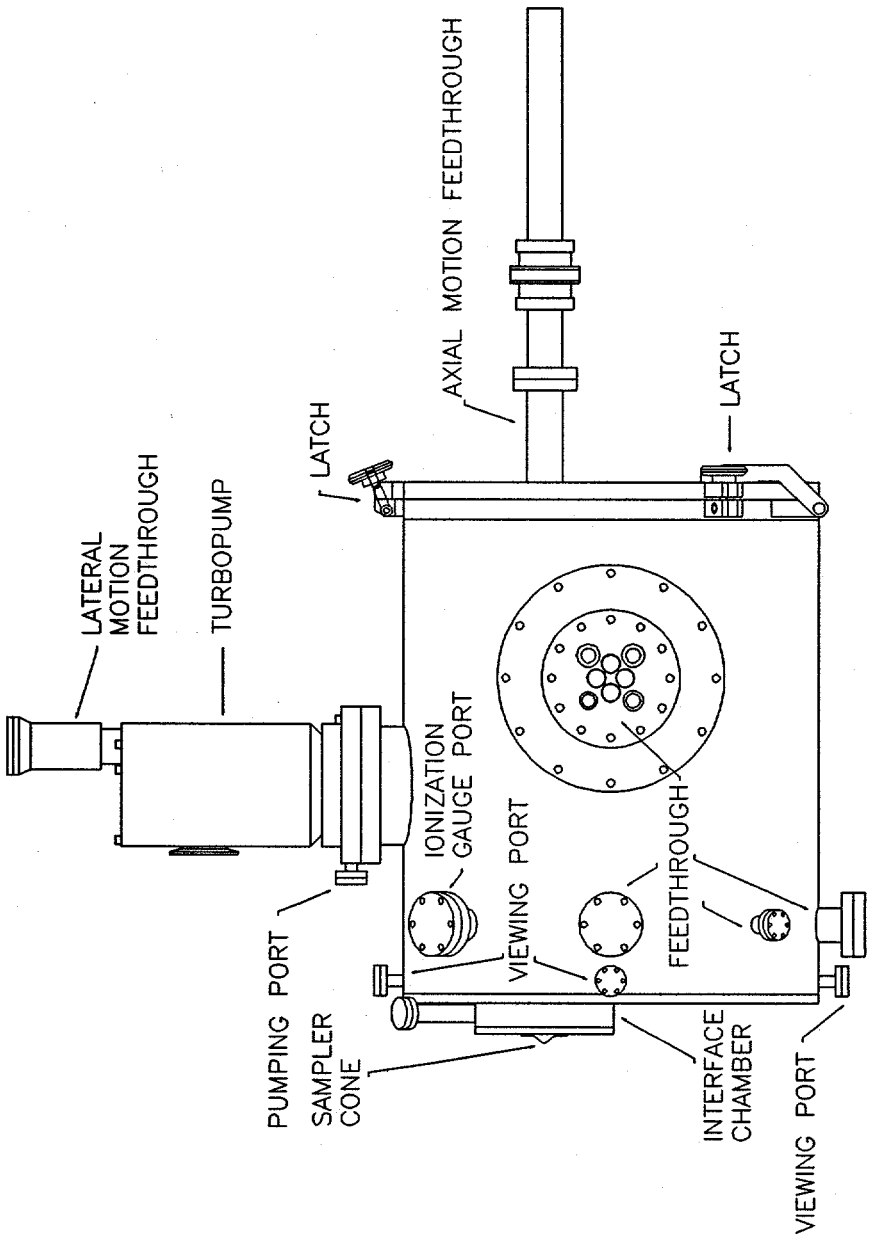

Figure 7. Top view of the outer chamber.

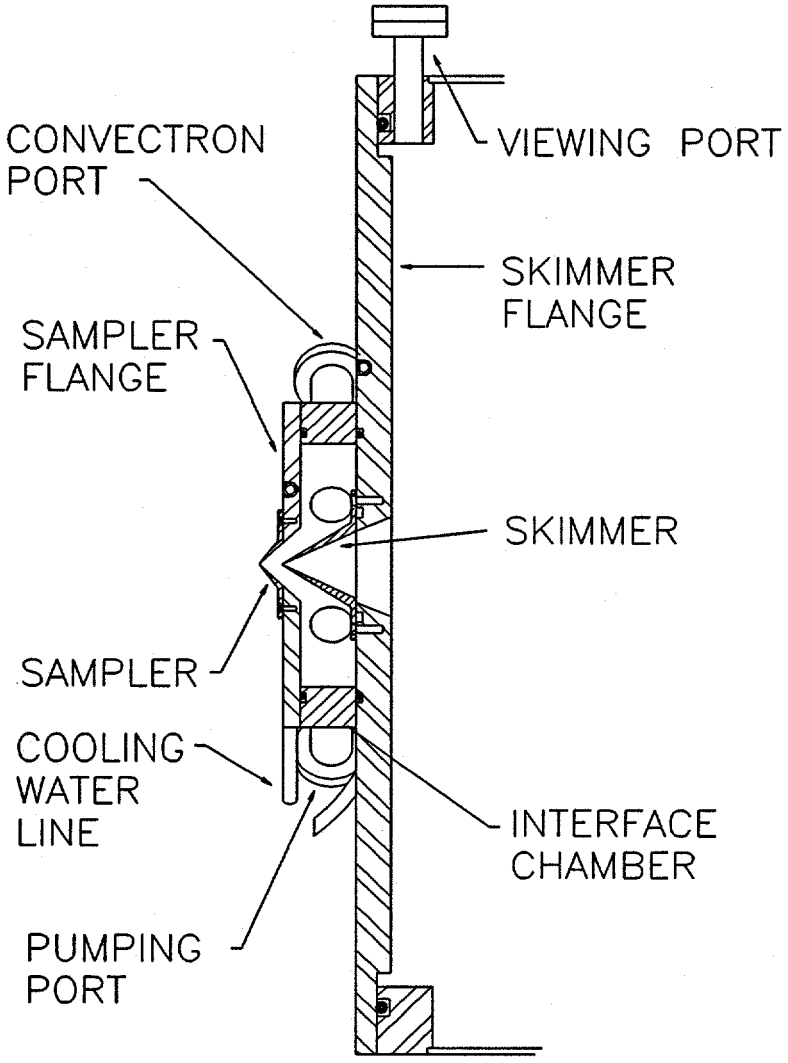

Figure 8. Section view of the ICP-MS interface.

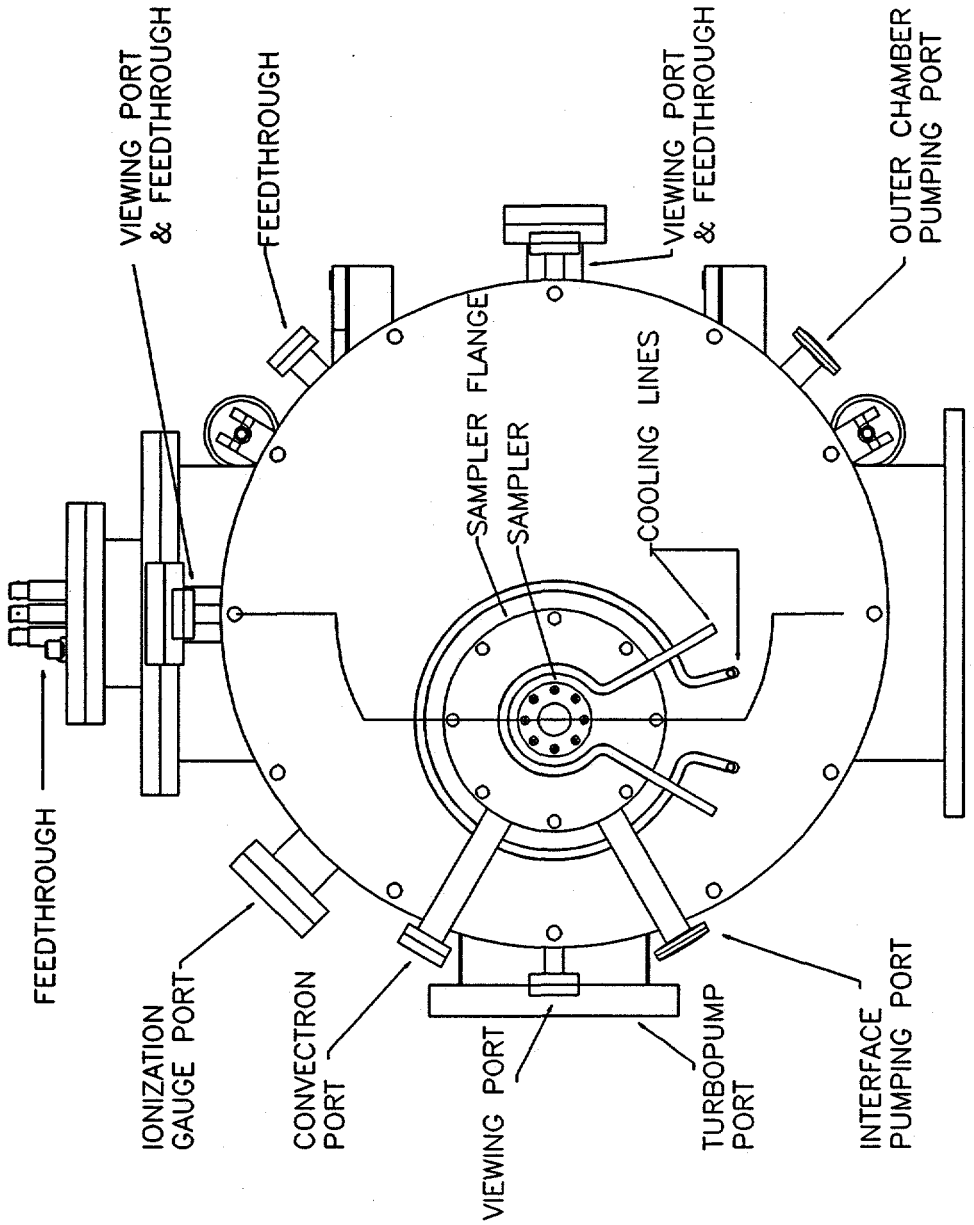

Figure 9. Front view of the ICP-MS device.

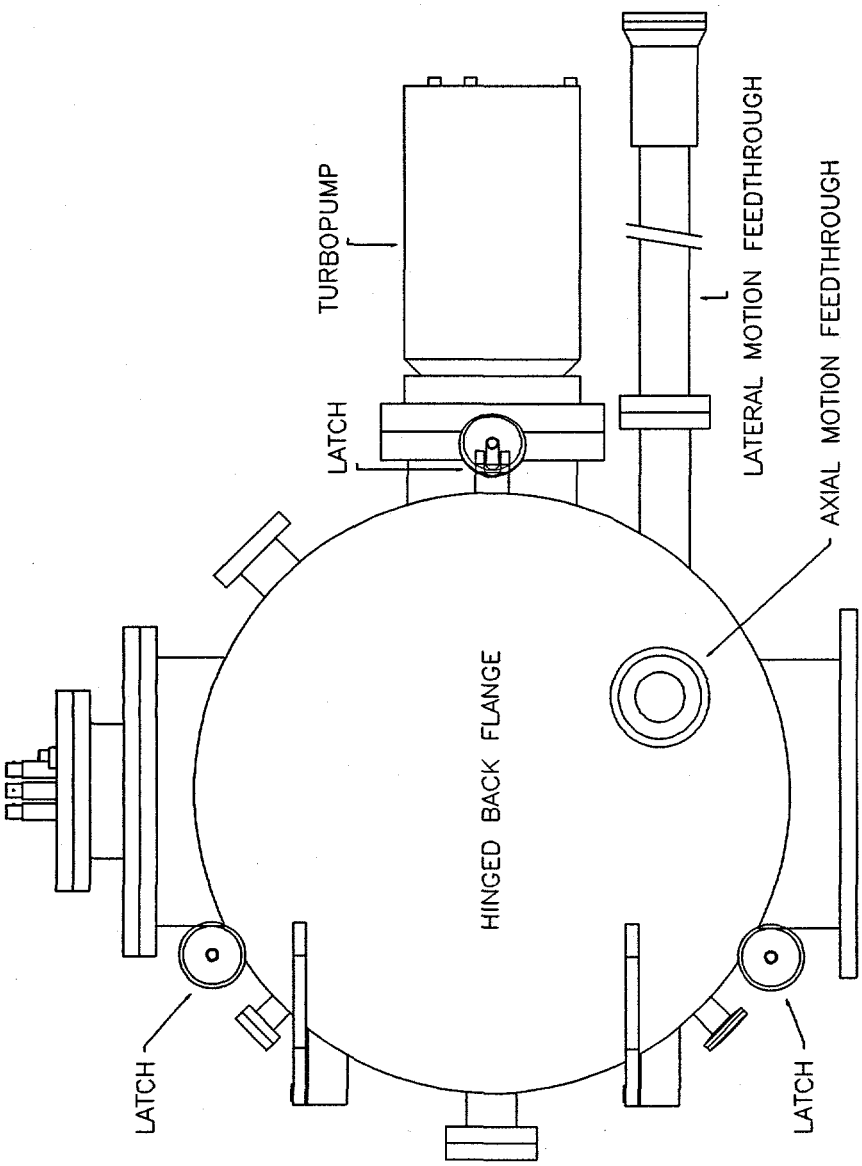

Figure 10. Rear view of the ICP-MS device.

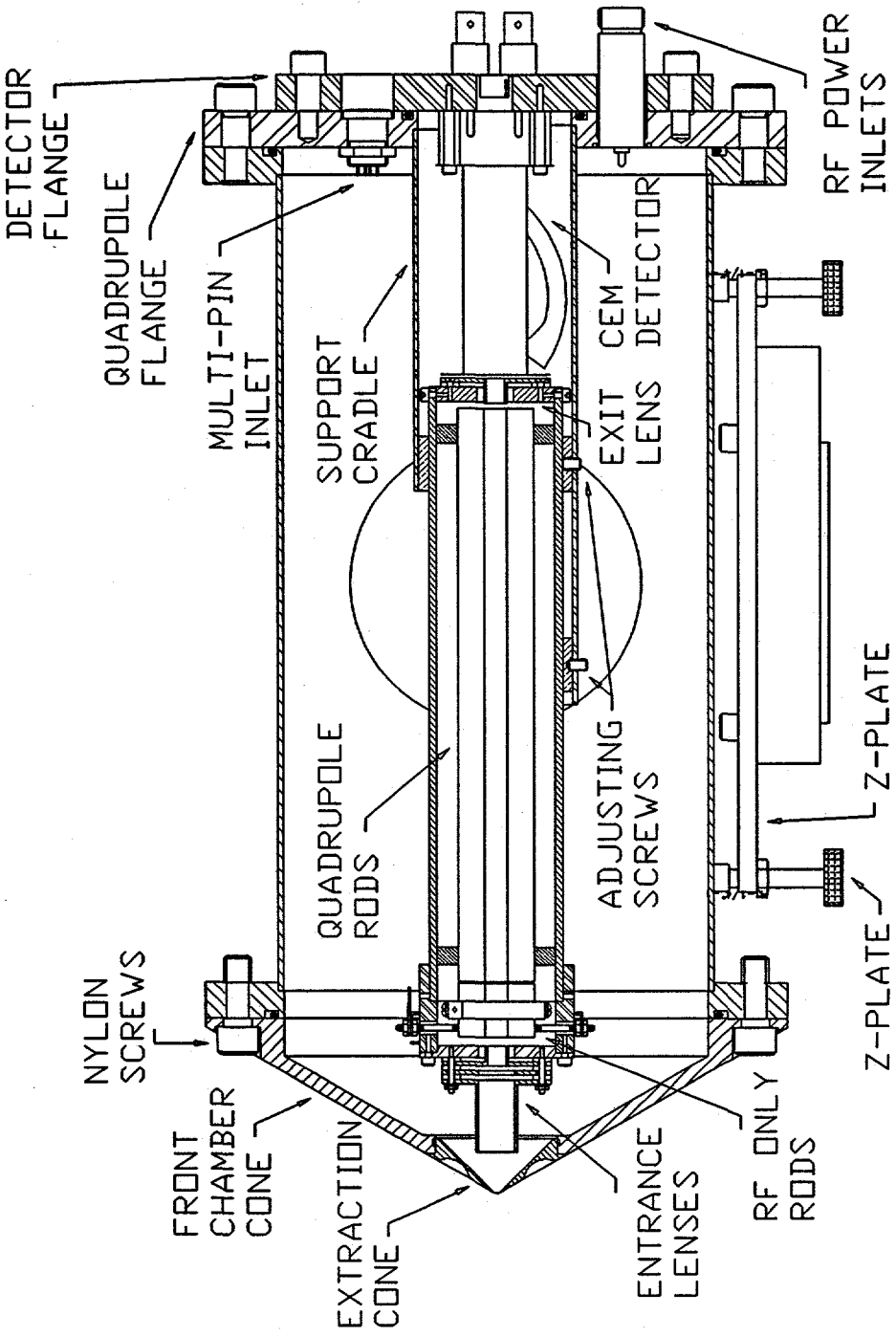

Figure 11. Section view of the inner chamber.

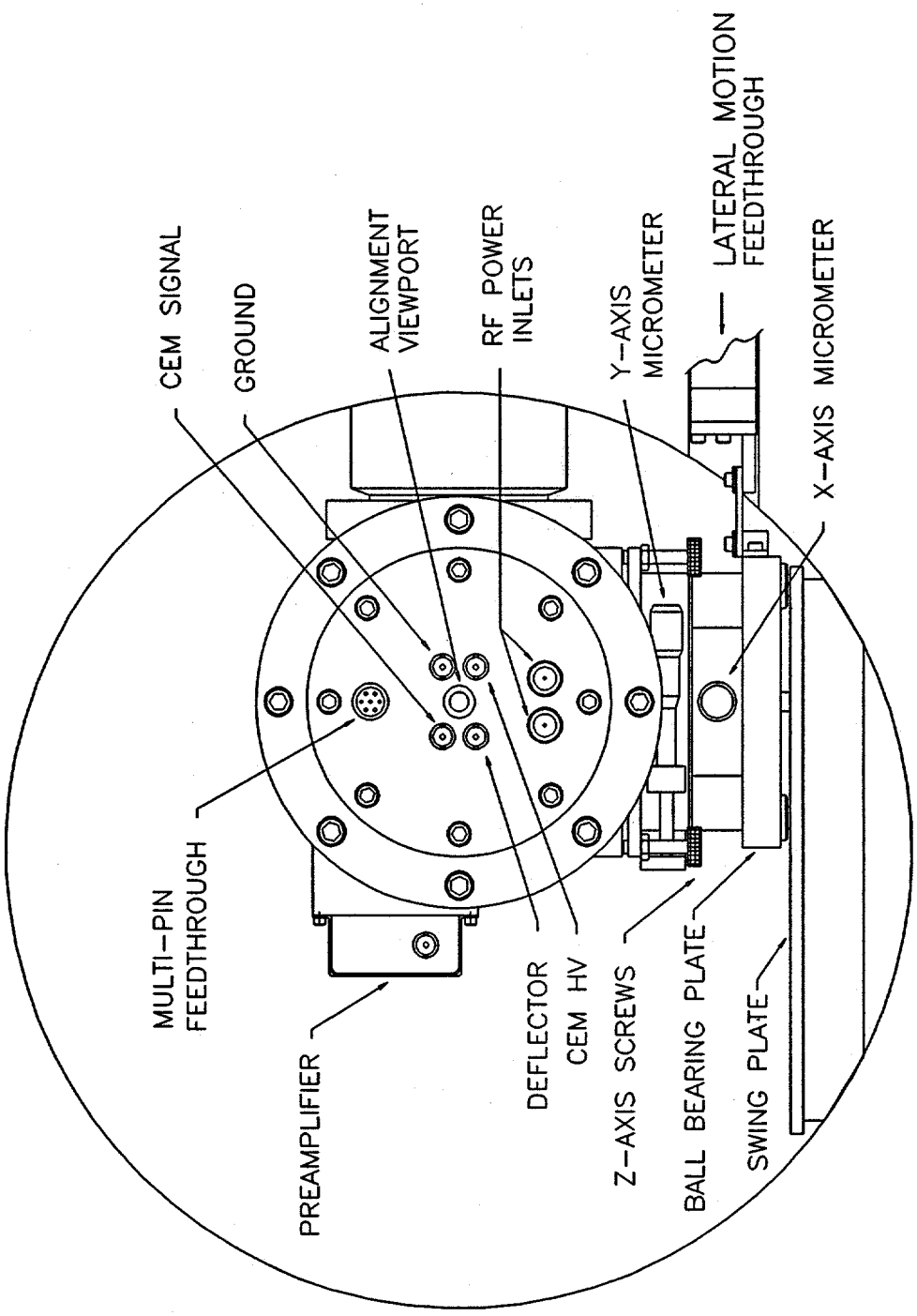

Figure 12. Rear view of the inner chamber.

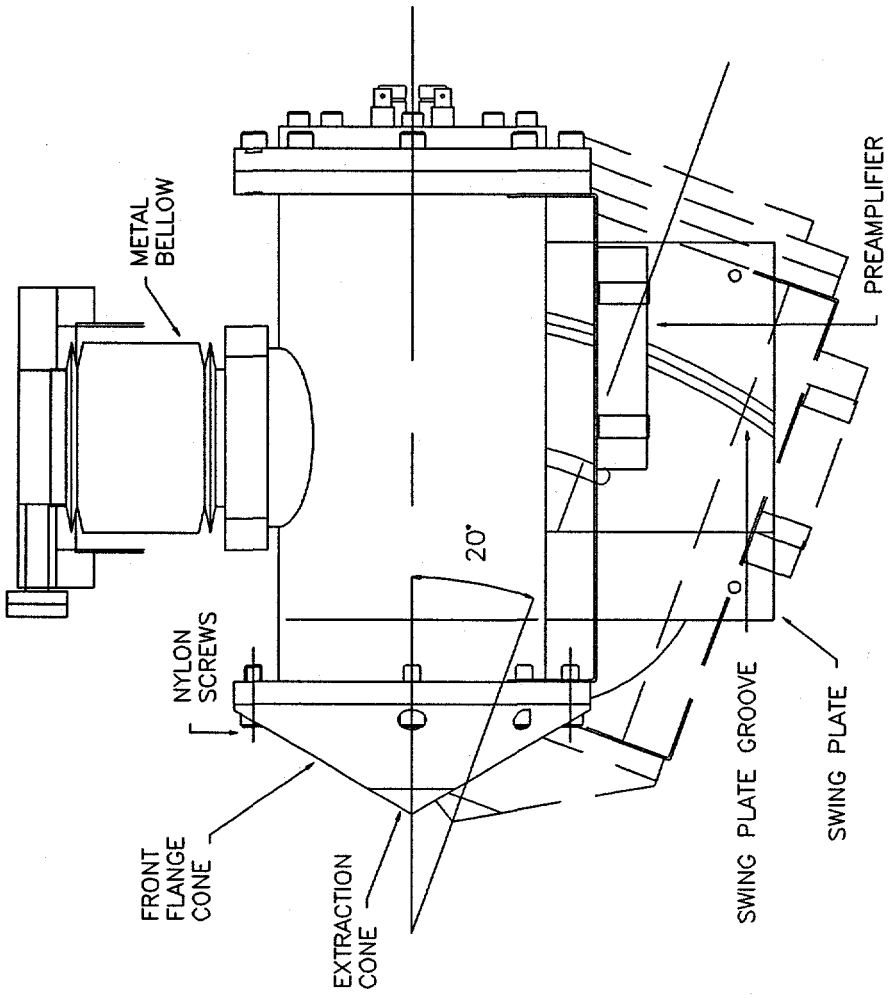

Figure 13. Top view of the inner chamber. The figure also shows the position of the inner chamber after pivoting 20° from the axis line.

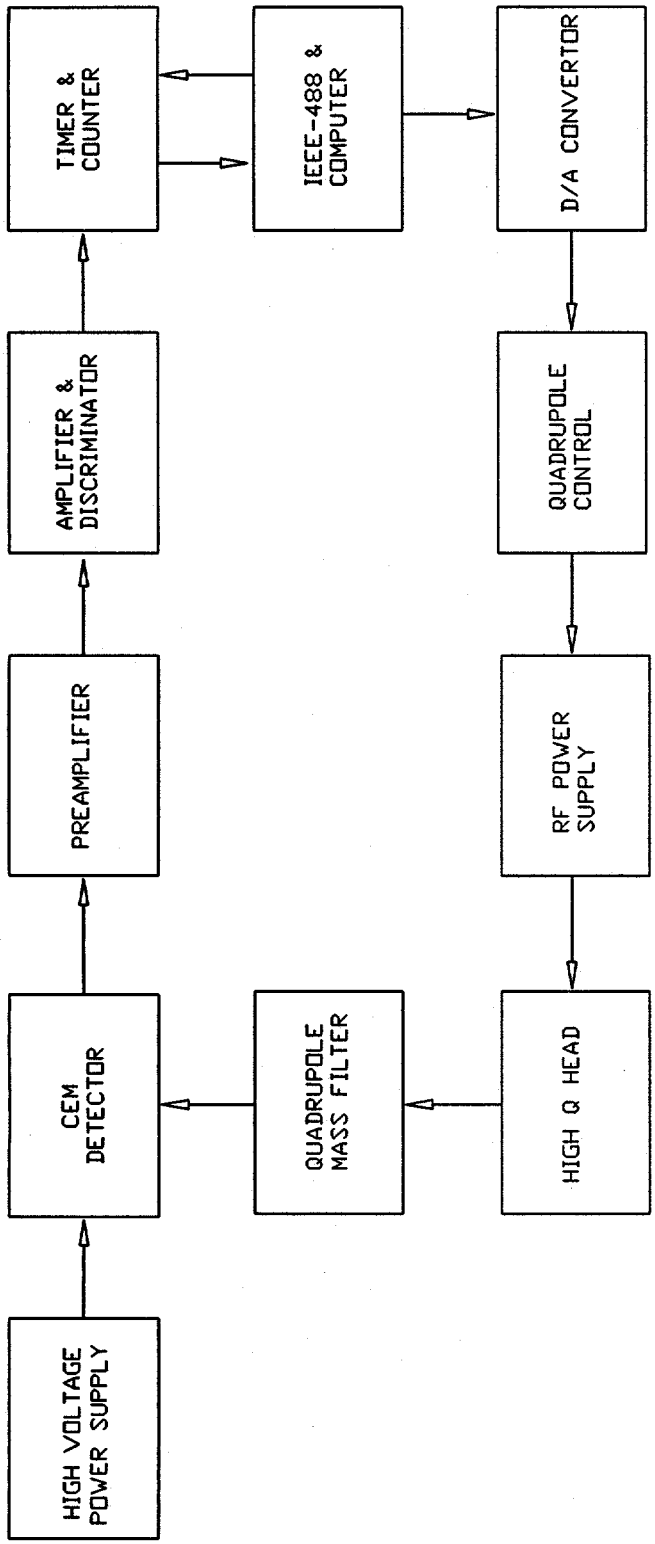

Figure 14. The quadrupole control and data acquisition system.

5. GENERAL CONCLUSIONS

Matrix effects, in most cases suppression effects, from easily ionized concomitant ions on the analyte ion signal in ICP-MS have been known ever since the earliest paper published in ICP-MS. Despite the amount of research and efforts in trying to understand the phenomenon, there is still a lot of work to be done.

The matrix effects are believed to originate from several processes. The first theory holds that the matrix effects originate in the plasma instead of in the mass spectrometer. The easily ionized matrix elements increase the electron density in the central channel of the plasma, thus decreasing the analyte ion signal. The second theory attributes the matrix effects to the space charge effect in the ion beam in the ICP-MS. Although there is still disagreement about where the charge separation occurs, computer simulated ion trajectory show that the presence of heavier matrix ions does decrease the transmission of analyte ions in the ICP-MS.

The research of this dissertation focus on some different aspects of the matrix effects. The first paper focused on a correction procedure for the matrix effects. It explored the idea of using the polyatomic ion signals that occur in the ICP-MS spectrum as internal standards to correct the matrix effects. The extent to which the matrix elements suppress both the analyte ion and the internal standards were the same, in most cases, if the polyatomic internal standard ion is chosen to be close in mass to the analyte ion. Therefore the ratio of the analyte ion signal to the internal standard remains the same. A calibration curve can be built and the matrix effects can thus be corrected.

The question the second and the third papers try to answer is that if the analyte ion beams are broadened or even lost in the presence of the matrix elements inside the ICP-MS. The second paper measured the radial distribution of the ion beam in the ICP-MS, to provide experimental information about the spatial resolution of the ion beam and ion intensities, and their changes with and without the presence of Cs as the matrix, under the influence of the ion lens potentials. The results showed that the broadening the analyte ion beam is not significant in the presence of the matrix, and the ion lens potentials can affect the ion transmission and reduce the matrix suppression. The Simion ion trajectory simulation shows that applying a slight positive potential on the first extraction lens makes the ion beam broader, and the ion density is lower in the ion beam. The ion deposition experiments showed that such an ion lens configuration alleviates the matrix effects. This is indication that the space charge effects behind the skimmer plays an important role in the ICP-MS.

The third paper is a project to design and build a special purpose ICP-MS device. The device is capable of measuring the spatial distribution of the ion beam in the ICP-MS device. The device includes a radially movable inner chamber with a quadrupole mass analyzer under the vacuum. The paper provided and discussed detailed information about the system design, with a number of design diagrams.

The ICP-MS is by far the most sensitive instrument for elemental analysis. It combines the speed of analysis, multiple elemental capabilities, refractory element capabilities of the ICP-AES with the sensitivity, simple spectrum and isotope information of the mass spectrometry. However, it still faces some problems of its own, including the matrix effects discussed in this dissertation. Future work using the device designed in the

third paper may provide more information about the matrix effects, hence a higher analyte ion transmission may be achieved, and a more sensitive instrument may be built.

ACKNOWLEDGMENTS

First and foremost, I would like to thank my parents Tingru Chen and Bizhen Cheng for all of their support during all the years of my education. They have never been to the United States in their lives, and they have probably only seen America on the TV. I, as their second son, have not been able to go back to China to visit with them ever since I came here to pursue my education in the United States. I feel I owe them a lot. They sure are proud of me at this moment, and I am proud of them, too.

I am very grateful to my wife, Fang Li, who helped raise our two daughters while at the same time being able to finish her master's degree at ISU. I am grateful to my daughters, too. Our first daughter, Diana, picked up English mostly on her own after she came to the U.S. at the age of four with no English experience. Seeing how she learned English reminded me my early years of learning English. Our second daughter, Joanna, was born in Ames, and she will remind us what a joy we had with her at ISU.

I am very grateful to my major professor, Dr. Sam Houk. When I decided to join the group in 1990, it was his personality, his friendliness to the students, his knowledge about the research, and his teaching skills that attributed to my decision. In my heart, I will always remember him as my friend and my professor. I sure have learned a lot from him during my graduate studies including English. It was in his group that I became an instrument oriented scientist. Without him, none of the work in this dissertation is possible. I would also like to thank Sam's wife Linda for all those nice conversations, all those parties, picnics, etc.

I would like to extend my appreciation to all my Program of Study Committee

members, Dr. Edward Yeung, Dr. James Espenson, and Dr. Terry King.

My appreciation also goes to Jerry Hand, Steve Lee, Jim Bernighaus and some others at the Ames Lab Machine Shop for helping me make many instrument parts and providing me with advice, and Terry Herman at the Ames Lab Engineering Services for helping me design the ICP-MS instrument and make the final drawings.

I would like to thank the ISU Office of Minority Student Affairs for the 1995 Outstanding Academic Achievement Award that they gave me.

I am also grateful to Perkin-Elmer SCIEX for the Graduate Fellowship awarded to me. The ultrasonic nebulizer provided by CETAC Technologies in our experiments is also appreciated.

I would like to thank all our group members for their friendliness and help. First, I would like to thank those who had helped me and left the group. Ke Hu is the first one that showed me how to light an ICP, and how the ion lenses are mounted. It was with him and his wife and others that we got the 1990 and 1991 Gilman Cup for the Departmental Volleyball Championships. He also showed me a lot of things I needed to know about the school here. Sam Shum showed me how to run the SCIEX ELAN 250 instrument, and helped me use the instrument. Hongsen Niu helped with my first experiment. I remember Dan Wiederin and Fred Smith, but I didn't have too much chance to talk to them before they graduated. I am impressed with Tonya Bricker, the first female group member I worked with. I would like also to thank John Hoekstra, who worked with me for a semester on the ion deposition studies. Secondly, I would like to thank the current group members including Scott Clemons, Lloyd Allen, and Steve Johnson (with whom I spent a week with at

PITTCON'95 in addition to all the other times), and Shen Luan, for all the discussions and their help. I would also like to thank Mike Minnich and Al Gwizdala for teaching me English, and Narong Praphairaksit and Renyi Duan (I feel so sad that she is going to drop out of the school) for their friendliness. I would like also thank a special group member, Ho-ming Pang, for all the help with instrumentation and computer. I am also grateful to another senior group member, Royce Winge, who did some experiments with me. I wish the best to all the other members, Elise Luong (the only female group member left), Ma'an Amad, and Jay Leach.

This work was performed at Ames Laboratory under Contract No. W-7405-eng-82 with the U.S. Department of Energy. The United States government has assigned the DOE Report number IS-T 1742 to this thesis.